

**THE MOLECULAR FUNCTION OF MuRF1  
AND ITS STABILITY IN SKELETAL MUSCLE**

By

IBRAHIM MUSA, B.Sc., M.Sc.

A Thesis Submitted to the University of Birmingham

in Partial Fulfilment of the Requirements for the Degree of

DOCTOR OF PHILOSOPHY

School of Sport, Exercise and Rehabilitation Sciences

College of Life and Environmental Sciences

University of Birmingham

March 2023

UNIVERSITY OF  
BIRMINGHAM

**University of Birmingham Research Archive**

**e-theses repository**

This unpublished thesis/dissertation is copyright of the author and/or third parties. The intellectual property rights of the author or third parties in respect of this work are as defined by The Copyright Designs and Patents Act 1988 or as modified by any successor legislation.

Any use made of information contained in this thesis/dissertation must be in accordance with that legislation and must be properly acknowledged. Further distribution or reproduction in any format is prohibited without the permission of the copyright holder.

## ACKNOWLEDGEMENTS

*In the name of Allah, the Most Gracious and the Most Merciful*

I give all glory to Allah for endowing me with the ability to finish this programme.

My heartfelt gratitude goes to my primary supervisor, Dr. Yu-Chiang Lai, for guiding me down the path of molecular physiology and biochemistry. To be honest, your first-hand approach to mechanistic studies was just what I admired. Indeed, you've given me a developing passion for molecular physiology research and helped me realise my potential in this scientific field. Your desire and passion for high-quality science has shaped who I am today. I would also like to extend my gratitude to my second supervisor, Prof. Gareth Wallis, for his impactful suggestions, supervision, and guidance.

A special note of appreciation goes to everyone in the Lai Lab including Alex Seabright, Yusuke Nishimura, Peter Dawson, Samuel Lord, and Jitpisute for the collaborative environment in which I have worked. Alex Seabright deserves special mention for his willingness to support and stand by me in any situation I have found myself in. My appreciation also goes to Yusuke Nishimura for his enthusiasm to share ideas and write research papers, which has provided me with unending joy.

My family deserves special recognition. Words cannot express how grateful I am to my parents. Your support and love for my education have shaped who I am today. I sincerely extend my appreciations to my wife and our lovely children for your understanding and patience over the last four years, as I was absent for most of your big days. Finally, I want to express my gratitude to TETFUND and Kogi State University Anyigba in Nigeria for the sponsorship and the opportunity accorded to me.

## DECLARATIONS

Except for the following, I declare that all of the work presented in this thesis is mine:

1. The proteomic data was collected from the University of Dundee's MRC PPU unit
2. The construct for HALO-UBA<sup>UBQLN1</sup> TUBE expression was generously supplied by the MRC PPU unit.
3. My supervisor, Dr. Yu-Chiang Lai, gave intellectual feedback at every stage.

## **SUPERVISORS**

Dr. Yu-Chiang Lai, Ph.D.

Prof Gareth Wallis, Ph.D.

## **ASSESSMENT COMMITTEE**

Dr. Craig Doig, Ph.D. (Nottingham Trent University)

Prof. Leigh Breen, Ph.D. (Internal examiner)

Dr. Samuel J E Lucas, Ph.D. (Chair)

## ABSTRACT

Skeletal muscle mass is essential for the maintenance of metabolic function. The amount of skeletal muscle mass depends on the net balance between muscle protein synthesis (MPS) and muscle protein breakdown (MPB). Skeletal muscle atrophy occurs when MPB exceeds MPS. MuRF1 (Muscle-specific ubiquitin ring finger 1), an E3 ligase, is a valid marker of skeletal muscle atrophy. However, its precise molecular function in the control of skeletal muscle mass is currently unclear. The present thesis establishes and addresses the gaps in the body of knowledge that, if addressed, may advance the knowledge of skeletal muscle mass regulation at molecular and cellular levels. MuRF1 is important in the degradation of muscle proteins, but recent studies suggest that it may also regulate a range of other non-degradative cellular processes. Herein, after making MuRF1 reporter and functional deficiency skeletal muscle cell lines, our data provide first evidence that MuRF1 regulates skeletal muscle mass by increasing muscle insulin resistance and inhibiting protein synthesis by upregulating the expression of TRIM72 protein. In addition, employing an ubiquitin-TUBE pulldown strategy, we have demonstrated that MuRF1 undergoes auto-ubiquitylation to regulate its own stability in skeletal muscle via K48- and K63- poly-ubiquitin chains signal. MuRF1 auto-ubiquitylation-mediated K48- and K63-poly-ubiquitin chains signal proteasomal and autophagy-mediated auto-degradation of MuRF1. Importantly, a novel two-step mechanism of MuRF1 auto-ubiquitylation was demonstrated *in vitro*, where recombinant MuRF1 first undergoes auto-mono-ubiquitylation in the presence of UBE2W, which in turn, convert into anchored poly-ubiquitin chains with further addition of UBE2D2 and UBE2N/V1, or UBE2N/V2, respectively. Overall, this thesis advances our understanding of MuRF1's mechanistic role and regulation in skeletal

muscle. Our novel findings have provided new directions for further exploration of the role of MuRF1 in the regulation of skeletal muscle mass.

## **LIST OF CONFERENCE ABSTRACTS AND COMMUNICATIONS**

- 1. GRK2243 Symposium "Understanding Ubiquitylation: From Molecular Mechanisms to Disease", Würzburg, Germany, May 2022 – Poster Communication – E3 ubiquitin ligase MuRF1 impairs IRS1/Akt signalling by stabilising TRIM72 in dexamethasone treated skeletal muscle.**

## LIST OF PUBLICATIONS

1. Nishimura, Y., Chunthong-Orn, J., Lord, S., **Musa, I.**, Dawson, P., Holm, L., & Lai, Y. C. (2022). Ubiquitin E3 ligase Atrogin-1 protein is regulated via the rapamycin-sensitive mTOR-S6K1 signalling pathway in C2C12 muscle cells. *American journal of physiology. Cell physiology*, 323(1), C215–C225. <https://doi.org/10.1152/ajpcell.00384.2021>
2. Yusuke Nishimura, **Ibrahim Musa**, Lars Holm, and Yu-Chiang Lai (2021). Recent advances in measuring and understanding the regulation of exercise-mediated protein degradation in skeletal muscle. *Am J Physiol Cell Physiol*. 1;321(2):C276-C287. Doi: 10.1152/ajpcell.00115.2021.
3. Seabright AP., Fine NHF., Barlow JP., Lord SO., **Musa I.**, Gray A., Bryant J., Banzhaf M., Lavery GG., Hardie DG., Hodson DJ., Philp A., Lai YC. (2020). AMPK activation induces mitophagy and promotes mitochondrial fission while activating TBK1 in a PINK1-Parkin independent manner. *The FASEB Journal*.
4. **Ibrahim Musa**, Yusuke Nishimura, and Yu-Chiang Lai. MuRF1 impairs IRS1/Akt signalling and its response by regulating TRIM72 in skeletal muscle. *Under manuscript preparation for publication*
5. **Ibrahim Musa**, Yusuke Nishimura, and Yu-Chiang Lai. Auto-ubiquitylation of MuRF1 regulates its stability in skeletal muscle. *Under manuscript preparation*

## LIST OF FIGURES

Figure 3. 1 Validation of L6 cell lines stably expressing GFP and GFP-MuRF1.....	25
Figure 3.2 Validation of Crispr/Cas9 generated GFP-MuRF1 knock-in C2C12 cell lines. .....	29
Figure 3.3 Validation of Crispr/Cas9-generated MuRF1 KO C2C12 cell lines.....	32
Figure 3.4 Generation of RING MUTANT GFP-MuRF1 C2C12 cell lines using retroviral system. ....	35
Figure 4.1. MuRF1 is interacting with TRIM72 in skeletal muscle cells .....	51
Figure 4.2. TRIM72 expression is associated with MuRF1 expression in C2C12 myotubes.....	54
Figure 4.3. Dexamethasone increases TRIM72 and MuRF1 protein expression while decreasing proximal insulin signalling in C2C12 myotubes. ....	57
Figure 4.4 MuRF1 KO prevents dexamethasone-induced downregulation of proximal insulin signalling, insulin-stimulated protein synthesis and glucose uptake in C2C12..	61
Figure 4.5. Restoration of TRIM72 in C2C12 MuRF1 KO myotubes decreases proximal insulin signalling .....	63
Figure 4.6. A working model of the molecular roles of MuRF1 in the regulation of skeletal muscle mass.....	70
Figure 5.1. Endogenous MuRF1 is stabilised by inhibition of the proteasome and autophagy in skeletal muscle.....	83
Figure 5.2. Exogenous MuRF1 is stabilised by inhibition of the proteasome and autophagy in skeletal muscle.....	87
Figure 5.3. MuRF1 ubiquitylation is not exclusively modified with K48 or K63 poly- ubiquitin chains in skeletal muscle.....	89

Figure 5.4. MuRF1 undergoes auto-ubiquitylation in skeletal muscle. ....	92
Figure 5.5. MuRF1 auto-ubiquitylation is controlled by ubiquitin conjugating enzymes UBE2s in vitro. ....	97
Figure 5.6. A working model of MuRF1 auto-ubiquitylation .....	103

## LIST OF ABBREVIATIONS

Akt	protein kinase B
ANOVA	analysis of variance
ATP	Adenosine triphosphate
BafA1	Bafilomycin A1
Bort	Bortezomib
BSA	bovine serum albumin
Cas9	CRISPR-associated protein
CC	coiled coil domain
CO <sub>2</sub>	carbon dioxide
CRISPR	clustered regularly interspaced short palindromic repeats.
Con	control
Dex	Dexamethasone
ddNTPs	dideoxynucleotides
DGpYMP	phospho-pentapeptide
DMEM	Dulbecco's modified eagles' medium
DMSO	dimethyl sulfoxide
DNA	deoxyribonucleic acid
dNTP	deoxynucleotide
eEF2	eukaryotic elongation factor 2
ER	endoplasmic reticulum.
FoxO	forkhead box
GAPDH	glyceraldehyde 3-phosphate dehydrogenase
GFP	green fluorescent protein

gRNA	Guide RNAs
GSK-3	Glycogen synthase kinase-3
h	hours
HCl	hydrochloric acid
HECT-type	homologous to the E6-AP C-terminus
HEPES	4-(2-hydroxyethyl)-1-piperazineethanesulfonic acid
IBR	Institute of Biomedical Research
IGF-1	insulin like growth factor 1
IRS1	insulin receptor substrate 1
kDa	kilodalton
KI	knock in
KO	knock out
LC3	microtubule-associated protein 1A/1B-light chain 3
mg	milligram
ml	millilitre
mmol	millimolar
MBP	Maltose binding protein
MPB	muscle protein breakdown
MPS	muscle protein synthesis
mRNA	messenger ribonucleic acid
mTOR	mammalian target of rapamycin
mTORC1	mammalian target of rapamycin complex 1
mTORC2	mammalian target of rapamycin complex 2
MuRF1	muscle-specific ring finger 1

MuRF2	muscle-specific ring finger 2
MuRF3	muscle-specific ring finger 3
MyBP-C	myosin-binding protein C
MyLC1	Myosin Light Chain 1
MyLC2	Myosin Light Chain 2
NBR1	next to BRCA1 gene 1 protein
O <sub>2</sub>	oxygen
PBS	phosphate buffered saline
pH	potential of hydrogen
PI3K	phosphoinositide-3-kinase
PIP2	Phosphatidylinositol 4,5-bisphosphate
PIP3	Phosphatidylinositol 3,4,5-trisphosphate
PVDF	polyvinylidene fluoride
RING	Really Interesting New Genes
RNA	ribonucleic acid
SDS	sodium dodecyl sulphate
SDS-PAGE	sodium dodecyl sulfate– polyacrylamide gel electrophoresis
SEM	standard error of the mean
Ser	serine
SKM	skeletal muscle mass
SM	Skeletal muscle
SQSTM1/p62	sequestosome-1
TBST	tris-buffered saline Tween-20
Thr	threonine

TRIM25	Tripartite Motif Containing 25
TRIM32	Tripartite Motif Containing 32
TRIM63	Tripartite Motif Containing 63
TRIM72	Tripartite Motif Containing 72
TUBE	tandem ubiquitin binding entity
Ub	ubiquitin
UBA <sup>UBQLN1</sup>	his-halo-ubiquilin1 UBA domain tetramer
UBE2D1	Ubiquitin Conjugating Enzyme E2 D1
UBE2W	Ubiquitin Conjugating Enzyme E2 W
UBE2N	Ubiquitin Conjugating Enzyme E2 N
UBE2V1	Ubiquitin Conjugating Enzyme E2 V1
UBE2V2	Ubiquitin Conjugating Enzyme E2 V2
ULK1	unc-51 like autophagy activating kinase 1
UPS	ubiquitin proteasome system
WT	wild type
°C	degrees Celsius
μg	microgram
μL	microlitre
μM	micromolar

# TABLE OF CONTENTS

## CHAPTER 1 1

GENERAL INTRODUCTION .....	1
1.1 Skeletal muscle and its role in health .....	2
1.2 Muscle protein synthesis and skeletal muscle mass .....	2
1.3 The ubiquitin proteasome system (UPS) and skeletal muscle mass.....	3
1.4 Skeletal muscle atrophy.....	4
1.5 MuRF1 as a valid marker of skeletal muscle atrophy .....	6
1.6 Role of MuRF1 in the regulation of skeletal Muscle Mass.....	7
1.7 MuRF1 auto-ubiquitylation .....	9
1.8 Significance of the thesis.....	10
1.9 Aim and objectives of the thesis.....	10

## CHAPTER 2 12

GENERAL METHODS .....	12
2.1 Reagents and general methods .....	13
2.1.1 Antibodies and Reagents .....	13
2.1.2 Mammalian cell lines and culture.....	14
2.1.3 C2C12.....	14
2.1.4 L6.....	14
2.1.5 HEK 293 and HEK293 FT cells .....	15

2.2	Transfection of mammalian cell lines .....	15
2.3	Cell lysis .....	16
2.4	Protein Measurement.....	16
2.5	GFP pulldown.....	17
2.6	Immunoprecipitation .....	17
2.7	TUBE-ubiquitin pulldown.....	18
2.8	Preparation of Samples .....	18
2.9	Immunoblotting (Western blotting).....	18
2.9.1	Gel electrophoresis .....	18
2.9.2	Transfer and blocking.....	19
2.9.3	Primary antibody .....	19
2.9.4	Secondary antibody .....	19
2.9.5	Antibody detection and Imaging .....	19
2.10	Data Analysis.....	20
2.11	Protein synthesis (SUnSET) .....	20
2.12	Glucose uptake measurements.....	20
2.13	Statistical analysis .....	21
CHAPTER 3		22
TOOLS DEVELOPMENT TO STUDY MURF1 PROTEIN AND ITS ROLE IN SKELETAL MUSCLE.....		22

3.1	Generation of L6 cell lines that stably expressed GFP-MuRF1 or GFP using a retrovirus.....	23
3.1.1	Background.....	23
3.1.2	Method.....	23
3.1.3	DNA construct.....	23
3.1.4	Transfection and retroviral generation .....	24
3.1.5	GFP- and GFP-MuRF1 retroviral transduction and selection in L6 .....	24
3.1.6	L6-GFP- and L6-GFP-MuRF1 cell lines sorting.....	24
3.1.7	Preparation of western samples .....	25
3.1.8	Validation by Immunoblotting (western blotting).....	25
3.2	GFP-MuRF1 knockin generation in C2C12 using CRISPR/Cas9 .....	26
3.2.1	Background.....	26
3.2.2	Method.....	26
3.2.3	DNA construct.....	26
3.2.4	Transfection and selection of GFP-MuRF1knock-in positive C2C12 myoblasts.....	27
3.2.5	Cell sorting .....	27
3.2.6	Sample preparation.....	28
3.2.7	Validation by Immunoblotting (Western blotting).....	28
3.3	MuRF1 knockout C2C12 cells generation using CRISPR/Cas9.....	30
3.3.1	Background.....	30
3.3.2	Method.....	30
3.3.3	DNA construct.....	30

3.3.4	Transfection and selection of MuRF1 knockout positive C2C12 myoblasts .	31
3.3.5	Cell sorting .....	31
3.3.6	Sample preparation .....	31
3.3.7	Validation by immunoblotting (Western blotting) .....	31
3.4	Generation of GFP-MuRF1 with Ring domain mutation at C23A in C2C12 cells using retrovirus .....	33
3.4.1	Background.....	33
3.4.2	DNA construct.....	33
3.4.3	Transfection and retroviral harvesting.....	33
3.4.4	<sup>GFP/GFP</sup> MuRF1 (C23A) retroviral transduction and selection in C2C12.....	34
3.4.5	Preparation of western samples .....	34
3.4.6	Validation by Immunoblotting (western blotting).....	34
CHAPTER 4 36		
MURF1 IMPAIRS IRS1/AKT SIGNALLING AND ITS RESPONSE BY REGULATING TRIM72 IN SKELETAL MUSCLE.....		
4.1	Abstract.....	37
4.2	Introduction .....	38
4.3	Materials and Methodologies .....	40
4.3.1	Antibodies and Reagents .....	40
4.3.2	Cell lines and Culture .....	41
4.3.3	Transient transfection of mammalian cell lines.....	42
4.3.4	Cell lysis .....	43
4.3.5	Protein Measurement.....	43

4.3.6	Sample preparation .....	44
4.3.7	GFP pulldown.....	44
4.3.8	Western blotting .....	44
4.3.9	Measurement of protein synthesis (SUnSET) .....	45
4.3.10	Measurement of glucose uptake .....	45
4.4	Data Analysis.....	46
4.5	Statistical analysis .....	46
4.6	Results .....	48
4.6.1	Identification of TRIM72 as a novel MuRF1-interacting protein. ....	48
4.6.2	TRIM72 protein expression correlates with MuRF1 protein expression in C2C12.....	52
4.6.3	Dexamethasone increases TRIM72 and MuRF1 protein expressions while decreasing IRS1/Akt signalling in C2C12 myotubes.....	55
4.6.4	The dexamethasone-induced downregulation of proximal insulin signalling, insulin-stimulated protein synthesis and glucose uptake is prevented in MuRF1 KO C2C12 myotubes. ....	58
4.6.5	Restoration of TRIM72 in C2C12 MuRF1 KO myotubes decreases proximal insulin signalling. ....	62
4.7	Discussion.....	65
4.8	Conclusion.....	69
CHAPTER 5		71

AUTO-UBIQUITYLATION OF MURF1 REGULATES ITS STABILITY IN SKELETAL MUSCLE.....	71
5.1 Abstract.....	72
5.2 Introduction .....	73
5.3 Materials and methods.....	75
5.3.1 Antibodies and Reagents .....	75
5.3.2 Cell lines and Culture .....	76
5.3.3 Cell lysis .....	77
5.3.4 Protein Measurement.....	77
5.3.5 Sample preparation .....	78
5.3.6 GFP pulldown.....	78
5.3.7 TUBE-ubiquitin pulldown.....	78
5.3.8 Western blotting .....	79
5.3.9 <i>In vitro</i> Analysis .....	79
5.4 RESULTS.....	81
5.4.1 Endogenous MuRF1 is stabilised by inhibition of the proteasome and autophagy in skeletal muscle.....	81
5.4.2 Exogenous MuRF1 is stabilised by inhibition of the proteasome and autophagy in skeletal muscle.....	84
5.4.3 MuRF1 ubiquitylation is not exclusively modified with K48 or K63 poly-ubiquitin chains in skeletal muscle.....	87
5.4.4 MuRF1 is the ubiquitin ligase that ubiquitylates itself in skeletal muscle.....	90

5.4.5	The UBE2D, UBE2N/V1/2 and UBE2W ubiquitin-conjugating enzymes are required for MuRF1 auto-ubiquitylation <i>in vitro</i> .	93
5.4.6	MuRF1 function as an E3 ligase enzyme and ubiquitylates itself <i>in vitro</i> .	98
5.5	Discussion	99
5.6	Conclusion	102
CHAPTER 6 104		
GENERAL DISCUSSION		104
6.1	GENERAL DISCUSSION	105
6.2	Limitations	109
6.3	Conclusion	110
CHAPTER 7 111		
REFERENCE		111

---

**CHAPTER 1**  
**GENERAL INTRODUCTION**

---

## **1.1 Skeletal muscle and its role in health**

Skeletal muscle (SKM) is quantitatively the largest tissue in the body accounting about half of the total body weight (1). SKM is a major mediator of metabolic health due to its role as a metabolic reservoir and adaptability (2). SKM regulates voluntary movements, thermogenesis, metabolic homeostasis and serves as a site for nearly all insulin-dependent glucose uptake and muscle protein storage (3, 4, 5, 6, 7). Therefore, the preservation of SKM mass is critical and significance to the metabolic functions of the body. Maintaining skeletal muscle mass requires a balance of SKM protein synthesis (MPS) and SKM protein breakdown (MPB). The imbalance between these pathways leads to loss of skeletal muscle mass. The UPS is widely acknowledged as the key regulatory system that mediates SKM mass remodelling (8). As a result, gaining understanding of the UPS's role in SKM mass regulation may lead to significant discoveries that could improve metabolic health.

## **1.2 Muscle protein synthesis and skeletal muscle mass**

The IRS1/Akt/mTORC1 signalling pathway is a crucial regulator of skeletal muscle mass (9, 10, 11, 12). IRS1 (insulin receptor substrate 1) is activated upon binding of insulin to the insulin receptor. The activated IRS1 in turn, recruits PI3K (phosphoinositol-3-kinase) to phosphorylate PIP2 into PIP3, resulting in the translocation of Akt onto the plasma membrane. Here, Akt activity is activated via phosphorylation by mTORC2 and PDK1 kinases. Activated Akt then translocates to the cytoplasm and nucleus to phosphorylate its downstream targets. Akt promotes protein synthesis by attenuating muscle protein breakdown via phosphorylation and inhibition of the FOXO transcription molecules (13, 14). In addition, Akt also phosphorylates and inhibits GSK-3 $\beta$  or activates mTOR to enhance protein synthesis. Upregulation of the

IRS1/Akt/mTORC1 pathway has been attributed to skeletal muscle mass hypertrophy (15) and increase in myotubes diameter (16, 17). Akt's function in the regulation of SKM mass has been demonstrated by previous authors. Akt knockout mice severely induced SKM atrophy (17). In contrast, Akt activation attenuates denervation-induced SKM atrophy in rat (9, 18). These previous studies suggest the importance of the Akt signalling molecule in the regulation of SKM mass. Furthermore, the inhibition of mTOR using rapamycin also show considerable loss of SKM mass (19), suggesting the importance of mTOR signalling in the regulation of SKM mass. Collectively, this pathway is essential for controlling SKM mass, and a thorough understanding of this pathway's upstream may lead to the development of novel therapeutic intervention.

### **1.3 The ubiquitin proteasome system (UPS) and skeletal muscle mass**

Multiple proteolytic pathways, including the UPS (20), autophagy lysosomal (21), calpain (22), and caspase (23) are involved in the breakdown of muscle proteins. However, the UPS plays a key role in the turnover of SKM protein during catabolic processes of SKM atrophy (24). In comparison to the autophagy, Zhao *et al.* (25) demonstrated that proteasome-mediated protein degradation accounted for at least two-thirds or 80% of the total protein degradation in both C2C12 myoblasts and myotubes (20, 25) using the proteasome inhibitor (bortezomib) and the autophagy inhibitor (concanamycin A), respectively. Proteins destined for degradation are usually tagged with the poly-ubiquitin chains generated by the UPS (26). The UPS comprises of the ubiquitin, E1 ubiquitin-activating enzyme, E2 ubiquitin-conjugating enzyme, E3 ubiquitin-ligase enzyme, and the 26S proteasome (27). The ubiquitylation phase is initiated by the E1, an enzyme that requires ATP to activate ubiquitin and establishes a thioester bond between ubiquitin's C-terminal Gly carboxyl group and its active Cysteine site. The activated ubiquitin is

transferred to the Cysteine residue of the E2 enzyme, and the final enzyme in the cascade, the RING (Really Interesting New Genes) or HECT-type E3 ligase (homologous to the E6-AP C-terminus), provides substrate specificity. Ubiquitin can be added to a protein as a single entity (mono-ubiquitin) or to ubiquitin molecule as a chain of variable length (poly-ubiquitin), referring to as “ubiquitin code”(28). The poly-ubiquitin chains are often linked by any of the seven lysine residues (Lys6, Lys11, Lys27, Lys29, Lys33, Lys48, and Lys63) or the N-terminal methionine residue of ubiquitin (29). The poly-ubiquitin chains on lysine 11 (K11) or 48 (K48) (28) are degraded in the 26S proteasome, a multicatalytic protease complex that breaks down ubiquitylated proteins into tiny peptides and free ubiquitin for recycling (30). In addition, mixed poly-ubiquitin chains, K48/K63 (31, 32) and K11/K48- branched chains promote proteasomal degradation for efficient elimination of aggregation of cytotoxic proteins by the 26S proteasome (33). This ubiquitylation pathway serves as a cue for protein turnover, which accelerates the loss of muscle mass (34). The process of ubiquitylation is not limited to UPS protein substrates; in fact, a number of UPS enzymes, including E3s, are ubiquitylated (35) to auto-regulate their own stability (36). Identifying the key components of the UPS that regulates SKM mass would help in developing novel therapies, including pharmacological strategies, to combat SKM atrophy.

#### **1.4 Skeletal muscle atrophy**

Skeletal muscle atrophy is the term describing the loss of skeletal muscle mass characterised by reduced protein content and myofiber diameter (37). Skeletal muscle atrophy occurs in response to limb immobilization, bed rest, mechanical ventilation, sepsis, cancer cachexia, diabetes, congestive heart failure, neurodegeneration, muscular dystrophies, aging, and side effect of synthetic glucocorticoid treatment (38, 39, 40). Lack of strength, falls, fractures, and disability

due to skeletal muscle atrophy has a detrimental impact on quality of life (41, 42). Currently, no effective pharmacological drug for skeletal muscle atrophy is available and the molecular mechanism of skeletal muscle atrophy is not fully understood (40). The only effective intervention that reverses skeletal muscle atrophy is physical exercise, but unfortunately not all patients have the capacity for physical exercise intervention (40). The absence of effective treatments for skeletal muscle atrophy implies that our understanding of the underlying mechanisms of skeletal muscle atrophy is still incomplete and requires more research. The most important proteolytic pathway known to drive muscle atrophy in both humans and rodents is the UPS (43). Components of the UPS including MuRF1 E3 ligase are amongst the most commonly upregulated genes in several humans and rodent models of skeletal muscle atrophy under catabolic circumstances (38, 44, 45). In contrast, MuRF1 gene deletion in rodents partially prevented skeletal muscle from atrophy (58, 59). But how MuRF1 regulates skeletal muscle mass at the molecular level remains unclear. The advent and adoption of cell-based skeletal muscle atrophy models have offer valuable molecular insights into muscle-specific signalling (46, 47). Models such as the dexamethasone-treated murine C2C12 skeletal muscle cells has been demonstrated to mimicked human atrophic muscle models (48). Thus, it would be possible to make useful contributions to this field by exploring the cell-based skeletal muscle atrophy models to understand the molecular mechanism of skeletal muscle atrophy.

## **1.5 MuRF1 as a valid marker of skeletal muscle atrophy**

The muscle-specific ring finger 1 (MuRF1, *TRIM63*) is an important E3 ubiquitin-ligase within the UPS that regulates skeletal muscle mass (35). MuRF1 is persistently overexpressed in nearly all conditions of skeletal muscle atrophy, both in rodents and human patients (49, 50). This suggests that MuRF1 is associated with skeletal muscle loss. Consistently, MuRF1 gene deletion partially prevented skeletal muscle atrophy in mice (51, 52). Similarly, in humans, mutant MuRF1 impairs muscle protein breakdown and causes hypertrophic cardiomyopathy (53). Altogether, these previous studies establish MuRF1 as a valid marker of skeletal muscle atrophy, making MuRF1 a potential therapeutic target to treat atrophy-related conditions (54). Although, most of these studies have concentrated on MuRF1 mRNA expression and muscle protein breakdown, it's currently unclear if MuRF1 protein is required for skeletal muscle protein breakdown (55). Consequently, direct measurement of the protein content is more pertinent to biological processes because protein is the ultimate product that carries out gene activity (56, 57). Importantly, the upregulation of the atrophy-promoting mRNA gene as noted by Sandri (58) is not always correlated with an increase in protein expression (58). It is believed that under catabolic conditions, an increase in ligase activity of skeletal muscle-specific ubiquitin E3 ligase would inevitably lead to an increase in autoubiquitylation (49), which is then degraded by proteasome- or lysosome-mediated degradation (58). Therefore, in order to prevent the loss of E3 ligase protein caused by increased autoubiquitylation, gene transcription must be upregulated (58). However, in the case of MuRF1, low antibody quality is frequently a major hindrance to revealing its protein expression in biological specimens (58, 59, 60). Thus, to establish an effective therapeutic strategy to ameliorate SKM atrophy, a substantial understanding of the molecular function of MuRF1 protein is necessary.

## 1.6 Role of MuRF1 in the regulation of skeletal Muscle Mass

Research aiming to understand MuRF1's role during skeletal muscle atrophy has advanced in recent years. MuRF1 is a candid biomarker of skeletal muscle atrophy, but how MuRF1 regulates skeletal muscle mass at the molecular level remains poorly understood. In a recent study, overexpression of MuRF1 was sufficient to cause atrophy, but the majority of its ubiquitylated targets do not undergo degradation (51). This suggests that MuRF1 could induce muscle atrophy via non-degradative mechanisms. Further analysis by Baehr *et al.*, indicates that MuRF2, MuRF3, and TRIM25 E3 protein abundance are positively correlated with MuRF1 overexpression (51), demonstrating that MuRF1 controls other E3 ligases to regulate skeletal muscle mass. Additionally, the mutation of MuRF1 RING domain at C44S/C47S attenuated skeletal muscle atrophy in mice (51). Similarly, MuRF1 was previously reported to ubiquitylate and promotes myofibrillar proteins degradation via the proteasome in C2C12 myotubes following dexamethasone treatment (61) and in transgenic mice (62). Consistently, the deletion of MuRF1's Ring-finger domain inhibited skeletal muscle atrophy and prevented the differential loss of MyBP-C, MyLC1, and MyLC2 in mice (62). These serial findings indicate that ligase activity of MuRF1 is also essential in skeletal muscle atrophy. Despite the fact that the crystal structure of MuRF1's RING domain has not yet been established due to its instability (35), the RING domain is needed for binding with E2 conjugating enzymes and catalysing ubiquitin transfer from E2 to target substrates (63).

Although MuRF1 is essential for the degradation of SKM myofibrillar proteins (61, 62), a previous study reported that muscle mass was preserved with enhanced protein synthesis in dexamethasone-treated MuRF1 knockout mice (64), as opposed to dexamethasone-treated mice

(65). Furthermore, in fasting induced atrophy, MuRF1 knockout mice also had higher protein synthesis than WT mice (66). Altogether, these previous findings indicate a probable MuRF1's role in the protein synthesis pathway, but the exact role remains unknown.

It is interesting to note that, besides MuRF1, several E3 ligases have been shown to regulate protein synthesis signalling pathway. Cbl-b (Casitas B-lineage lymphoma proto-oncogene-b), another RING-type E3 ligase catalyses the ubiquitylation of IRS1 protein and promotes its degradation in glucocorticoid induced atrophy (67). Blocking the interaction between Cbl-b and the IRS1 protein using phosphopeptide DGpYMP, prevents glucocorticoid induced atrophy (68). SCF-Fbxo40 is also another E3 ligase that ubiquitylates and degrades IRS1 upon IGF-1 stimulation (69). In a previous study, SCF-Fbxo40 was found to be overexpressed in denervation-induced atrophy (70), whereas SCF-Fbxo40 knockdown in mice using siRNA (small-interfering RNA) results in thicker myotubes diameter (69). TRIM72, a RING-type E3 ligase, ubiquitylate and promotes the degradation of IRS1 in cells (71, 72), whereas TRIM72 Knockdown in mice activates Akt and promotes myogenesis (72, 73). Furthermore, TRIM32, another E3 ligase, downregulates Akt signalling by promoting plakoglobin and phosphatidylinositol 3-kinase dissociation (74).

Accumulating evidence suggests that MuRF1 also mediates varieties of other cellular functions including protein ubiquitylation (51, 64), amino acid and carbohydrate metabolism (66), fatty acid oxidation (75), mitochondrial function (76), apoptosis (77), endoplasmic reticulum (ER) stress response (78), and insulin resistance (54). These findings indicate that MuRF1 participates in a wide range of cellular processes. Undiscovered co-protein partners of MuRF1 may involve

in the regulation of SKM mass. Investigating the candid role of MuRF1 in the regulation of SKM mass is therefore essential for efficient therapeutical intervention for ameliorating skeletal muscle disorders.

### **1.7 MuRF1 auto-ubiquitylation**

The specificity of substrate ubiquitylation is solely a function of the E3 ubiquitin ligases (79). Due to the precise regulation of ubiquitylation and its ability to determine the fate and functions of substrates suggest that the E3 ligase might be regulated by other E3 ligases or by targeting themselves for ubiquitylation (Auto-ubiquitylation) (80). Auto-ubiquitylation is one of the notable features of the E3 ligases which describes the ligase's activities and functional interactions with sets of E2s (80). In addition, auto-ubiquitylation could also be a means by which E3 ligases auto-regulate their stability *in vivo* (36). MuRF1 auto-ubiquitylation in skeletal muscle has not been previously reported, but it has been reported in peripheral blood plasma as a circulating marker for cancer cachexia (81). The acquired signals were compatible with mono, multi-mono or short poly-ubiquitin chains, implying that they might not be necessarily degradation signals. More recently, overexpression of MuRF1 in mice resulted in the ubiquitylation of 16 lysine sites on MuRF1 in addition to other substrates ubiquitylated (51). However, it is yet unknown if these multiple ubiquitylation on MuRF1 were auto-ubiquitylation or/and they were ubiquitylated by other E3 ligases. The upregulation of MuRF2, MuRF3, and TRIM25 E3 ligases following the overexpression of MuRF1 makes it difficult to draw a definite conclusion. MuRF1 auto-ubiquitylation is thus largely used in *in vitro* assay to demonstrate its ligase activities and functional interactions with sets of E2s (82, 83). A previous study had demonstrated that MuRF1 auto-ubiquitylation with UBE2D1 acts as a prerequisite to specifically

accelerates the ubiquitylation of S5a but inhibits the ubiquitylation of troponin I *in vitro* (84). Taken together, MuRF1 auto-ubiquitylation could play diverse role during catabolic processes of skeletal muscle atrophy. Thus, further studies are clearly needed for clarifying the presence and role of MuRF1- ubiquitylation in skeletal muscles.

## **1.8 Significance of the thesis**

Skeletal muscle atrophy is a major clinical condition that hinders independence and quality of life. However, despite its prevalence and debilitating effects, there are no effective pharmaceutical agents/drugs against skeletal muscle atrophy. This deficit is due to our lack of understanding of its pathogenesis at the mechanistic level. While MuRF1 is a reliable marker of skeletal muscle atrophy, its precise role in the regulation of skeletal muscle mass is currently unclear. This mechanistic study will significantly improve our understanding on the molecular role of MuRF1 and its protein regulation in skeletal muscle for efficient therapeutical intervention for ameliorating skeletal muscle disorders.

## **1.9 Aim and objectives of the thesis**

The primary aim of the present thesis is to improve our understanding of MuRF1's function in the regulation of skeletal muscle mass. Thus, the specific objectives of this thesis include:

- i) To develop MuRF1 reporter and functional deficiency in skeletal muscle cell lines.
- ii) To determine the interacting partners of MuRF1 protein and their associated role in the regulation of skeletal muscle mass.
- iii) To determine the auto-ubiquitylation of MuRF1 and its stability in skeletal muscle.

Within the present thesis:

Chapter 2 describes the general methodological and analytical techniques employed in the thesis.

Chapter 3 describes the development of MuRF1 reporter and functional deficiency cell lines to examine the function of MuRF1 E3 ligase in skeletal muscle.

Chapter 4 describes the interacting partners of MuRF1 protein and how they regulate muscle mass.

Chapter 5 describes the auto-ubiquitylation of MuRF1 and its stability in skeletal muscle.

Chapter 6 discusses the discoveries from Chapters 4 and 5, as well as addressing the gaps in the body of knowledge within this field and its limitations.

---

**CHAPTER 2**  
**GENERAL METHODS**

---

## **2.1 Reagents and general methods**

### **2.1.1 Antibodies and Reagents**

The antibodies used for Western blot analysis were Anti-MuRF1 (Santa Cruz SC-398608; 1:1000), Unpublished data from our lab validated that Anti-MuRF1 from Santa Cruz was capable of detecting the predicted band of ~40 kDa (85), Anti-TRIM72 (Antibodies.com A84884; 1:8000), Anti-phospho Akt (Ser473) (Cell Signalling Technology 4060; 1:1000), Anti-phospho-Akt (T308) (Cell Signalling Technology 2965; 1:1000), Anti-phospho-P70 S6K1 (T389) (Cell Signalling Technology 9234; 1:1000), Anti-GAPDH (Cell Signalling Technology 5174; 1:1000), Anti IRS1 (Cell Signalling Technology 3407; 1:1000), Anti-GFP (Chromotek 3H9-100; 1:2000), Anti-FLAG M2 (Sigma-Aldrich F1804-200UG; 1:1000) Anti-Vinculin (Abcam ab73412; 1:1000), and puromycin (Sigma-Aldrich P8833; 1:1000) respectively. The secondary antibodies used were Anti-mouse IgG, HRP-linked Antibody (Cell Signalling Technology 7076; 1:10 000), Anti-goat IgG, HRP-linked Antibody (Cell Signalling Technology 7077; 1:10 000), Anti-rabbit IgG, HRP-linked Antibody (Cell Signalling Technology 7074; 1:10 000), and Anti-Rat IgG, HRP-linked Antibody (Cell Signalling Technology 7077; 1:5000). The cells culture reagents used were Dulbecco's Modified Eagle Medium (DMEM; Thermo Fisher Scientific, Loughborough, UK, 31966021) containing GlutaMAX, 25 mM of glucose, and 1 mM of sodium pyruvate, Hyclone fetal bovine serum (FBS, Fisher Scientific, Loughborough, UK, SV30180.03), Penicillin-Streptomycin (10 000 Units/mL- $\mu$ g/mL, Thermo Fisher Scientific, Loughborough, UK, 15140122). Horse Serum (HS) (Sigma-Aldrich, Cambridgeshire, UK, H1270), Bradford protein assay kit (ThermoFisher Scientific, Leicestershire, UK, 23209), Dexamethasone (Sigma-Aldrich D4902) was prepared in ethanol and the treatment procedures were described in the figure. Insulin solution was purchased from Sigma Aldrich (Dorset, UK,

I927), GAG/POL and VSV-G plasmids were purchased from Clontech (Saint-Germain-en-Laye, France) polybrene was purchased from Sigma Aldrich (Cambridgeshire, UK).

### **2.1.2 Mammalian cell lines and culture**

#### **2.1.3 C2C12**

C2C12 mouse skeletal muscle myoblasts were purchased from the American Type Culture Collection (ATCC, Manassas, VA, USA). The C2C12 myoblasts of passage number 3 to 8 were cultured and grown in high-glucose Dulbecco's Modified Eagle Medium (DMEM) supplemented with 10% (v/v) foetal bovine serum (GE Healthcare, Buckinghamshire, UK) and 1% (v/v) Penicillin-Streptomycin (10 000 units/mL- $\mu$ g/mL) until desired confluency in an incubator with 37°C and a 5% CO<sub>2</sub> atmosphere. At about 90% confluency, C2C12 mouse skeletal muscle myoblasts were differentiated into myotubes for at least five days using high-glucose DMEM supplemented with 2% (v/v) horse serum (HS) and 1% (v/v) penicillin-streptomycin (10 000 units/mL- $\mu$ g/mL). To maintain cells or myotubes viability, the medium was changed every two days.

#### **2.1.4 L6**

Rat skeletal muscle L6 myoblast cells of passage number 3 to 8 were obtained from the American Type Culture Collection (ATCC, Manassas, VA, USA). L6 myoblasts were cultured in high-glucose Dulbecco's Modified Eagle Medium (DMEM) supplemented with 10% (v/v) foetal bovine serum (GE Healthcare, Buckinghamshire, UK) and 1% (v/v) Penicillin-Streptomycin (10 000 units/mL- $\mu$ g/mL) until desired confluency in an incubator with 37°C and a 5% CO<sub>2</sub> atmosphere. At about 90% confluency, L6 skeletal muscle myoblasts were differentiated into

myotubes for six days using high-glucose DMEM supplemented with 2% (v/v) horse serum (HS) and 1% (v/v) penicillin-streptomycin (10 000 units/mL- $\mu$ g/mL). To maintain cells or myotubes viability, the medium was changed every two days.

### **2.1.5 HEK 293 and HEK293 FT cells**

HEK293 myoblast cells were purchased from the American Type Culture Collection (ATCC, Manassas, VA, USA). HEK293 FT myoblast was obtained from University of Dundee, UK (MRC PPU) as a gift from Professor Miratul Muqit. HEK293 or HEK293 FT myoblast cells were cultured in high-glucose Dulbecco's Modified Eagle Medium (DMEM) supplemented with 10% (v/v) foetal bovine serum (GE Healthcare, Buckinghamshire, UK) and 1% (v/v) Penicillin-Streptomycin (10 000 units/mL- $\mu$ g/mL) until desired confluency in an incubator with 37°C and a 5% CO<sub>2</sub> atmosphere. To maintain cells viability, the medium was changed every two days.

## **2.2 Transfection of mammalian cell lines**

Transient transfections were performed using Polyethylenimine (PEI) transfection reagent. Specifically, maintained culture cells or myotubes were transfected with the required plasmid DNA in a 1:2.5 ratio ( $\mu$ l/ $\mu$ g) of PEI to the plasmid. In brief, PEI and plasmid DNA were firstly mixed individually, in a separate eppendorf tubes containing 500  $\mu$ l DMEM devoid of serum for 5 min at room temperature. After 5 min incubation, the PEI/DNA mixture was combined into one and was further incubated for 20 min before added dropwise onto the cells or myotubes. After overnight incubation, fresh media was replaced to wash out PEI remnant after transfection. At 48 h post transfection, cells were lysed and harvested for analysis.

### **2.3 Cell lysis**

At the end of the experiments, Cells prewashed with ice-cold Dulbecco's phosphate buffered saline (DPBS, ThermoFisher Scientific, Leicestershire, UK), were lysed and collected in cold sucrose lysis buffer containing 250 mM of sucrose, 10 mM of sodium  $\beta$ -glycerolphosphate, 50 mM of Tris-base (pH 7.5), 5 mM of sodium pyrophosphate, 50 mM of sodium fluoride, 1 mM of EDTA, 1 mM of benzamidine, 1 mM of EGTA, 1 mM of sodium orthovanodate, 1% of Triton X-100, 1 x complete Mini EDTA-free protease inhibitor cocktail, and 100 mM of 2-chloroacetamide for a 2 cm and 10 cm dish, respectively. Lysates were pelleted for 15 minutes in 4°C at 13,000 rpm and the supernatant was collected and stored at -80°C for analysis.

### **2.4 Protein Measurement**

Protein measurement was quantified using the Bradford protein assay (ThermoFisher Scientific, Leicestershire, UK). Firstly, 10  $\mu$ L of lysates (samples) were diluted in 90  $\mu$ L of ddH<sub>2</sub>O. In a 96-well microplate containing 300  $\mu$ L Bradford protein reagent, diluted samples were loaded in duplicate. After a brief incubation period, the absorbance at 595 nm was measured using a FluoStar Omega microplate reader (BMG Labtech, Aylesbury, UK). The results were analysed using MARS software. Protein in each sample was quantified from a standard curve using BSA standards ranging from 125 to 1000  $\mu$ g/ml (Thermo Fisher Scientific, Leicestershire, UK, 23209). As a control, 10  $\mu$ l of dH<sub>2</sub>O was used as a blank.

## **2.5 GFP pulldown**

20 µl of GFP-trap agarose or IgG bead slurry pre-washed with an ice-cold phosphate buffered saline (PBS) was then washed twice with ice-cold sucrose lysis buffer before incubated with 2 mg lysates overnight on a rotating wheel at 4 °C. Beads were then pelleted by centrifugation at 3500 rpm for 1 min at 4°C. After washing three times with sucrose lysis buffer, the co-immunoprecipitated proteins were eluted with 2x NuPAGE LDS sample buffer. Samples were left overnight in 1.5% of 2-mercaptoethanol to denature at room temperature before analysis.

## **2.6 Immunoprecipitation**

20 µl of protein A sepharose bead slurry prewashed with ice-cold PBS (phosphate buffered saline) was washed twice in 750 µl ice-cold sucrose lysis buffer. Protein lysates of 1.0 mg and 2 µg specific coupled antibodies was mixed with the pre-washed beads on a rotational wheel overnight at 4°C. Beads were then pelleted for 1 min in 4°C at 3500 rpm and the flow through was retained. The immunoprecipitates were extensively (three times) washed with ice-cold lysis buffer containing 150 mM NaCl to exclude non-specific bound proteins. The beads was resuspended in 400 µl ice-cold sucrose lysis buffer per IP and transferred to a spin column. The immunoprecipitated proteins were eluted with 1x NuPAGE LDS sample buffer. Samples were left to denature overnight at room temperature in 1.5% of 2-mercaptoethanol.

## **2.7 TUBE-ubiquitin pulldown**

Escherichia coli BL21 cells were used to express and purify the His-halo-ubiquitin UBA domain tetramer (UBA<sup>UBQLN1</sup>) as previously described (86). In 750 µl of binding buffer, 1 mg of the HALOUBA<sup>UBQLN1</sup> TUBE protein was incubated for 2 hours at 4°C with 200 µl of HaloLink resin that had been pre-washed with cold PBS (phosphate buffered saline). 1 mg of protein from cell lysates was incubated to the conjugated UBA<sup>UBQLN1</sup> TUBE protein and HaloLink resin overnight on a rotational wheel at 4°C. Following 3 washes in sucrose lysis buffer, the captured ubiquitin and poly-ubiquitin chains were eluted in 1x LDS sample buffer (NuPAGE, Invitrogen, NP0008). Samples were left overnight in 1.5% of 2-mercaptoethanol to denature at room temperature before analysis.

## **2.8 Preparation of Samples**

Protein lysates were prepared using 1x LDS sample buffer (NuPAGE, Invitrogen, NP0008). Samples were left overnight in 1.5% of 2-mercaptoethanol to denature at room temperature before analysis.

## **2.9 Immunoblotting (Western blotting)**

### **2.9.1 Gel electrophoresis**

Aliquots from the prepared samples were loaded and run on 10% Bis/Tris gels (ThermoFisher Scientific, Leicestershire, UK) in 1x MOPS buffer (ThermoFisher Scientific, Leicestershire, UK) for approximately 75 minutes at 140 V.

### **2.9.2 Transfer and blocking**

Proteins from the gel were transferred to 0.2  $\mu$ M PVDF (polyvinylidene fluoride) membranes (Millipore, Hertfordshire, UK) in 1x transfer buffer containing; 20 mM Tris base, 150 mM glycine, and 20% methanol for 1 h at 100 V and 4°C condition. The membranes were blocked for 1 hour in 5% (w/v) dried skimmed milk diluted with Tris-buffered saline Tween 20 (TBS-T): 137 mM of sodium chloride, 20 mM of Tris-base 7.5 pH and 0.1% of Tween-20.

### **2.9.3 Primary antibody**

To wash off the residual milk solution, membranes were washed three times for 10 minutes each in TBS-T prior to incubation in primary antibodies prepared in 3% of BSA diluted with TBST. Membranes were incubated in primary antibody on a rocker at 4°C overnight.

### **2.9.4 Secondary antibody**

Membranes were washed three times for 10 minutes each in TBST before incubating in horse radish peroxidase conjugated secondary antibodies for 1 h at room temperature.

### **2.9.5 Antibody detection and Imaging**

After membranes were washed three times for 10 minutes each in TBST, antibody binding detection was performed using enhanced chemiluminescence (ECL) horseradish peroxidase substrate detection kit (Millipore, Hertfordshire, UK). G: BOX Chemi-XR5 (Syngene, Cambridgeshire, UK) was used to acquire images.

## **2.10 Data Analysis**

ImageJ/Fiji (National Institutes of Health, USA) was used for protein band quantification. The proteins of interest were normalised in relation to the experimental controls.

## **2.11 Protein synthesis (SUnSET)**

Protein synthesis was assessed using the surface sensing of translation (SUnSET) technique, as previously described (87), except that puromycin was incorporated for 24 h. Briefly, fully formed myotubes were pre-treated with 1  $\mu$ M of puromycin (P8833, Sigma-Aldrich) simultaneously with the indicated treatments for 24 h in a serum free media. Subsequently, protein synthesis was stimulated by 100 nM of insulin for 30 minutes in a serum-free media prior to cell lysis. The incorporation of puromycin-labeled peptides was determined by immunoblotting with anti-puromycin antibody.

## **2.12 Glucose uptake measurements**

Glucose uptake was measured using the glucose uptake 'Promega Glo™ assay kit'. Briefly, 20,000 cells were seeded into each well of a 96-well plate. At confluent, differentiation was initiated by adding 100 $\mu$ l DMEM + 2% horse serum. One day before the assay, Myotubes were incubated in 100  $\mu$ l serum free DMEM overnight. On the day of the assay, wells were washed once with 100 $\mu$ l PBS and myotubes were incubated with or without 1 $\mu$ M insulin for 1 hour at 37°C in 5% CO<sub>2</sub>. After 1 hour incubation, myotubes were washed once with 100 $\mu$ l PBS. Next, 50 $\mu$ l 1mM 2DG was added to each well (including myotubes free wells as blank control) for 30 min at 25°C. 25 $\mu$ l Stop Buffer was added with a brief shaken to lyse cells at 25°C. Next, samples were transferred to 384 well plates at 15 $\mu$ l/well. 5 $\mu$ l Neutralization Buffer was then added to

each well with brief shake. Finally, 20µl 2DG Detection Reagent was added to all wells with brief shake and then dark-adapted for one hour at 25°C. Retained luminescence was then measured using a FLUOstar Omega microplate reader. Control wells (2DG: without myotubes), provided the assay background and were subtracted from all conditions.

### **2.13 Statistical analysis**

GraphPad Prism Software version 9 (San Diego, California, USA) was used to run all the statistical analysis. One way ANOVA (analysis of variance) was applied to analyse multiple means. For the MuRF1 KO and MuRF1 restoration experiments, the differentiation time course experiment, the dexamethasone dose response experiments, and the TRIM72 restoration experiment, one way ANOVA (analysis of variance) was applied before Dunnett's multiple comparisons post-hoc test analysis. For the experiment on the role of MuRF1 on IRS1/Akt signalling, insulin-induced protein synthesis, and insulin-induced glucose uptake, a two way ANOVA was performed before Tukey's multiple comparisons post-hoc test analysis. All presented data are mean  $\pm$  SD. (\*) Statistical analyses were considered significant at  $P < 0.05$ .

---

**CHAPTER 3**

**TOOLS DEVELOPMENT TO STUDY**

**MuRF1 PROTEIN AND ITS ROLE IN**

**SKELETAL MUSCLE**

---

### **3.1 Generation of L6 cell lines that stably expressed GFP-MuRF1 or GFP using a retrovirus.**

#### **3.1.1 Background**

Studies that describe changes in the mRNA and protein expression of MuRF1 have shown that this gene regulates skeletal muscle mass and function in both healthy and diseased conditions (35, 51, 52). More mechanistic studies via yeast-2-hybrid (Y2H) screens, have also revealed proteins that interact with MuRF1, some of which have been identified as MuRF1 substrates (35); however, the nature of targeted analysis of Y2H (88) limits the identification of interacting proteins with MuRF1. In contrast, affinity purification mass spectrometry-based method offers high sensitivity and increased coverage of protein-protein interaction network in an unbiased manner (89). Thereafter, our aim was to use a retrovirus encoding human MuRF1 protein fused with a GFP tag at the N-terminus to generate GFP tag MuRF1 L6 skeletal muscle cell lines. L6 cells were also infected with a retrovirus encoding a GFP as a control (GFP-empty).

#### **3.1.2 Method**

#### **3.1.3 DNA construct**

A retrovirus encoding human MuRF1 protein fused with a GFP tag at the N-terminus was used to infect L6 muscle cells. L6 cells were also infected with a retrovirus encoding a GFP as a control (GFP-empty).

### **3.1.4 Transfection and retroviral generation**

HEK293-FT cells were transiently co-transfected with 3.8 µg GAG/POL (retroviral packaging vector) and 2.2 µg VSV-G (retroviral envelope vector) and either with 6 µg of each pBABED.puro GFP and pBABED.puro<sup>GFP/GFP</sup> MuRF1 vectors, to generate GFP and GFP-MuRF1 retroviruses using polyethylenimine (PEI) transfection reagent. Following 48 hours of incubation, the pelleted retroviral media supernatant was collected via a 0.45 µM sterile syringe filter into sterile eppendorf tubes and was stored in -80°C freezer before analysis.

### **3.1.5 GFP- and GFP-MuRF1 retroviral transduction and selection in L6**

5 mL from the collected GFP and GFP-MuRF1 retroviral media containing 10 µg/mL polybrene was used to transduce (infect) L6 rat skeletal muscle cell for 48 h. After 48 h transduction, the transduced L6 rat skeletal muscle cell was selected using 2 µg/mL puromycin. The resistant clones were further culture until desire confluency before sorting.

### **3.1.6 L6-GFP- and L6-GFP-MuRF1 cell lines sorting**

The infected clones were subsequently sorted and collected into 5 ml FACS tubes using the ARIA fusion sorter (BD Biosciences, Berkshire, UK). This was carried out by a specialist at the University of Birmingham's flow cytometry center (Institute of Biomedical Research). The sorted L6 cells that stably express relative GFP signals for both GFP and GFP-MuRF1 were re-cultured for further expansion and cryopreserved after being validated by western blotting.

### 3.1.7 Preparation of western samples

Protein lysates from GFP pulldown samples were prepared using 1x LDS sample buffer (NuPAGE, Thermo Fisher Scientific, NP0008). Samples were left overnight in 1.5% of 2-mercaptoethanol at room temperature to denature before western blotting analysis.

### 3.1.8 Validation by Immunoblotting (western blotting)

Detail western blotting descriptions are presented in section 2.9 of Chapter 2.

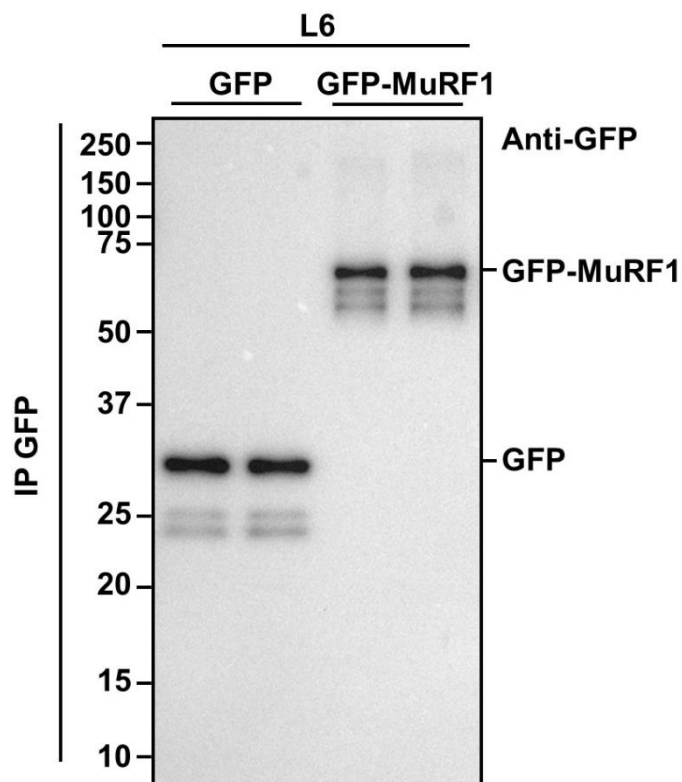


**Figure 3. 1 Validation of L6 cell lines stably expressing GFP and GFP-MuRF1.**

After L6 cells were infected and selected, sorted L6 myoblast cell stably expressing GFP and GFP-MuRF1 were differentiated and subjected to GFP pulldown before immunoblotting with GFP antibody.

## **3.2 GFP-MuRF1 knockin generation in C2C12 using CRISPR/Cas9**

### **3.2.1 Background**

The sole aim of the present thesis was to dissect the functional role of MuRF1 protein and of its expression in skeletal muscle. However, early research on MuRF1 protein expression in biological samples was scant due to the lack of MuRF1-specific antibodies (59, 60, 90). Additionally, one method to mimic the expression of endogenous proteins is to use CRISPR/Cas9 to insert a reporter into an endogenous gene within cells. This method has been successfully used for gene editing in several labs (91). The merit of this editing tool is that it is quick, efficient, highly specific, and easy to use for cellular genomic engineering. The fundamental principle of this gene editing tool is that each of the crRNA (CRISPR RNA) comprises of 20-nucleotide guide sequence that uses Watson-Crick base pairing to direct Cas9 (CRISPR associated protein 9) to the target 20-nucleotide DNA (91). Thereafter, our aim was to use CRISPR/Cas9 to generate GFP tag MuRF1 knockin skeletal muscle cell lines.

### **3.2.2 Method**

#### **3.2.3 DNA construct**

The sense and antisense sgRNA constructs for A (tCTGATTCCTGATGGAAACGCTA, GCTGATCTGCCCCATCTGCCTtG); sense and antisense sgRNA constructs for B (tCTGGAGAAGCAGCTGATCTGCC, tGAGATGTTTACCAAGCCTGTcG), which target the N-terminal GFP knock-in to the MuRF1 locus, and the Nter GFP donor (pMK-RQ vector, DU60520) were generated via the CRISPR vector designing tool (<http://tools.genome-engineering.org>). The generated oligonucleotides identified were annealed to their respective

complements with the cloning tag 'a,' 'g' as was shown in the following: Nter KI as A (TAGCGTTTCCATCAGGAATCAGa, CaAGGCAGATGGGGCAGATCAGC) and Nter KI as B (GGCAGATCAGCTGCTTCTCCAAGa, CgACAGGCTTGGTAAACATCTCa) to generate dsDNA inserts with compatible over-hangs to BbsI-restriction site of pBabeD-puro and pX335-Cas9-D10A vectors (92). The antisense sgRNA was cloned onto pX335-spCas9-D10A (Addgene, 42335) and the sense sgRNA cloned onto the pBabeD-puro (puromycin selectable plasmid P U6).

#### **3.2.4 Transfection and selection of GFP-MuRF1 knock-in positive C2C12 myoblasts**

C2C12 myoblasts cells of 60-70% confluency were co-transfected with 1 µg CRISPR plasmids and 3 µg of the fluorescent GFP tag donor plasmid using polyethylenimine (PEI) transfection reagent. After 48 h co-transfection, the transfected C2C12 mouse skeletal muscle cell was selected using 2 µg/mL puromycin. The resistant clones were further culture until desire confluency before sorting.

#### **3.2.5 Cell sorting**

The selected pools of clones were subsequently single-cell sorted and collected into 96 well plates using the ARIA fusion sorter (BD Biosciences, Berkshire, UK). This was carried out by a specialist at the University of Birmingham's flow cytometry center (Institute of Biomedical Research). The sorted clonal C2C12 cells were cultured and maintain over a week for recovery. The C2C12 myoblast cells expressing GFP-MuRF1 knock-in were re-cultured for further expansion and cryopreserved after being validated by western blotting.

### **3.2.6 Sample preparation**

Colonies from 24 well plates were lysed and prepared using 1x urea laemli buffer (6M Urea, 8% SDS, 40% glycerol, 0.005% Bromophenol Blue, 0.2M Tris-HCl pH 6.8, 5% B-ME, and H<sub>2</sub>O). Samples were then sonicated and left overnight at room temperature to denature before western blotting analysis.

### **3.2.7 Validation by Immunoblotting (Western blotting)**

Detail western blotting descriptions are presented in section 2.9 of Chapter 2

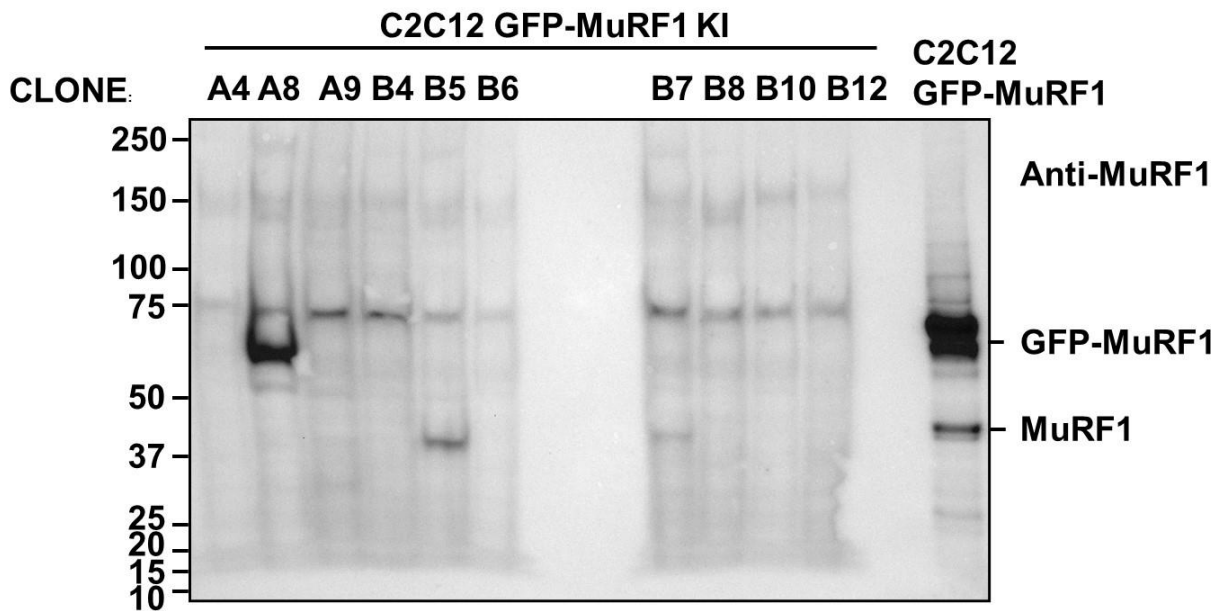
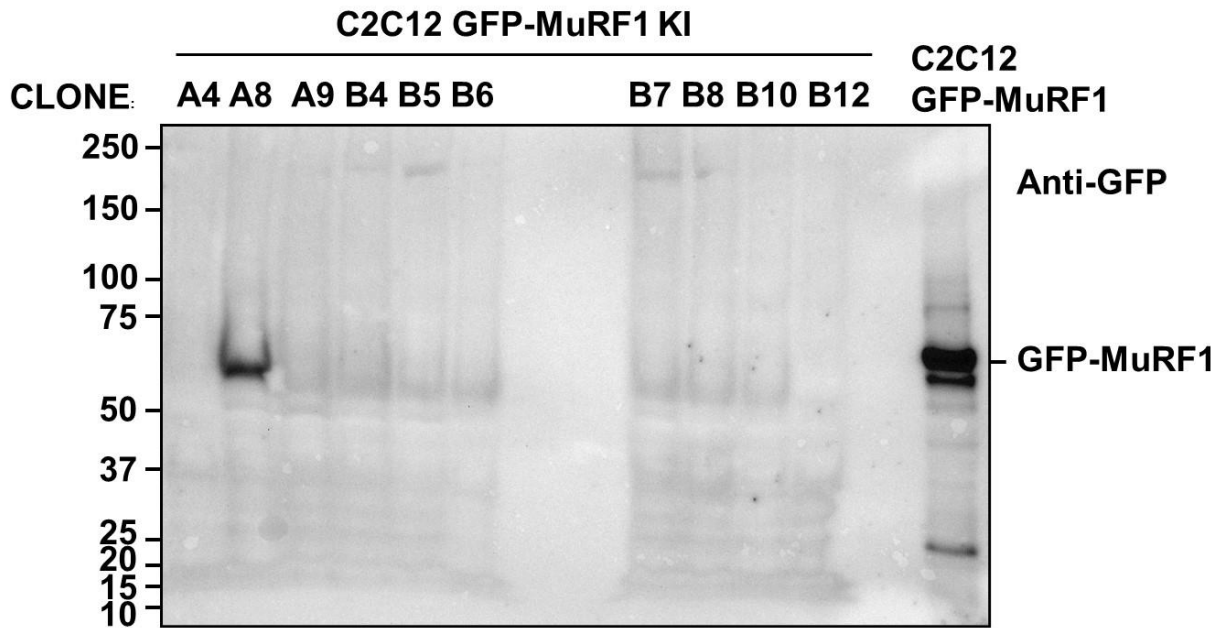


**Figure 3.2 Validation of Crispr/Cas9 generated GFP-MuRF1 knock-in C2C12 cell lines.**

CRISPR/Cas9-generated GFP-MuRF1 knock-in clones and C2C12 cells over-expressing GFP-MuRF1 (as a control) were lysed before immunoblotting with GFP (A) and MuRF1 (B) antibody, respectively.

### **3.3 MuRF1 knockout C2C12 cells generation using CRISPR/Cas9**

#### **3.3.1 Background**

Targeted gene deletion in cells is a common strategy used in physiological research to identify the function of a gene (93, 94). After validating the association between MuRF1 and TRIM72 proteins, we sought to determine whether TRIM72 served as a MuRF1 interaction partner or as a MuRF1 protein substrate using MuRF1-deficient (KO) skeletal muscle cell lines. Thereafter, our aim was to use CRISPR/Cas9 to generate MuRF1 KO C2C12 skeletal muscle cell lines.

#### **3.3.2 Method**

#### **3.3.3 DNA construct**

The sense and antisense sgRNA constructs for A (tCTGATTCCTGATGGAAACGCTA, GCTGATCTGCCCCATCTGCCTtG); sense and antisense sgRNA constructs for B (tCTGGAGAAGCAGCTGATCTGCC, tGAGATGTTTACCAAGCCTGTcG), which target the N-terminal GFP knock-in to the MuRF1 locus, and the Nter GFP donor (pMK-RQ vector, DU60520) were generated via the CRISPR vector designing tool (<http://tools.genome-engineering.org>). The generated oligonucleotides identified were annealed to their respective complements with the cloning tag 'a,' 'g' as was shown in the following: Nter KI as A (TAGCGTTTCCATCAGGAATCAGa, CaAGGCAGATGGGGCAGATCAGC) and Nter KI as B (GGCAGATCAGCTGCTTCTCCAAGa, CgACAGGCTTGGTAAACATCTCa) to generate dsDNA inserts with compatible over-hangs to BbsI-restriction site of pBabeD-puro and pX335-Cas9-D10A vectors (92). The antisense sgRNA was cloned onto pX335-spCas9-D10A (Addgene, 42335) and the sense sgRNA cloned onto the pBabeD-puro (puromycin selectable plasmid P U6).

### **3.3.4 Transfection and selection of MuRF1 knockout positive C2C12 myoblasts**

C2C12 myoblasts cells of 60-70% confluency were co-transfected with 1 µg CRISPR plasmids and 3 µg of the fluorescent GFP tag donor plasmid using polyethylenimine (PEI) transfection reagent. After 48 h co-transfection, the transfected C2C12 mouse skeletal muscle cell was selected using 2 µg/mL puromycin. The resistant clones were further culture until desire confluency before sorting.

### **3.3.5 Cell sorting**

The selected pools of clones were subsequently single-cell sorted and collected into 96 well plates using the ARIA fusion sorter (BD Biosciences, Berkshire, UK). This was carried out by a specialist at the University of Birmingham's flow cytometry center (Institute of Biomedical Research). The sorted clonal C2C12 cells were cultured and maintain over a week for recovery. The C2C12 myoblast cells expressing GFP-MuRF1 knock-in were re-cultured for further expansion and cryopreserved after being validated by western blotting.

### **3.3.6 Sample preparation**

Protein lysates from samples were prepared using 1x LDS sample buffer (NuPAGE, Invitrogen, NP0008). Samples were left overnight in 1.5% of 2-mercaptoethanol at room temperature to denature before western blotting analysis.

### **3.3.7 Validation by immunoblotting (Western blotting)**

Detail western blotting descriptions are presented in section 2.9 of Chapter 2

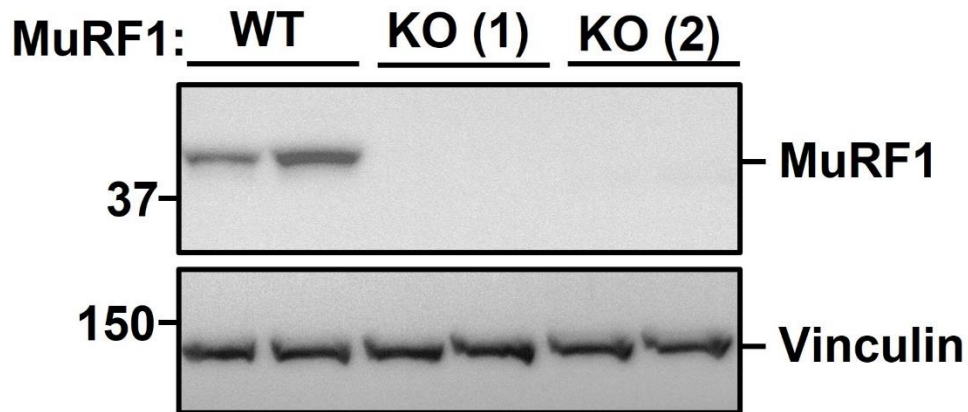


**Figure 3.3 Validation of Crispr/Cas9-generated MuRF1 KO C2C12 cell lines.**

CRISPR/Cas9-generated GFP-MuRF1 knockout clones and C2C12 wild type (WT) cell (as a control) were lysed before immunoblotting with Anti-MuRF1 and Anti-Vinculin (as a loading control), respectively.

### **3.4 Generation of GFP-MuRF1 with Ring domain mutation at C23A in C2C12 cells using retrovirus**

#### **3.4.1 Background**

Although MuRF1 is essential in the catabolic processes occurring during skeletal muscle atrophy (51), it is unknown how MuRF1 activity is deregulated in skeletal muscle. MuRF1 auto-ubiquitylation has been demonstrated in *vitro* (82, 83) and in peripheral blood cells (81). But, to date, no studies have described MuRF1 auto-ubiquitylation in striated muscles. The inadequate, appropriate, and applicable tools for measuring substrate target ubiquitylation (95) limit the study of MuRF1 protein auto-ubiquitylation in skeletal muscle. Modification of the E3 ligase ring domain is a common strategy used in physiological research to identify E3 ligase activities (51). Thus, techniques developed to evaluate the regulation of MuRF1 protein expression and its ligase activities will be useful in the understanding of MuRF1 deregulation in skeletal muscle. On this basis, our aim was to generate a C2C12 skeletal muscle cell lines stably expressing GFP-MuRF1 with a ring domain point mutation at C23A using retroviral system.

#### **3.4.2 DNA construct**

A retrovirus encoding human MuRF1 protein fused with a GFP tag at the N-terminus with a ring domain mutant was used to infect C2C12 skeletal muscle cells.

#### **3.4.3 Transfection and retroviral harvesting**

HEK293-FT cells were transiently co-transfected with 3.8 µg GAG/POL (retroviral packaging vector) and 2.2 µg VSV-G (retroviral envelope vector) and either with 6 µg of pBABED.puro<sup>GFP/GFP</sup> MuRF1 vector with ring domain point mutation at C23A, to generate GFP/GFPMuRF1

retroviruses with ring domain point mutation at C23A using polyethylenimine (PEI) transfection reagent. Following 48 hours of incubation, the pelleted retroviral media supernatant was collected via a 0.45  $\mu$ M sterile syringe filter into sterile eppendorf tubes and was stored in -80°C freezer before analysis.

#### **3.4.4 <sup>GFP/GFP</sup>MuRF1 (C23A) retroviral transduction and selection in C2C12**

5 mL from the collected <sup>GFP/GFP</sup>MuRF1 (C23A).Puro retroviral media containing 10  $\mu$ g/mL polybrene was used to transduce C2C12 mouse skeletal muscle cell for 48 h. After 48 h transduction, the transduced C2C12 mouse skeletal muscle cell was selected using 2  $\mu$ g/mL puromycin. The resistant clones were cultured for further expansion and cryopreserved after being validated by western blotting.

#### **3.4.5 Preparation of western samples**

Protein lysates from GFP pulldown samples were prepared using 1x LDS sample buffer (NuPAGE, Thermo Fisher Scientific, NP0008). Samples were left overnight in 1.5% of 2-mercaptoethanol at room temperature to denature before western blotting analysis.

#### **3.4.6 Validation by Immunoblotting (western blotting)**

Detail western blotting descriptions are presented in section 2.9 of Chapter 2

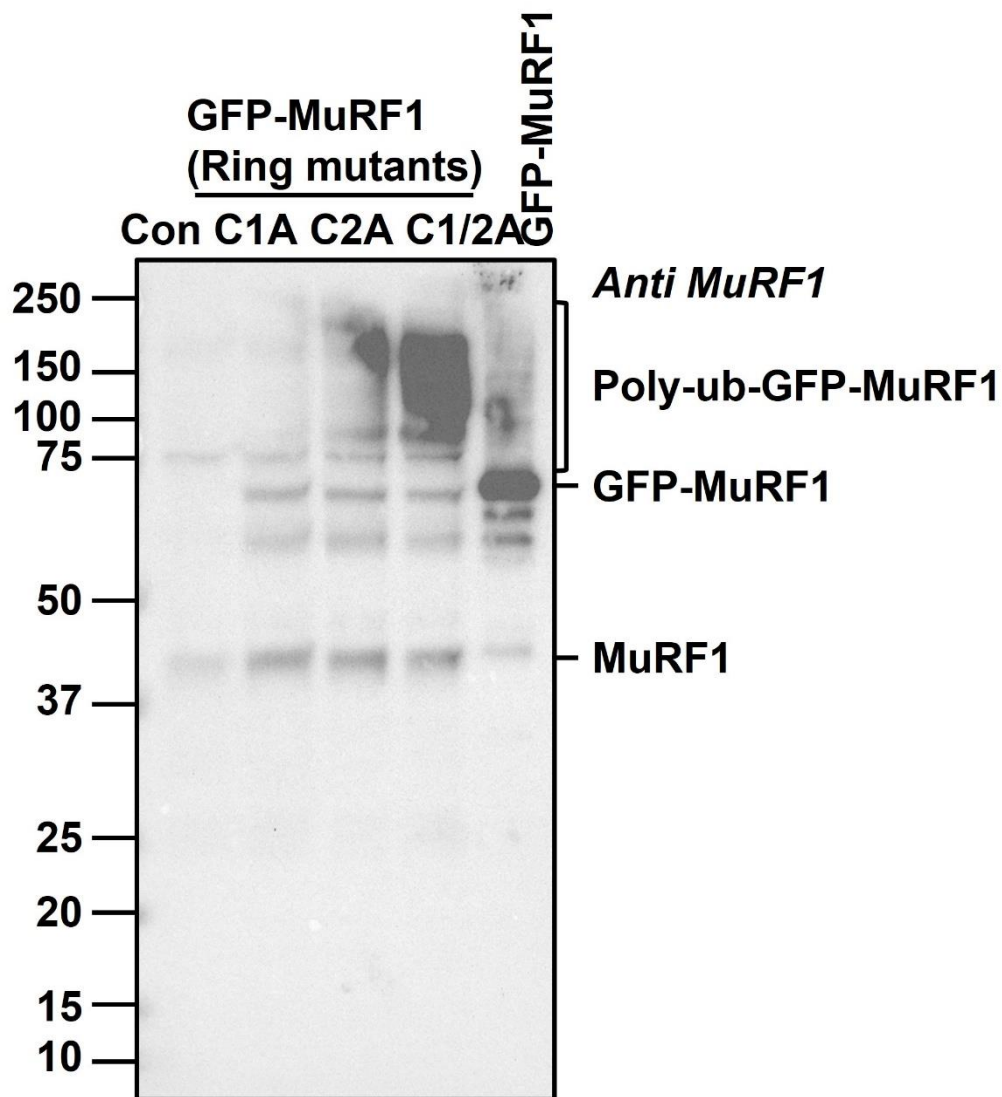


**Figure 3.4 Generation of RING MUTANT GFP-MuRF1 C2C12 cell lines using retroviral system.** After transduction and selection of C2C12 cells, lysates of generated clones for potential RING Mutant GFP-MuRF1 C2C12, C2C12 WT (Con), and C2C12 cells over-expressing GFP-MuRF1 (as a control) were subjected to immunoblot analysis and probed with MuRF1 antibody. N.B C1A=C23A, C2A=C26A, C1/2=C23A/C26A cysteine residues respectively. Due to the efficiency of the mutation, C23A mutant clone was used for the subsequent experiment.

---

## **CHAPTER 4**

# **MURF1 IMPAIRS IRS1/Akt SIGNALLING AND ITS RESPONSE BY REGULATING TRIM72 IN SKELETAL MUSCLE.**

---

#### 4.1 Abstract

Muscle-specific RING-finger protein 1 (MuRF1, *TRIM63*) is a key participant in the catabolic process of skeletal muscle atrophy. Despite the identification of numerous putative interacting partners, the molecular mechanism by which increasing MuRF1 expression causes skeletal muscle atrophy remains unclear. To gain mechanistic insight into the function of MuRF1, we applied quantitative affinity purification mass spectrometry (APMS) to further identify MuRF1's interacting partners in skeletal muscle. While confirming other previously identified MuRF1 interactors such as MuRF2, MuRF3, and Mylpf: myosin regulatory light chain 2, APMS led to the identification of another tripartite motif-containing protein 72 (*TRIM72*) as a novel MuRF1 interacting partner in skeletal muscle. Subsequent analysis using MuRF1 knockout and rescue experiments showed that *TRIM72* protein abundance is positively correlated with MuRF1 protein expression. *TRIM72* protein abundance was increased by dexamethasone treatment in C2C12 myotubes, alongside MuRF1 protein expression. Dexamethasone treatment decreases IRS1/Akt signalling, protein synthesis, and glucose uptake in wild type myotubes but not in MuRF1 KO myotubes. Further analysis showed that overexpression of *TRIM72* impairs IRS1/Akt signalling in MuRF1 KO myotubes. These findings provide the first evidence that MuRF1 overexpression can lead to skeletal muscle insulin resistance in addition to decreased protein synthesis by interacting with and stabilising the *TRIM72* protein.

## 4.2 Introduction

MuRF1 is an indispensable constituent of the UPS that regulates skeletal muscle mass (35), yet the mechanistic function of MuRF1 is not well understood. MuRF1 gene is overexpressed in numerous conditions of skeletal muscle atrophy, and MuRF1 knockout mice spare skeletal muscle mass from denervation- and dexamethasone induced atrophy (38, 51, 52, 64, 96). MuRF1 was reported to target myofibrillar proteins for ubiquitylation and subsequent degradation via the UPS (61, 62) to promote skeletal muscle atrophy. In addition, MuRF1 appears to target muscle creatine kinase for proteasome-dependent degradation to regulate the metabolism of skeletal muscle energy in mice (66, 97). Some previous studies report that MuRF1 translocates to the sarcomere for interaction with titin and promotes sarcomeric M-line stabilisation (98, 99). Furthermore, examination of protein synthesis rate in MuRF1 knockout mice following dexamethasone treatment revealed higher protein synthesis rate (64) when compared with wild type dexamethasone treated mice (65). These findings suggest a probable role of MuRF1 in the protein synthesis pathway, but the exact role remains unknown.

The numerous reported MuRF1 activities suggest that MuRF1 requires interacting partners to exhibit distinct cellular functions. Therefore, undiscovered co-protein partners of MuRF1 may play a key role in the regulation of skeletal muscle mass. To date, most protein interactors linked to MuRF1 have been identified through the yeast-2-hybrid (Y2H) screens using a tagged MuRF1 protein as bait (66, 97, 99, 100). However, the nature of targeted analysis of Y2H (88) limits the identification of interacting proteins with MuRF1. In contrast, affinity purification mass spectrometry provides high sensitivity and increased coverage of protein-protein interaction network (non-binary) in an unbiased manner (89).

In this present study, we used affinity purification mass spectrometry following the generation of skeletal muscle cell line that stably express GFP-MuRF1 to discover novel interacting partners of MuRF1. While confirming other previously identified MuRF1 interactors such as MuRF2, MuRF3, and Mylpf: myosin regulatory light chain 2, this led to the identification of another tripartite motif-containing protein 72 (TRIM72) as a novel MuRF1 interacting partner in skeletal muscle. TRIM72 is also a key player in the event of skeletal muscle atrophy (101). TRIM72 is persistently overexpressed in mouse models of cancer-induced cachexia, dexamethasone induced muscle atrophy, and hind limb unloading (101). TRIM72 gene deletion partially prevented skeletal muscle atrophy in these afore mentioned mouse models (101). However, how the interaction between MuRF1 and TRIM72 ligases collectively evokes augmented levels of protein expression and atrophy remains unexplored. We discovered that MuRF1 is required for TRIM72 expression in skeletal muscle. Dexamethasone treatment increased the abundance of TRIM72 protein in C2C12 myotubes, as did the expression of MuRF1 protein. Dexamethasone treatment reduces IRS1/Akt signalling, protein synthesis, and glucose uptake in wild type myotubes but not in MuRF1 KO myotubes. Subsequent investigation revealed that overexpression of TRIM72 inhibits IRS1/Akt signalling in MuRF1 KO myotubes. These findings provide the first evidence that MuRF1 interacts with and stabilises the TRIM72 protein, causing skeletal muscle insulin resistance as well as reduced protein synthesis.

### **4.3 Materials and Methodologies**

#### **4.3.1 Antibodies and Reagents**

The following antibodies were applied for western blot analysis: Anti-MuRF1 (Santa Cruz SC-398608; 1:1000), Anti-TRIM72 (Antibodies.com A84884; 1:8000), Anti-phospho Akt (Ser473) (Cell Signalling Technology 4060; 1:1000), Anti-phospho-Akt (T308) (Cell Signalling Technology 2965; 1:1000), Anti-phospho-P70 S6K1 (T389) (Cell Signalling Technology 9234; 1:1000), Anti-GAPDH (Cell Signalling Technology 5174; 1:1000), Anti IRS1 (Cell Signalling Technology 3407; 1:1000), Anti-GFP (Chromotek 3H9-100; 1:2000), Anti-FLAG M2 (Sigma-Aldrich F1804; 1:1000), Anti-Vinculin (Abcam ab73412; 1:1000), and Anti-puromycin (Sigma-Aldrich P8833; 1:1000). Anti-Myosin (fast) (Sigma M4276; 1:1000), Anti-PAX7 antibody (ThermoFisher; PA1-117, 1:1000), and Anti-Myosin (Slow) (Sigma M8421; 1:1000). The following secondary HRP-linked antibodies were applied: Anti-goat (Cell Signalling Technology 7077; 1:10 000), Anti-mouse (Cell Signalling Technology 7076; 1:10 000), Anti-rabbit (Cell Signalling Technology 7074; 1:10 000), and Anti-rat (Cell Signalling Technology 7077; 1:5000) Antibodies. The reagents for cell culture that were used includes: High glucose GlutaMAX Dulbecco's Modified Eagle Medium with 1 mM of sodium pyruvate (Thermo Fisher Scientific, Loughborough, UK, 31966021); Cytiva Hyclone Foetal bovine serum (Fisher Scientific, South America, 10309133); Penicillin-Streptomycin (10 000 Units/mL-ug/mL); Horse serum (Sigma-Aldrich, Cambridgeshire, UK, H1270); DPBS (Sigma, 14190); polybrene infection reagent (Merck life scientific UK, TR-1003); and 0.05% Phenol red Trypsin-EDTA (Fisher Scientific, 25300062); Polyethylenimine (PEI) solution (Sigma, 408727); GAG/POL and VSV-G plasmids purchased from Clontech (Saint-Germain-en-Laye, France). Chemicals/compounds such as

Dexamethasone (Sigma-Aldrich D4902) and Insulin solution (Sigma Aldrich Dorset, UK, I927) were used.

#### **4.3.2 Cell lines and Culture**

C2C12 mouse skeletal muscle myoblasts were purchased from the American Type Culture Collection (ATCC, Manassas, VA, USA). GFP-MuRF1 knocked-in (KI) and MuRF1 knockout (KO) C2C12 cell lines were developed using CRISPR/Cas9 system as was described previously (102). Briefly, C2C12 myoblasts cells of 60-70% confluency were co-transfected with 1 µg CRISPR plasmids and 3 µg of the fluorescent GFP tag donor plasmid using polyethylenimine (PEI) transfection reagent. After 48 h co-transfection, the transfected C2C12 mouse skeletal muscle cell was selected using 2 µg/mL puromycin. The selected pool of clones were subsequently single-cell sorted and collected into 96 well plate using the ARIA fusion sorter (BD Biosciences, Berkshire, UK). This was carried out by a specialist at the University of Birmingham's flow cytometry center (Institute of Biomedical Research). Positive clones for GFP-MuRF1 KI- and MuRF1 KO C2C12 were validated by immunoblotting. L6 stably expressing GFP-MuRF1 and GFP empty were generated using a retroviral system. Briefly, L6 skeletal muscle cells was infected with a GFP-MuRF1 and GFP (control) retroviral media containing 10 µg/mL polybrene for 48 h respectively. After 48 h infection, the infected L6 rat skeletal muscle cell was selected using 2 µg/mL puromycin. The infected resistant clones were subsequently sorted and collected into 5 ml FACS tubes using the ARIA fusion sorter (BD Biosciences, Berkshire, UK). This was carried out by a specialist at the University of Birmingham's flow cytometry center (Institute of Biomedical Research). The sorted L6 skeletal muscle cells that stably express relative GFP signals for both GFP-MuRF1 and GFP were re-

cultured for further expansion and cryopreserved after being validated by western blotting. All myoblasts cells were cultured and grown in high-glucose Dulbecco's Modified Eagle Medium (DMEM) supplemented with 10% (v/v) foetal bovine serum and 1% (v/v) Penicillin-Streptomycin (10 000 units/mL- $\mu$ g/mL). At about 90% confluency, skeletal muscle myoblasts were differentiated into myotubes for at least five days using high-glucose DMEM supplemented with 2% (v/v) horse serum (HS) and 1% (v/v) penicillin-streptomycin (10 000 units/mL- $\mu$ g/mL). To maintain cells or myotubes viability, the medium was changed every two days until cells were fully differentiated. Description of drug treatment on myotubes were discussed in the respectively figure legends.

#### **4.3.3 Transient transfection of mammalian cell lines**

Transient transfections were performed using Polyethylenimine (PEI) transfection reagent. Specifically, maintained culture cells or myotubes were transfected with the required plasmid DNA in a 1:2.5 ratio ( $\mu$ l/ $\mu$ g) of PEI to the plasmid. Briefly, PEI and plasmid DNA were firstly mixed individually, in a separate eppendorf tubes containing 500  $\mu$ l DMEM devoid of serum for 5 min at room temperature. After 5 min incubation, the PEI/DNA mixture was combined into one and was further incubated for 20 min before added dropwise onto the cells or myotubes. After overnight incubation, fresh media were replaced to wash out PEI remnant after transfection. At 48 h post transfection, cells were lysed and harvested for analysis.

#### **4.3.4 Cell lysis**

At the end of the experiments, the prewashed cells or myotubes with ice-cold DPBS were lysed and collected in cold sucrose lysis buffer containing 250 mM of sucrose, 10 mM of sodium  $\beta$ -glycerolphosphate, 50 mM of Tris-base (pH 7.5), 5 mM of sodium pyrophosphate, 50 mM of sodium fluoride, 1 mM of EDTA, 1 mM of benzamidine, 1 mM of EGTA, 1 mM of sodium orthovanadate, 1% of Triton X-100, 1 x complete Mini EDTA-free protease inhibitor cocktail, and 100 mM of 2-chloroacetamide for a 2 cm and 10 cm dish, respectively. Lysates were pelleted for 15 minutes at 4°C at 13,000 rpm, and the supernatant was collected and stored at -80°C for analysis.

#### **4.3.5 Protein Measurement**

Bradford protein quantification assay was performed on the supernatant. Briefly, 300  $\mu$ l of Coomassie Protein Assay Reagent were loaded in duplicate onto a flat bottom clear 96 well plate. 10  $\mu$ l of dH<sub>2</sub>O acts as a background control. 10  $\mu$ l of serial dilution of BSA protein standards (125, 250, 500, 750, 1000  $\mu$ g/ml) were used to obtain a standard curve. 10  $\mu$ l from 10 x diluted protein lysate sample supernatants was added to the corresponding well in duplicate and were mixed thoroughly using a plate shaker for 10 sec twice at 1250 rpm. The plate was briefly incubated at room temperature, after which the absorbance was measured at 595 nm using a BMG Labtech FluoStar Omega micro plate reader (Aylesbury, UK). MARS software was used to analyse the results.

#### **4.3.6 Sample preparation**

Protein lysates were prepared using 1x LDS sample buffer (NuPAGE, Invitrogen, NP0008). Samples were left overnight in 1.5% of 2-mercaptoethanol to denature at room temperature before analysis.

#### **4.3.7 GFP pulldown**

20  $\mu$ l of GFP-trap agarose or IgG bead slurry pre-washed with an ice-cold DPBS was then washed twice with ice-cold sucrose lysis buffer before incubated with 2 mg lysates overnight on a rotating wheel at 4 °C. Beads were then pelleted by centrifugation at 3500 rpm for 1 min at 4°C. After pelleted (washing) three times with sucrose lysis buffer, the co-immunoprecipitated proteins were eluted with 2x NuPAGE LDS sample buffer. Samples were left overnight in 1.5% of 2-mercaptoethanol to denature at room temperature before analysis.

#### **4.3.8 Western blotting**

Aliquots from the prepared samples were loaded and run on 10% Bis/Tris gels (ThermoFisher Scientific, Leicestershire, UK) in 1x MOPS buffer (ThermoFisher Scientific, Leicestershire, UK) for approximately 75 minutes at 140 V. Proteins from the gel were transferred to 0.2  $\mu$ M PVDF (polyvinylidene fluoride) membranes (Millipore, Hertfordshire, UK) in 1x transfer buffer containing; 20 mM Tris base, 150 mM glycine, and 20% methanol for 1 h at 100 V and 4°C condition. The membranes were blocked for 1 hour in 5% (w/v) dried skimmed milk diluted with TBS-T (Tris-buffered saline Tween 20): 20 mM of Tris-base 7.5 P<sup>H</sup>, 137 mM of sodium chloride, and 0.1% of Tween-20. To wash off the residual milk solution, membranes were washed three times for 10 minutes each in TBS-T prior to incubation in primary antibodies

prepared in 3% of BSA diluted with TBST. Membranes were incubated in primary antibody on a rocker at 4°C overnight. Membranes were washed three times for 10 minutes each in TBST before incubating in horse radish peroxidase conjugated secondary antibodies for 1 h at room temperature. After membranes were washed three times for 10 minutes each in TBST, antibody binding detection was performed using enhanced chemiluminescence (ECL) horseradish peroxidase substrate detection kit (Millipore, Hertfordshire, UK). G: BOX Chemi-XR5 (Syngene, Cambridgeshire, UK) was used to acquire images.

#### **4.3.9 Measurement of protein synthesis (SUnSET)**

Measurement of the protein synthesis was done using SUnSET (Surface sensing of translation) technique, as was previously described (87), except that puromycin was incorporated for 24 h. Briefly, fully formed myotubes were pre-treated with 1µM of puromycin (P8833, Sigma-Aldrich) simultaneously with the indicated treatments for 24 h in a serum free media. Subsequently, protein synthesis was stimulated by 100 nM of insulin for 30 minutes in a serum-free media prior to cell lysis. The incorporation of puromycin-labelled peptides was determined by western blotting with anti-puromycin antibody (Sigma-Aldrich P8833; 1:1000).

#### **4.3.10 Measurement of glucose uptake**

Glucose uptake was measured using the glucose uptake 'Promega Glo™ assay kit'. Briefly, 20,000 cells were seeded into each well of a 96-well plate. At confluent, differentiation was initiated by adding 100 µl DMEM + 2% horse serum. C2C12 WT and MuRF1 KO myotubes pre-treated with 1 µM of dexamethasone (Dex) or 0.1% ethanol (vehicle control) for 24 hours were serum starved overnight before the assay. After overnight serum starvation, wells were

once washed with 100  $\mu$ l DPBS and myotubes were incubated with or without 1  $\mu$ M insulin under a 5% CO<sub>2</sub> incubator at 37°C for 1 hour. After the incubation, myotubes were once washed with 100  $\mu$ l DPBS. Next, 50  $\mu$ l 1 mM 2DG in DPBS was added to each well (including myotube free wells as blank control) for 30 min at 25°C. 25  $\mu$ l Stop Buffer was added with a brief shaken to lyse cells at 25°C. Next, samples were transferred to 384 well plate at 15  $\mu$ l/well. 5  $\mu$ l Neutralization Buffer was then applied to each well with brief shake. Finally, 20  $\mu$ l of the 2DG detecting reagent was then applied to all wells with brief shake before dark-adapted for one hour at 25°C. Retained luminescence was then acquired using a BMG Labtech FLUOstar Omega microplate reader (Aylesbury, UK). Control wells (2DG: without myotubes), provided the assay background and were subtracted from all conditions.

#### **4.4 Data Analysis**

ImageJ/Fiji (National Institutes of Health, USA) was used for protein band quantification. The proteins of interest were normalised in relation to the experimental controls.

#### **4.5 Statistical analysis**

GraphPad Prism Software version 9 (San Diego, California, USA) was used to run all the statistical analysis. One way ANOVA (analysis of variance) was applied for multiple means analysis. For the MuRF1 KO and MuRF1 restoration experiments, the differentiation time course experiment, the dexamethasone dose response experiments, and the TRIM72 restoration experiment, one way ANOVA (analysis of variance) was applied before Dunnett's multiple comparisons post-hoc test analysis. For the experiment on the role of MuRF1 on IRS1/Akt signalling, insulin-induced protein synthesis, and insulin-induced glucose uptake, a two way

ANOVA was performed before Tukey's multiple comparisons post-hoc test analysis. All presented data are mean  $\pm$  SD. (\*) Statistical analysis was considered significant at  $P < 0.05$ .

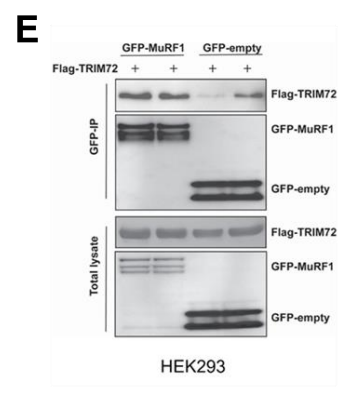
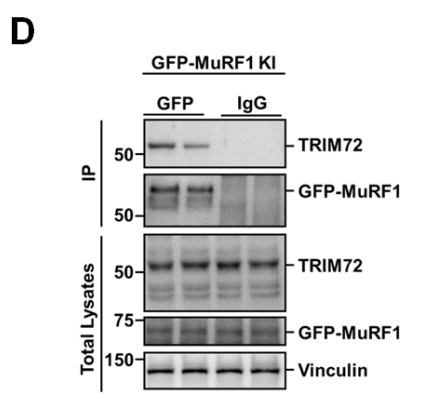
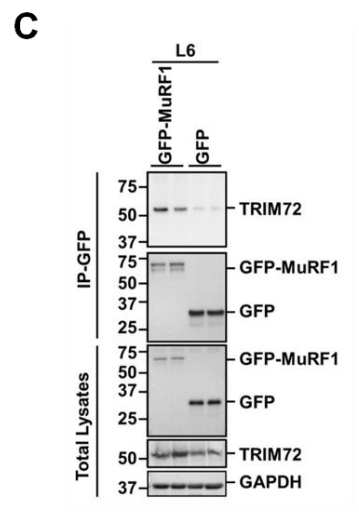
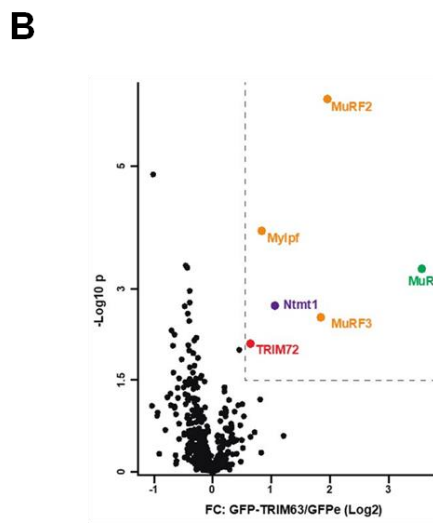
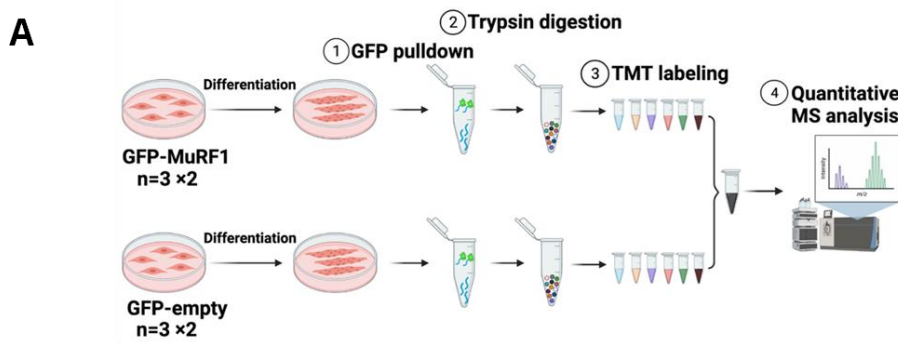
## 4.6 Results

### 4.6.1 Identification of TRIM72 as a novel MuRF1-interacting protein.

To gain insights into the molecular functions of MuRF1, we searched for its binding partners by an affinity purification and quantitative proteomic screening (Fig 4.1 A). First, we generated L6 skeletal muscle cell lines that stably expressing GFP-MuRF1 or GFP alone. L6 skeletal muscle cell were infected with a retrovirus encoding human MuRF1 protein fused with a GFP tag at the N-terminus or a retrovirus encoding a GFP as a control (GFP-empty). The generated cells were differentiated for 6 days into myotubes. Lysates from the differentiated cells were then subjected to GFP pulldown using agarose GFP-Trap slurry beads. Before proceeding with the on-bead digestion, the pulldown products were thoroughly washed in sucrose lysis buffer with 150 mM NaCl. Following peptide elution, each sample was labelled with TMT6 reagents before being mixed. To achieve high peptide detection sensitivity, the mixed peptides were subjected to high pH reversed-phase chromatography using spin columns, and then fractionated into six fractions before being analysed by mass spectrometer (Fig 4.1 A). From the volcano plot analysis, several MuRF1 putative binding partners were identified (Fig 4.1 B). While confirming previously found MuRF1 interactors such as MuRF2, MuRF3 (99), and myosin regulatory light chain 2 (MyIpf) (62), another TRIM72 (tripartite motif-containing protein 72) protein was identified as a novel MuRF1 interacting partner in skeletal muscle. Importantly, TRIM72 is an E3 enzyme and was previously reported to negatively regulate protein synthesis via its ligase activity by targeting skeletal muscle IRS1 protein (Yi et al., 2013, Song et al., 2013). TRIM72 proteins also contain a RING-finger, B-box- and a Coiled-Coil domain, which together form the RBCC motif (103). TRIM72 could also play a role in the regulation of skeletal muscle mass. Thus, the significance of the interaction between MuRF1 and TRIM72 was explored further.

To verify the binding of TRIM72 to MuRF1 in living cell, GFP pulldown assay was performed. Lysates of L6 myotubes infected with the expression plasmid for GFP-MuRF1 or GFP alone were incubated with GFP-Trap agarose beads. TRIM72 was co-immunoprecipitated by MuRF1 after pulldown assay (Fig 4.1 C, upper panel), however much less TRIM72 protein was discovered when control lysates were analysed. Total levels of TRIM72 were determined by western blot to confirm TRIM72 protein expression (Fig 4.1 C, fourth panel). The present data demonstrate that MuRF1 is interacting with TRIM72 protein. To ascertain the interaction between endogenous MuRF1 and TRIM72, a CRISPR/Cas9 generated GFP-MuRF1 knock-in C2C12 cell lines were used because both MuRF1 and TRIM72 are expressed in mouse skeletal muscle C2C12 cell. First, the mouse skeletal muscle C2C12 cell was co-transfected with CRISPR/Cas9 sgRNA plasmid pairs and GFP expression donor using PEI in a 10-cm dish. After puromycin selection, resistant clones were successfully determined by western blot (Data not shown). The knock-in cells were differentiated into myotubes for 6 days. Lysates were prepared for GFP pulldown using GFP-Trap agarose beads. Beads without GFP as IgG were also analysed. The pulldown products were thoroughly washed in lysis buffer containing 150 mM NaCl before immunoblotted for TRIM72 using TRIM72 antibody. After pulldown assay, MuRF1 co-immunoprecipitated TRIM72 in the GFP-MuRF1 knock-in lysates (Fig 4.1 D, upper panel) but not IgG. A total protein level for TRIM72 was examined by western blotting and was seemed to correlate with GFP-MuRF1 expression (Fig 4.1 D, fourth panel). Taken together, our results demonstrate that MuRF1 and TRIM72 physically interact in skeletal muscle cells. However, to confirm this interaction via reversal strategy was not successful. This is because TRIM72 antibody cannot recognize the endogenous MuRF1 binding site. To address this gap, a co-IP experiment was performed using a non-muscle cell line, HEK293. HEK293 cells were

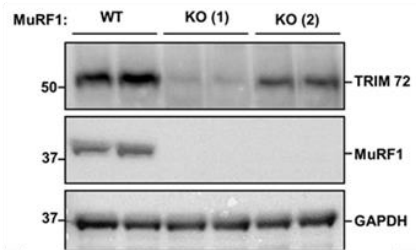
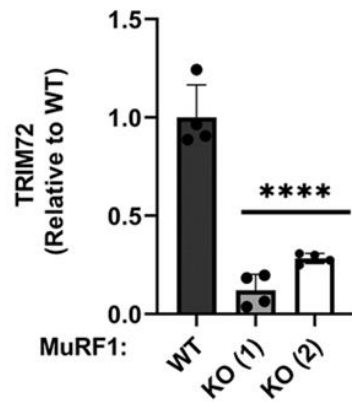
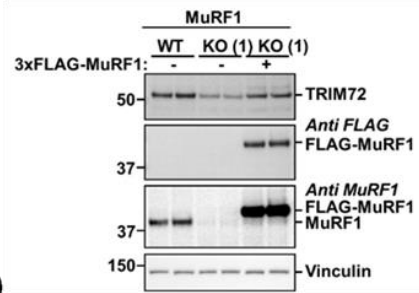
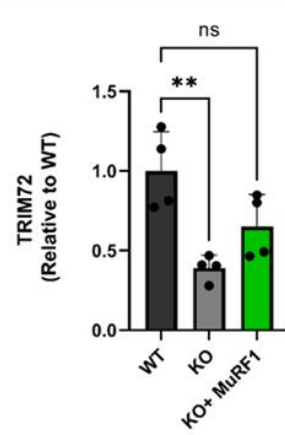
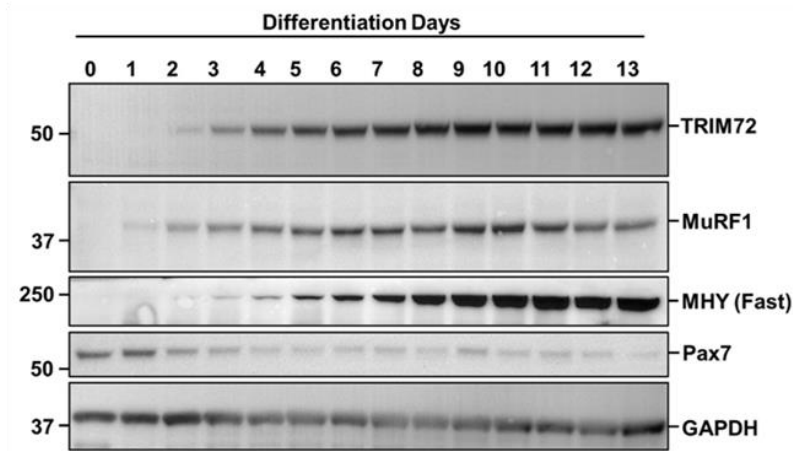
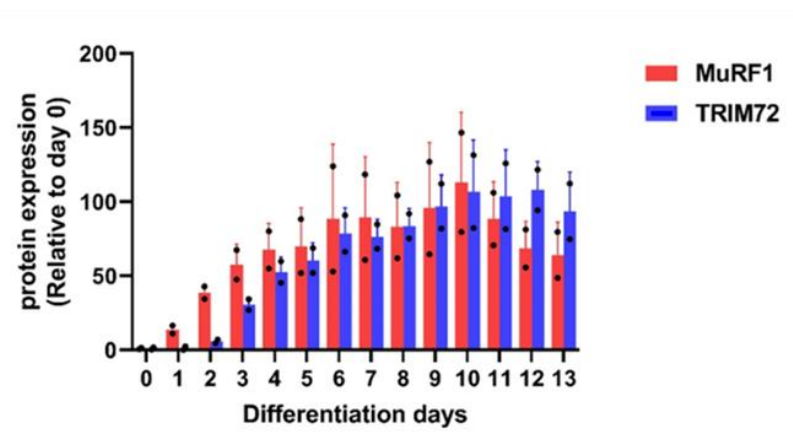
transiently co-transfected with FLAG-TRIM72 and either with GFP-MuRF1 or GFP-empty. The lysates from the transfected cells was subjected to a GFP pulldown using GFP-Trap agarose beads. The pulldown products were immunoblotted with the Flag-tagged HRP conjugated antibody for TRIM72. This shows a successful pulldown of TRIM72 by MuRF1 (Fig 4.1 E, upper panel), confirming the specificity of the MuRF1-TRIM72 interaction in cell.



**Figure 4.1. MuRF1 is interacting with TRIM72 in skeletal muscle cells.** (A) Experimental flow-chart depicting the proteomic workflow to identify MuRF1 interacting partners. (1) Protein lysates from L6 myotubes that stably expressed GFP-MuRF1 and GFP-empty was subjected to a GFP pulldown using agarose GFP-Trap slurry beads. The GFP pulldown products from GFP-MuRF1 and GFP empty were subjected to (2) trypsin digestion and (3) TMT labelling. (4) The TMT labelled peptides were then mixed before conducting MS analysis on an orbitrap Fusion Tribrid mass spectrometer. Data were analysed by MaxQuant software packages. (B) Volcano plot showing the Log<sub>2</sub> fold change (GFP-TRIM63/GFP-empty) against the -Log<sub>10</sub> p value highlighting significantly upregulated peptides. The dotted lines separate the upregulated hits for MuRF1-interacting proteins. (C) Verification of MuRF1 interaction with endogenous TRIM72 in L6 myotubes that stably expressed GFP-MuRF1. Total lysates (1 mg) from L6 myotubes that stably expressed GFP-MuRF1 or GFP-empty were subjected to GFP pulldown using GFP-Trap agarose beads. The pulldown products were immunoblotted with the indicated antibodies. To confirm protein expression and loading control, total lysates (lower panel) were immunoblotted with the indicated antibodies. Immunoblots were representative of three independent experiments. (D) Verification of endogenous MuRF1 interaction with endogenous TRIM72 in GFP-MuRF1 knock-in C2C12 myotubes. Total lysates (1 mg) from GFP-MuRF1 knock-in C2C12 myotubes were subjected to GFP pulldown using GFP-Trap agarose beads or beads bound with IgG (as a control). The pulldown products and immunoprecipitates were immunoblotted with the indicated antibodies. To confirm protein expression and loading control, total lysates (lower panel) were immunoblotted with the indicated antibodies. Immunoblots were representative of three independent experiments. (E) Verification of MuRF1 and TRIM72 interaction in HEK293 cells. HEK293 cells were transiently co-transfected with FLAG-TRIM72 and either with GFP-MuRF1 or GFP-empty (as a control). Total lysates (0.5 mg) were subject to pulldown using GFP-Trap agarose beads. The pulldown products were immunoblotted with the indicated antibodies. To confirm exogenous protein expression, total lysates (lower panel) were immunoblotted with the indicated antibodies.

#### **4.6.2 TRIM72 protein expression correlates with MuRF1 protein expression in C2C12.**

We next examined whether TRIM72 constitutes a functional interaction partner or represents a substrate of MuRF1 protein. Thus, we used CRISPR/Cas9 technology to generate a MuRF1 knockout (KO) C2C12 cell line. First, C2C12 cells were co-transfected with CRISPR/Cas9 sgRNA plasmid pairs in a 10-cm dish using PEI to direct the cas9 protein to induce a site-specific double strand break in MuRF1 genomic DNA. After puromycin selection, western blot analysis was used to identify successful C2C12 MuRF1 KO clones (Fig 3.3). Myoblasts of wild-type (WT) or two different clones of MuRF1 KO C2C12 were differentiated into myotubes for 6 days. Myotubes were then lysed, and the same amounts of protein extracts were prepared for immunoblotting to monitor TRIM72 and MuRF1 protein contents (Fig 4.2 A). As expected, MuRF1 protein content was not detected in MuRF1 KO cells, indicating the successful knock out of MuRF1 in C2C12 cells (Fig 4.2 A). Notably, TRIM72 protein levels were significantly reduced ( $P < 0.05$ ) in MuRF1 KO C2C12 myotubes compared to WT (Fig 4.2 A and B). The KO models used in this study permanently deleted MuRF1 unlike a transient Cre-inducible system. Thus, we next examined if a transient reintroduction of MuRF1 could restore TRIM72 expression. Interestingly, when FLAG-MuRF1 was transiently added to MuRF1 KO C2C12 myotubes, TRIM72 protein expression was restored (Fig 4.2 C and D). These results suggest that the expression of TRIM72 protein is MuRF1 protein dependent. The restoration of TRIM72 expression when MuRF1 was added in KO myotubes motivated us to compare the expression of TRIM72 and MuRF1 proteins in differentiating C2C12 cells over a 13-day period (Fig 4.2 E and F). Consistently, MuRF1 proteins begin to express prior to TRIM72 proteins, and this pattern continues throughout the differentiation process (Fig 4.2 E and F). Taken together, our findings show that MuRF1 regulates the expression of skeletal muscle TRIM72 protein.

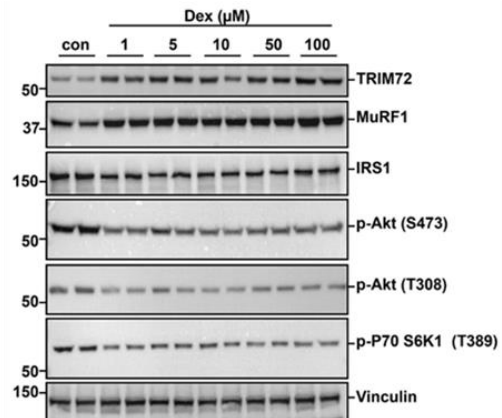
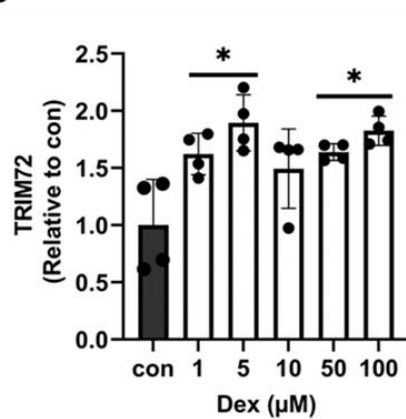
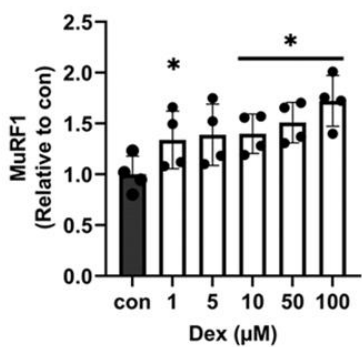
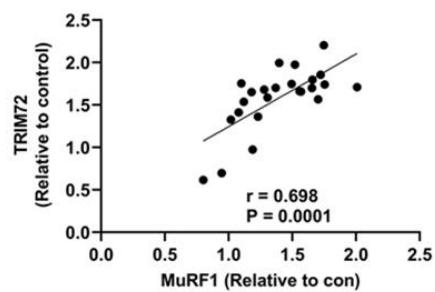
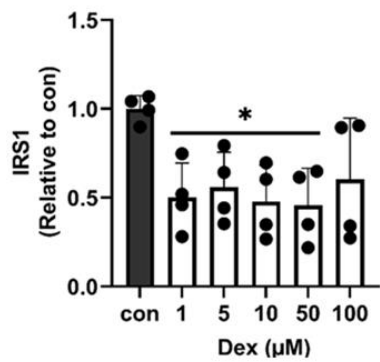
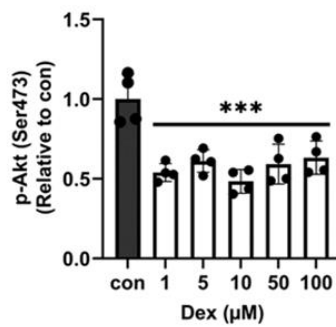
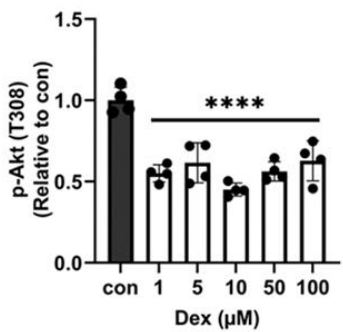
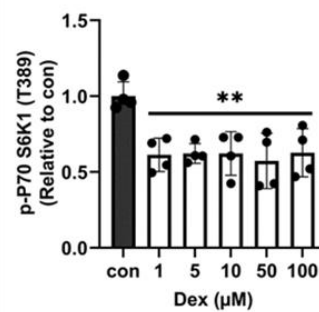
**A****B****C****D****E****F**

**Figure 4.2. TRIM72 expression is associated with MuRF1 expression in C2C12 myotubes.**

(A) TRIM72 protein levels are reduced in MuRF1 knockout C2C12 myotubes. Total lysates from WT (wild type) or two different MuRF1 knockout (KO 1 & 2) C2C12 myotubes were analysed by immunoblotting and probed with the indicated antibodies. Immunoblots were representative of four independent experiments (B) Quantification of TRIM72 protein expression in WT and MuRF1 KO C2C12 myotubes. Quantitative data from (A) were normalized to WT and subjected to one way analysis of variance (ANOVA) before Dunnett's multiple comparisons post-hoc test analysis. Error bars indicate the mean  $\pm$  standard deviation (n = 4). \*\*\*\* p < 0.0001 compared to WT. (C) Transient overexpression of MuRF1 restored TRIM72 protein expression in MuRF1 KO myotubes. Total lysates of C2C12 myotubes from WT or MuRF1 KO with and without transient transfection of 3xFLAG-MuRF1 for 48 h were analysed by immunoblotting and probed with the indicated antibodies. Immunoblots were representative of four independent experiments. (D) Quantification of TRIM72 protein expression in WT and MuRF1 KO with and without transient transfection of 3xFLAG-MuRF1. Quantitative data from (C) were normalized to WT and subjected to one way analysis of variance (ANOVA) before Dunnett's multiple comparisons post-hoc test analysis. Error bars indicate the mean  $\pm$  standard deviation (n = 4). \*\*\*\* p < 0.0001 compared to WT. (E) Representative blots of two independent experiments showing MuRF1 and TRIM72 protein expressions during differentiation time course for up to 13 days in C2C12 cells. Total lysates from C2C12 cells at the designated days of differentiation were analysed by immunoblotting and probed with the indicated antibodies. (F) Bar chart analysis of MuRF1 and TRIM72 protein expressions during differentiation time course in C2C12 cells. Quantitative data from (E) were normalised to day 0 and presented as bar chart. n = 2 in each time point.

#### **4.6.3 Dexamethasone increases TRIM72 and MuRF1 protein expressions while decreasing IRS1/Akt signalling in C2C12 myotubes.**

In a previous study, MuRF1 protein is upregulated in dexamethasone treated C2C12 myotubes (104). We next examine whether TRIM72 protein is similarly upregulated in dexamethasone treated C2C12 myotubes. To answer this question, mouse skeletal C2C12 cells were first differentiated for 5 days into myotubes. The myotubes were then treated with ethanol (EtOH), a vehicle control (con), or different dexamethasone concentrations for 24 h before immunoblotted with the indicated antibodies (Fig 4.3 A). For the first time, Dex treatments dose-dependently upregulated TRIM72 protein expression (Fig 4.3 B). As expected, Dex treatment dose-dependently increased MuRF1 protein expression (Fig 4.3 C). Pearson's correlation coefficient analysis from the dose-response data (Fig 4.3 D), shows a positively correlation between TRIM72 and MuRF1 protein expressions ( $r = 0.698$ ,  $P < 0.0001$ ). In a previous study, overexpression of TRIM72 in C2C12 myotubes markedly reduces IRS1 protein levels (71). After showing that MuRF1 and TRIM72 proteins are both upregulated after Dex treatment, we wanted to know whether IRS1 protein levels were also reduced by Dex treatment. To answer this question, the same lysates were immunoblotted and probed with the appropriate antibodies (Fig 4.3 A). Notably, the protein level of IRS1 (Fig 4.3 E), Akt phosphorylation at Ser 473 (Fig 4.3 F) and Thr 308 (Fig 4.3 G) were significantly reduced after Dex treatment in a dose-dependent manner. Additionally, the decreased phosphorylation of Akt's downstream target, p70 S6K1 at Thr 389, further supported the decreased Akt activity (Fig 4.3 H). Taken together, our findings show that MuRF1 and TRIM72 proteins are both upregulated after Dex treatment with a simultaneous reduction of the IRS1 protein levels. Based on the efficiency of the Dex concentrations, 1  $\mu$ M Dex was chosen for the subsequent experiments.

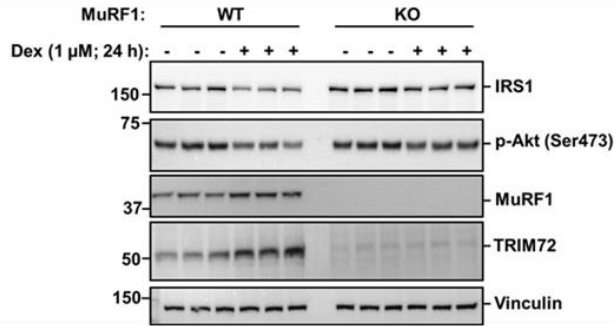
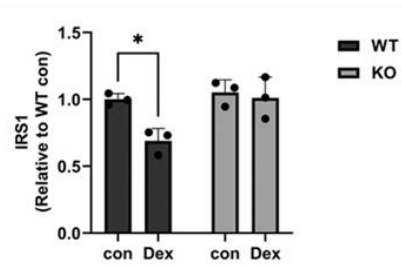
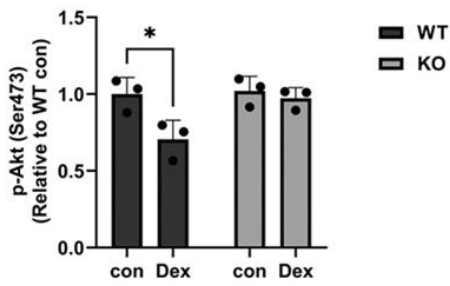
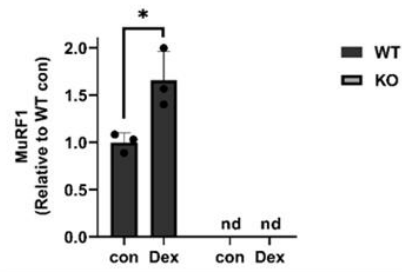
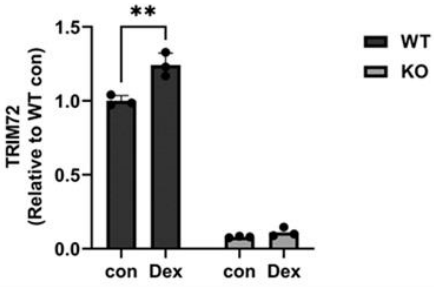
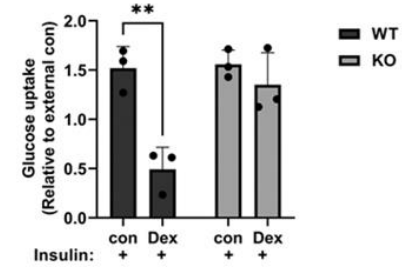
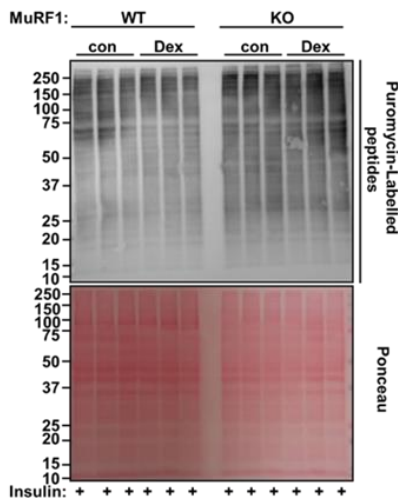
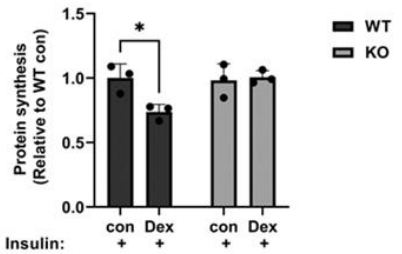
**A****B****C****D****E****F****G****H**

**Figure 4.3. Dexamethasone increases TRIM72 and MuRF1 protein expression while decreasing proximal insulin signalling in C2C12 myotubes.** Total lysates from C2C12 myotubes treated with 0.1% ethanol as controls (con) or with indicated concentrations of dexamethasone (Dex) for 24 h were analysed by immunoblotting and probed with the indicated antibodies. (A) Representative blots showing the effect of dexamethasone on TRIM72, MuRF1 proteins, and proximal insulin signalling in C2C12 myotubes. Immunoblots were representative of four independent experiments. (B, C, E-H) Quantitative data of TRIM72, MuRF1 and IRS1 protein expressions and proximal insulin signalling, including Akt and p70 S6K1 phosphorylation status. Quantitative data were normalised to control (con) and subjected to one way analysis of variance (ANOVA) before Dunnett's multiple comparisons post-hoc test analysis. Error bars indicate the mean  $\pm$  standard deviation ( $n = 4$ ). Statistical analysis were considered significant at \*  $p < 0.05$ , \*\*  $p < 0.01$ , \*\*\*  $p < 0.001$ , \*\*\*\*  $p < 0.0001$ , compared with control. (D) TRIM72 expression is associated with MuRF1 protein expression in C2C12 myotubes treated with dexamethasone. Quantitative data of TRIM72 and MuRF1 from four independent experiments were subjected to Pearson's correlation coefficient analysis to examine their protein expression correlation.

#### **4.6.4 The dexamethasone-induced downregulation of proximal insulin signalling, insulin-stimulated protein synthesis and glucose uptake is prevented in MuRF1 KO C2C12 myotubes.**

To further examine whether MuRF1 and TRIM72 interaction participate in the down regulation of IRS1/Akt signalling observed in Dex treated C2C12 myotubes, western blotting was performed on WT (wild type) and KO (MuRF1-knockout) myotubes treated with 1  $\mu$ M Dex for 24 hour. The result showed that Dex treatment significantly reduced IRS1 protein levels and Akt phosphorylation at serine 473 in WT but not in MuRF1 KO myotubes compared with controls (Fig 4.4 A). This present data demonstrated that MuRF1 and TRIM72 interaction are essential for the downregulation of IRS1 and Akt signalling in Dex treated C2C12 myotubes. In a previous study, glucocorticoids were shown to decrease protein synthesis in muscle (105). After our discovery that the MuRF1/TRIM72 interaction are required for the downregulation of IRS1/Akt signalling in Dex treated C2C12 myotubes, we wanted to know whether the MuRF1/TRIM72 interaction also affect the global insulin-induced protein synthesis following Dexamethasone treatment in mouse skeletal muscle C2C12 myotubes. To test this, we used a SUnSET (Surface sensing of translation) technique in conjunction with puromycin incorporation in culture cells (87, 106). Briefly, WT and MuRF1 KO C2C12 skeletal muscle myotubes were pre-treated with 1  $\mu$ M puromycin and either 0.1% ethanol (control), or 1  $\mu$ M dexamethasone for 24 h before stimulating by 100 nM insulin for 30 minutes prior to cell lysis in a serum free media. The level of protein synthesis (incorporated puromycin peptides) was determined by western blotting with the appropriate antibody against puromycin. Notably, Dex treatment significantly reduced protein synthesis in WT. In contrast, Dex did not decrease protein synthesis in myotubes of MuRF1 KO when compared to controls (Fig 4.4 F and G). Next, we examined

whether MuRF1/TRIM72 interaction also affect glucose uptake in Dex treated C2C12 myotubes. To answer this question, we measured Insulin-stimulated 2-Deoxyglucose (2DG) uptake in WT and MuRF1 KO myotubes treated with 1  $\mu$ M dexamethasone for 24 h. While Dex treatment significantly reduced glucose uptake in WT, Dex treatment did not suppress glucose uptake in myotubes of MuRF1 KO when compared to controls (Fig 4.4 H). These results indicate that MuRF1/TRIM72 interaction are required for the reduced IRS1/Akt signalling and its response.

**A****B****C****D****E****H****F****G**

**Figure 4.4 MuRF1 KO prevents dexamethasone-induced downregulation of proximal insulin signalling, insulin-stimulated protein synthesis and glucose uptake in C2C12.** (A)

Immunoblots from three independent experiments showing IRS1, p-Akt (Ser473), MuRF1 and TRIM72 in WT and MuRF1 KO C2C12 myotubes treated with and without dexamethasone. Total lysates from WT or MuRF1 KO C2C12 myotubes treated with and without 1  $\mu$ M dexamethasone (Dex) for 24 hours were analysed by immunoblotting before probing with the appropriate antibodies. (B-E) Figures showing quantitative data of IRS1 protein expression (B), Akt Ser473 phosphorylation (C), MuRF1 (D) and TRIM72 (E) protein expressions. Quantitative data from (A) were normalised to wild-type control (WT con) and subjected to a two way ANOVA before Tukey's multiple comparisons post-hoc test analysis. Error bars indicate the mean  $\pm$  standard deviation ( $n = 3$ ). \* $p < 0.05$ , \*\* $p < 0.01$ , compared to WT con. nd: non-detectable. (F) Immunoblot showing insulin-stimulated protein synthesis and loading control (ponceau) in WT or MuRF1 KO C2C12 myotubes treated with and without dexamethasone. WT or MuRF1 KO C2C12 myotubes were pre-treated with 1  $\mu$ M puromycin and either 0.1% ethanol (control), or 1  $\mu$ M dexamethasone for 24 h before stimulating by 100 nM insulin for 30 minutes prior to cell lysis in a serum free media. The protein synthesis (incorporated puromycin-labelled peptides) was determined by immunoblotting with anti-puromycin antibody. (G) Quantification of insulin-stimulated protein synthesis in WT or MuRF1 KO myotubes. Quantitative data from (F) were normalised to wild-type control (WT con) and subjected to a two way ANOVA before Tukey's multiple comparisons post-hoc test analysis. Error bars indicate the mean  $\pm$  standard deviation ( $n = 3$ ). \* $p < 0.05$ , compared to WT con. (H) Insulin-stimulated 2-Deoxyglucose (2DG) uptake in WT and MuRF1 KO treated with or without dexamethasone. C2C12 WT and MuRF1 KO myotubes pre-treated with or without 1  $\mu$ M dexamethasone for 24 hours were serum starved overnight, stimulated by 1  $\mu$ M insulin for 1 h before measuring 2DG uptake for 30 min. Results were presented as glucose uptake (2DG fold-changes) relative to external controls (without insulin stimulation). Data were analysed by a two way ANOVA before Tukey's multiple comparisons post-hoc test analysis. Error bars indicate the mean  $\pm$  standard deviation ( $n = 3$ ). \*\* $p < 0.01$  compared with insulin-stimulated control.

#### **4.6.5 Restoration of TRIM72 in C2C12 MuRF1 KO myotubes decreases proximal insulin signalling.**

In a previous study, overexpression of TRIM72 in C2C12 myotubes markedly reduces IRS1 protein levels (71). Our findings show that MuRF1 and TRIM72 proteins are both upregulated after Dex treatment with a concomitant decrease in the IRS1 protein levels. To exclude the possibility that MuRF1 protein is responsible for the reduced IRS1/Akt signalling, we transiently transfected FLAG-TRIM72 plasmid into MuRF1 KO myoblasts. Overexpression of TRIM72 in MuRF1 KO significantly reduced IRS1 protein (Fig 4.5 A and B) and phosphorylation of its downstream target, Akt at Ser 473 (Fig 4.5 A and C). Furthermore, the reduced Akt phosphorylation at Ser 473 was also confirmed by the decrease in the phosphorylation of its downstream target, p70 S6K1 at Thr 389 (Fig 4.5 A and D). Our data indicate that overexpression of TRIM72 in MuRF1 KO is sufficient to cause significant reduction of the IRS1 protein and its downstream signalling targets. This observation confirms that MuRF1 stabilises TRIM72 to impair IRS1/Akt signalling and its response in Dex treated C2C12 myotubes.

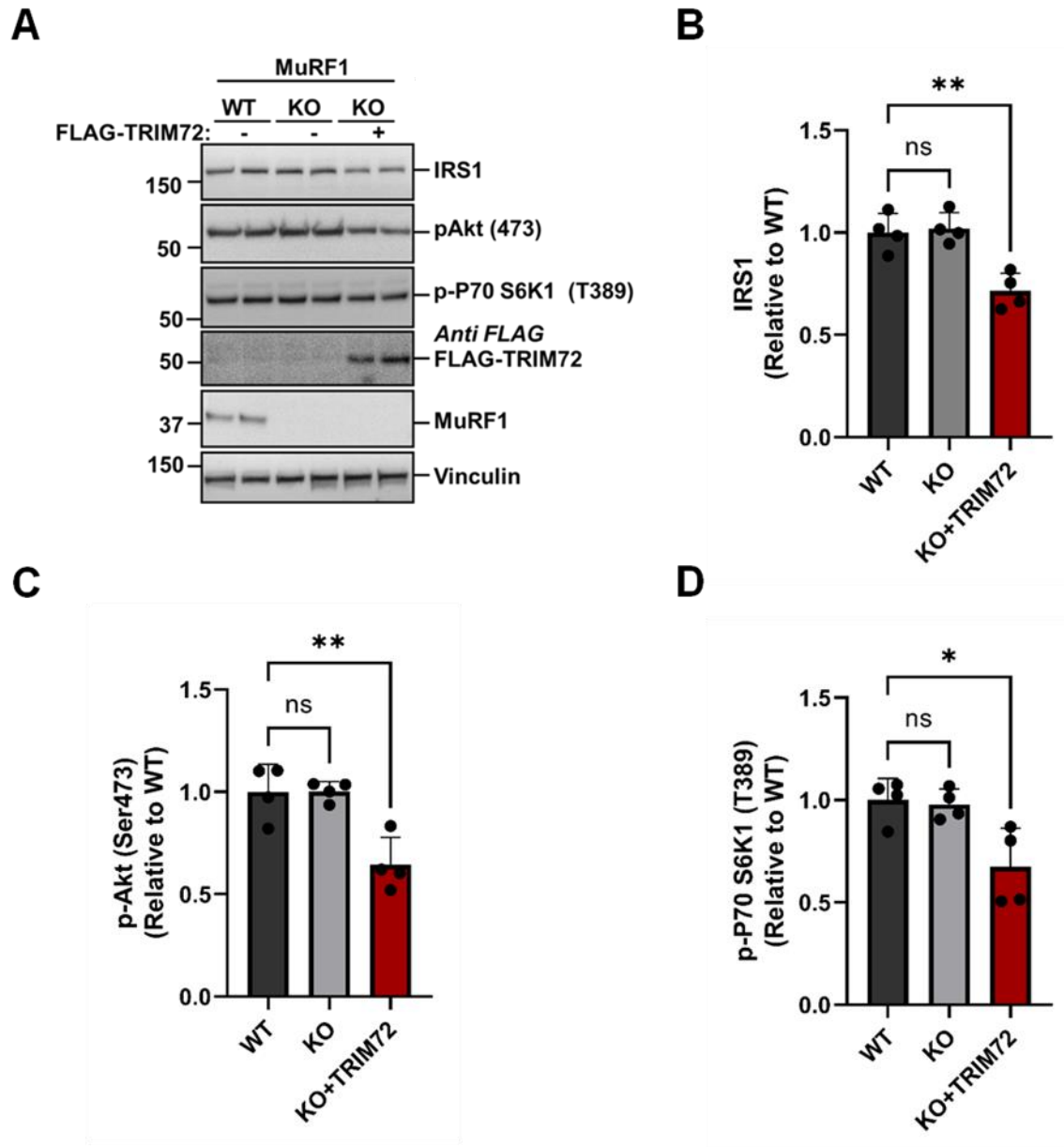


**Figure 4.5. Restoration of TRIM72 in C2C12 MuRF1 KO myotubes decreases proximal insulin signalling.** (A) Immunoblots from four independent experiments showing IRS1, p-Akt (Ser473), p70 S6K1 (T389), TRIM72 and MuRF1 in WT and MuRF1 KO C2C12 myotubes. Total lysates of C2C12 myotubes from WT or MuRF1 KO with and without transient transfection of FLAG-TRIM72 for 48 hours were analysed by immunoblotting and probed with the appropriate antibodies. (B-D) Figures showing quantitative data of IRS1 protein expression (B), Akt Ser (473) phosphorylation (C) and p70 S6K1 (T389) phosphorylation (D). Quantitative

data from (A) were normalised to wild-type (WT) and subjected to a one way ANOVA before Dunnett's multiple comparisons post-hoc test analysis. Error bars indicating: mean  $\pm$  standard deviation ( $n = 4$ ). \* $p < 0.05$ , \*\* $p < 0.01$ , compared to Wild Type. ns: non-significant.

## 4.7 Discussion

MuRF1 protein is important in the myofibrillar proteins degradation, but recent studies suggest that it may also regulate a range of other non-degradative cellular processes (64, 66, 107). Identification of yet discovered co-protein partners of MuRF1 may provide more insights into molecular roles of MuRF1 protein in the regulation of skeletal muscle mass. Here, we used affinity purification mass spectrometry and discovered TRIM72 as a novel interaction partner of MuRF1 in mouse skeletal muscle cells. We found that MuRF1 is required to stabilize TRIM72, but TRIM72 is sufficient to impair IRS1/Akt signalling, protein synthesis, and glucose uptake in skeletal muscle. Moreover, dexamethasone reduced IRS1/Akt signalling, protein synthesis, and glucose uptake in wild type myotubes, but MuRF1 KO myotubes were resistant to the detrimental effects of dexamethasone, suggesting MuRF1 as a negative regulator of anabolic pathways. Our data provide evidence that MuRF1 plays a non-degradative role to modulate skeletal muscle mass homeostasis, encouraging further exploration of the molecular roles of MuRF1.

To determine the functional significance of protein-protein interaction between TRIM72 and MuRF1, we first inquired whether TRIM72 is a MuRF1 substrate or simply an interaction partner whose activity is controlled by MuRF1. It is interesting to note that TRIM72 protein abundance was reduced in MuRF1 knockout myotubes (KO) but was restored when MuRF1 was added (Fig 2). This suggests that TRIM72 is not a MuRF1 substrate but rather a partner whose protein expression is regulated by MuRF1. Consistently, developing C2C12 cells start to express MuRF1 proteins before TRIM72 proteins over a 13-day period of differentiation (Fig 2), supporting our notion that MuRF1 regulates the stability of TRIM72 in skeletal muscle. In

agreement with this, MuRF1 and TRIM72 were downregulated in *tibialis anterior* (TA) muscle after MuRF1 inhibitor (MyoMed 205) was administered to obese ZSF1 rats in a previous study (108). This further affirms that MuRF1 interacts with and modulates TRIM72, another E3 ligase, to regulate skeletal muscle mass. Recently, Baehr *et al.* demonstrated that MuRF1 overexpression upregulates MuRF2, MuRF3, TRIM25 and DCAF8 protein abundance, albeit the biological significance is unknown (51). All these findings together support the notion that MuRF1 regulates skeletal muscle mass by exerting control over other E3 ubiquitin ligases (8, 51, 100).

In a common model of skeletal muscle atrophy, dexamethasone (Dex) treatment is thought to cause atrophy in part through activating MuRF1 (61, 64, 67, 104, 109). Following Dex treatment, Dex dose-dependently increase skeletal muscle MuRF1 protein levels (Fig 4.3 C), supporting the finding of the earlier investigations. For the first time, Dex treatment led to a dose-dependent upregulation of the TRIM72 protein (Fig 4.3 B). Overexpression of TRIM72 in C2C12 myotubes significantly lowers IRS1 protein levels, according to a previous study (71). Consistently, in this study, we show that the protein level of IRS1 (Fig 4.3 E), including its downstream target, Akt phosphorylation at Ser 473 (Fig 4.3 F) and Thr 308 (Fig 4.3 G) were significantly reduced after Dex treatment in a dose-dependent manner. Furthermore, the reduced Akt phosphorylation observed was supported by the decrease in the phosphorylation of its downstream target, p70 S6K1 at Thr 389 (Fig 4.3 H). Taken together, our findings show that MuRF1 and TRIM72 proteins are both upregulated after Dex treatment with a concomitant decrease in the IRS1 protein levels and its downstream target in C2C12 myotubes. This data aligned with a previous study where IRS1 deficiency was shown to promote muscle atrophy *in*

*vivo* and *in vitro* (110, 111). Thus, we speculated that when the upstream target, MuRF1, is elevated, TRIM72 is also raised, which in turn plays a role in the initiation of muscle atrophy via the insulin signalling pathway. Consistently, previous study with MuRF1 knockout mice revealed that MuRF1 can negatively regulate insulin sensitivity (97), raising the possibility that MuRF1 may be responsible for the insulin-resistance linked to muscle wasting (112). In line with this, MuRF1 overexpression has previously been linked to a reduction in IRS1 protein levels (67), but the molecular basis for this change was not discussed by the authors. Thus, our data provide a link between these previous studies that MuRF1 stabilizes TRIM72 as a protein interacting partner to ubiquitylate and degrade IRS1 (71, 72, 73) via the 26S proteasome, leading to an impaired IRS1 signalling pathway and the subsequent muscle wasting. In supporting our finding that IRS1/Akt activity is regulated by TRIM72, the restoration of TRIM72 in MuRF1 KO significantly reduced IRS1 protein (Fig 5 A and B).

MuRF1 was reported to negatively regulate protein synthesis (66), however the underlying molecular mechanism was not explored. It was previously reported that the IRS1/Akt/mTORC1 pathway can activate protein synthesis (9, 10, 11, 12). In agreement with this, a previous study showed MuRF1 overexpression with a concomitant reduction in IRS1 protein levels (67), but the underlying molecular basis for this change was not explored by the authors. Our findings indicate that MuRF1 and its related interaction partner, TRIM72, negatively affect insulin-induced protein synthesis after dexamethasone treatment (Fig 4). Overexpression of MuRF1 also raises TRIM72 protein levels after Dex treatment. In skeletal muscle, TRIM72 functions as an autonomous ubiquitin ligase to remove the IRS1 protein as a negative regulator of protein synthesis (71, 72, 73). The increase in the insulin-induced protein synthesis observed in MuRF1

KO C2C12 myotubes (Fig 4), could be attributed to the restored insulin signalling activity caused by the marked loss of TRIM72 in the MuRF1 KO C2C12 myotubes. This is consistent with a previous study in which MuRF1 KO was demonstrated to be resistant to reductions in protein synthesis induced by dexamethasone (64). Unfortunately, the molecular mechanism was not investigated by the previous authors.

Glucose metabolism has a contributory role for maintaining organ function in humans (113). To assess the function of MuRF1 on glucose metabolism, we measured insulin-induced glucose uptake in MuRF1 WT and KO myotubes after Dex treatment. Dex treatment significantly reduced insulin-induced glucose uptake in WT but not in MuRF1 KO myotubes when compared with controls (Fig 4 H), raising the possibility that MuRF1 negatively regulates glucose uptake. Recently, Labeit *et al.*, examined the effect of MuRF1 on glucose metabolism in diabetic mice. They found increase in serum glucose and decreased glucose tolerance with an altered PI3K/Akt signalling, as well as increased Akt phosphorylation at Ser473 in MuRF1 KO mice skeletal muscle (114). Unfortunately, no molecular studies were previously performed to ascertain the role of MuRF1 in glucose metabolism. Consistently, MuRF1 inhibitor (MyoMed-205), was shown to stabilise serum glucose in diabetic mice (114). Though, the molecular mechanism by which MuRF1 negatively regulates glucose uptake was not reported by these previous authors, our data provide evidence that MuRF1 interact and stabilizes TRIM72 to impair insulin-induced glucose uptake via downregulation of IRS1 signalling in skeletal muscle. In line with our findings, reports from (71, 115, 116) also showed that TRIM72 is sufficient to promote diabetes, via downregulation of IRS1. However, findings by other authors (117, 118) do not support their conclusions. Neither the injection of rhTRIM72 nor the adenoviral gene transfer of TRIM72 was

able to cause changes in blood glucose in either diabetic db/db or nondiabetic mice in these earlier investigations (117, 118). Interestingly, the disparity in these earlier studies revealed that the negative effects of rhTRIM72 on metabolism are only seen in cases of advanced diabetes (116). In the study by Feng *et al.* (116), all the db/db mice had fasting blood glucose greater than 10 mmol/L and fed blood glucose greater than 20 mmol/L at 10 weeks of age. Whereas, in the other mouse studies, the average fasting blood glucose was 7 mmol/L and the average fed blood glucose was 13.9 mmol/L at 18-32 weeks of age (117, 118). This implies that the negative effects of rhTRIM72 on metabolism are only observed in cases of severe diabetes. While the TRIM72's impact on insulin signalling and glucose metabolism in skeletal muscle has come from diabetic models, our findings have come from studies conducted on C2C12 myotubes that have been exposed to dexamethasone treatment. Overall, the results of this present study are indicating that TRIM72 protein regulates insulin signalling via multiple mechanisms. The mechanism of protein synthesis and glucose uptake after the restoration of TRIM72 in MuRF1 KO skeletal muscle, however, should be examined in further research to support these findings.

#### **4.8 Conclusion**

As summarised in Fig 4.6, we used affinity purification mass spectrometry and discovered TRIM72 as a novel interacting partner of MuRF1. Our findings provide the first evidence that MuRF1 partner with TRIM72 to regulates skeletal muscle mass by enhancing skeletal muscle insulin resistance in addition to decreased protein synthesis. Our finding is encouraging further exploration of the molecular roles of MuRF1 in developing a new therapeutic option for the amelioration of skeletal muscle atrophy and its associate complications.

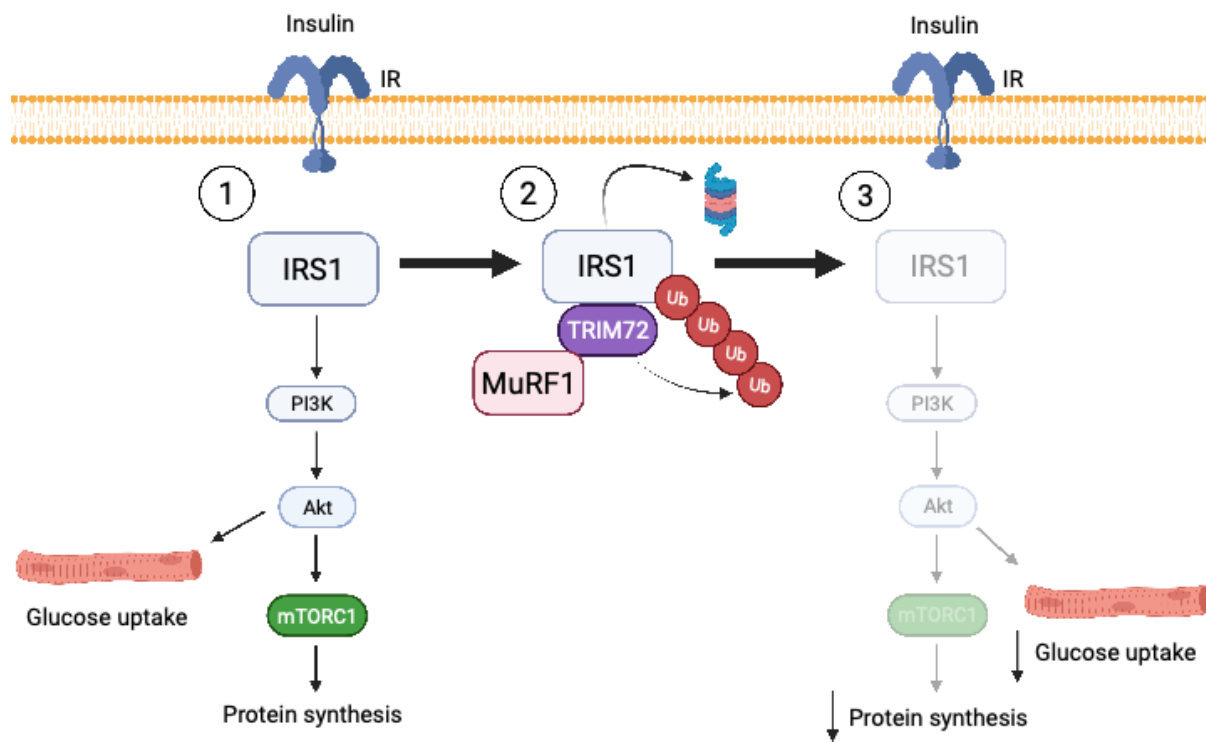


**Figure 4.6. A working model of the molecular roles of MuRF1 in the regulation of skeletal muscle mass.** (1) IRS1 is activated and PI3K is recruited when insulin binds to its receptor (IR). The phosphorylation of Akt is initiated as a response to 1 above. Phosphorylated Akt, in turn, targets its downstream mTORC1 to regulate synthesis of protein and glucose uptake; (2) MuRF1 overexpression increases and stabilises TRIM72. TRIM72, in turn, ubiquitylates and degrades IRS1 via the proteasome. (3) It is suggested that this would impair IRS1/Akt signalling events, leading to decreased insulin-stimulated protein synthesis and glucose uptake. → indicates direction of signalling in the figure. IR: indicates Insulin Receptor, IRS1: indicates Insulin Receptor Substrate 1.

---

**CHAPTER 5**  
**AUTO-UBIQUITYLATION OF MURF1**  
**REGULATES ITS STABILITY IN**  
**SKELETAL MUSCLE.**

---

## 5.1 Abstract

Auto-ubiquitylation is an important mechanism that regulates the stability of RING-type E3 ligases in cells. MuRF1 is a RING-type E3 ubiquitin ligase. MuRF1 auto-ubiquitylation has been demonstrated in *in vitro* and in blood cells, but MuRF1 auto-ubiquitylation has not been reported in skeletal muscle. We generated mouse skeletal muscle cell line stably expressing GFP-MuRF1 with an intact or point mutant cysteine residue at C23A in the RING domain and employed a ubiquitin-TUBE pulldown assay to measure MuRF1 auto-ubiquitylation. Our data demonstrated that auto-ubiquitylation regulates E3 ligase activity of MuRF1 in skeletal muscle. Like other RING type E3 ubiquitin ligases, the ubiquitylation activity of MuRF1 is abolished by point mutation of the cysteine residues at C23A in the RING domain in skeletal muscle. Our result indicated that MuRF1 catalyses the addition of mono-ubiquitylation, K48, and K63 specific poly-ubiquitin chains to itself in skeletal muscle. Further *in vitro* analysis reflects similar result as in the skeletal muscle; MuRF1 interacts with cognate UBE2D, UBE2N/Vs and UBE2W to catalyse mono-ubiquitylation, K48, and K63 specific poly-ubiquitin chains in a UBE2-dependent manner. We found a novel 2-step auto-ubiquitylation ubiquitylation mechanism, where MuRF1 interacts with cognate UBE2W to mono-ubiquitylates itself to serves as an anchor for UBE2N/V and UBE2D generated poly-ubiquitin chains. Furthermore, we show that the auto-ubiquitylation of MuRF1 protein could direct MuRF1 degradation via autophagy for its stability. Overall, we show novel mechanisms for protein stability of MuRF1 in skeletal muscle.

## 5.2 Introduction

Ubiquitylation is a key post-translational modification in many cellular processes, including the regulation of protein stability and endocytosis (119, 120, 121). Ubiquitylation involves the activation and conjugation of the 8.5 kDa ubiquitin to the lysine residues or on occasion, to the NH<sub>2</sub> terminus of other protein substrates (79). Ubiquitylation occurs via the sequential activities of the E1 (ubiquitin-activating), E2 (ubiquitin-conjugating), and E3 (ubiquitin-ligase) enzymes (79, 122). E3 ubiquitin ligases play a critical role in the ubiquitylation process by specifying the target substrate and catalysing ubiquitin transfer from the E2 (RING-type E3) or from the E3 itself (HECT-type E3) to the target lysine residues (123). Ubiquitin can be added to a protein as a single entity (mono-ubiquitin) or to ubiquitin molecule as a chain of variable length (poly-ubiquitin). The poly-ubiquitin chains are often linked by any of the seven lysine residues (Lys6, Lys11, Lys27, Lys29, Lys33, Lys48, and Lys63) or the N-terminal methionine residue of ubiquitin (29) which determines the fate of the substrates. The human genome encodes 2 E1s, 40 E2s and approximately 600 E3s (124).

MuRF1, a RING-type E3 ligase (125), plays a crucial role in the catabolic processes of skeletal muscle atrophy. MuRF1 overexpression in mice results in substrates ubiquitylation and skeletal muscle atrophy, whereas MuRF1 RING domain mutant at C44S/C47S partially attenuated skeletal muscle atrophy in mice (51). The evidence indicates that the RING domain is important for the function of MuRF1 in the catabolic processes of skeletal muscle atrophy. It is hypothesized that under catabolic process, increased RING-type E3 ligase activity would inevitably promote auto-ubiquitylation (52) leading to auto-degradation via proteasome or autophagic route for its stability (58). Interestingly, Baehr *et al.* showed that, MuRF1 was

ubiquitylated on 16 lysine sites following MuRF1 overexpression in mice (51). However, the mechanisms of MuRF1 ubiquitylation were not determined, and it is unclear whether MuRF1 overexpression *per se* facilitated auto-ubiquitylation of MuRF1. Auto-ubiquitylation is one of the notable features of the RING-type E3 ligases to auto-regulate their stability *in vivo* (36), describes the ligase's activities or their interactions with cognate E2s (80). A previous study showed that MuRF1 auto-ubiquitylation with UBE2D1 was a prerequisite to specifically accelerate the ubiquitylation of S5a but inhibits the ubiquitylation of troponin I *in vitro* (84). This suggests that MuRF1 auto-ubiquitylation is also important in the catabolic processes of skeletal muscle atrophy either by regulating its stability via degradation for replenishment or increasing its ligase activity to ubiquitylate target substrates (58). MuRF1 auto-ubiquitylation has been reported in peripheral blood plasma as a circulating marker for cancer cachexia (81). The acquired signals were compatible with mono, multi-mono or short poly-ubiquitin chains, implying that they might not necessarily be degradation signals. To date, the lack of valid and applicable tools for measuring substrate ubiquitylation (126) limits the study of MuRF1 protein auto-ubiquitylation in skeletal muscle.

We employed a more controlled skeletal muscle cell line models to investigate MuRF1 auto-ubiquitylation under catabolic conditions using a recently developed tandem ubiquitin-binding entity (TUBE) technique by our lab (126). TUBE has a tetra ubiquitin-binding domain structure that has strong affinity for all poly-ubiquitin chain types. Thus, TUBE is a novel technique to better understand the precise functional role of MuRF1 ligase activity, which is not only essential for therapeutic potentials but could also pave a way for restricting their functions until required.

## **5.3 Materials and methods**

### **5.3.1 Antibodies and Reagents**

The antibodies used for Western blot analysis were Anti-MuRF1 (Santa Cruz SC-398608; 1:1000), Anti-GAPDH (Cell Signalling Technology 5174; 1:1000), Anti-GFP (Chromotek 3H9-100; 1:2000), Anti-Vinculin (Abcam ab73412; 1:1000), Anti-MBP (New England Biolabs; E8038S, 1:20,000), Anti-Ubiquitin (Biolegend 646302; 1:1000), Anti-K48 specific poly-ubiquitin (Merck-Millipore 05-1307; 1:1000), Anti-K63-specific poly-ubiquitin (Cell Signalling Technology 5621; 1:1000), Anti-LC3A/B (Cell Signalling Technology 4108; 1:1000), Anti-P62 (Cell Signalling Technology 5114; 1:1000), Anti-Actin (Sigma A2103; 1:1000) respectively. The secondary antibodies used were Anti-mouse IgG, HRP-linked Antibody (Cell Signalling Technology 7076; 1:10 000), Anti-rabbit IgG, HRP-linked Antibody (Cell Signalling Technology 7074; 1:10 000), and Anti-Rat IgG, HRP-linked Antibody (Cell Signalling Technology 7077; 1:5000). The cells culture reagents used were Dulbecco's Modified Eagle Medium (DMEM; Thermo Fisher Scientific, Loughborough, UK, 31966021) containing GlutaMAX, 25 mM of glucose, and 1 mM of sodium pyruvate, Hyclone fetal bovine serum (FBS, Fisher Scientific, Loughborough, UK, SV30180.03), Penicillin-Streptomycin (10 000 Units/mL- $\mu$ g/mL, Thermo Fisher Scientific, Loughborough, UK, 15140122). Horse Serum (HS) (Sigma-Aldrich, Cambridgeshire, UK, H1270), Bradford protein assay (ThermoFisher Scientific, Leicestershire, UK, 23209), Dexamethasone (Sigma-Aldrich D4902) were prepared in ethanol and treatment conditions were described in the figure. Bortezomib, M132, and Bafilomycin A1 were prepared in DMSO and treatment conditions were described in their respective figures.

### 5.3.2 Cell lines and Culture

C2C12 mouse skeletal muscle myoblasts were purchased from the American Type Culture Collection (ATCC, Manassas, VA, USA). L6 stably expressing GFP-MuRF1 and GFP empty were generated using a retroviral system. Briefly, L6 skeletal muscle cells were infected with a GFP-MuRF1 and GFP (control) retroviral media containing 10 µg/mL polybrene for 48 h respectively. After 48 h infection, the infected L6 rat skeletal muscle cell was selected using 2 µg/mL puromycin. The infected resistant clones were subsequently sorted and collected into 5 ml FACS tubes using the ARIA fusion sorter (BD Biosciences, Berkshire, UK). This was carried out by a specialist at the University of Birmingham's flow cytometry center (Institute of Biomedical Research). The sorted L6 skeletal muscle cells that stably express relative GFP signals for both GFP-MuRF1 and GFP were re-cultured for further expansion and cryopreserved after being validated by western blotting. Wild-type and RING finger mutant at C23A<sup>GFP/GFP</sup>PMuRF1 C2C12 cells were generated using retroviral system. Briefly, <sup>GFP/GFP</sup>PMuRF1 (C23A).Puro retroviral media containing 10 µg/mL polybrene was used to transduce C2C12 mouse skeletal muscle cell for 48 h. After 48 h transduction, the transduced C2C12 mouse skeletal muscle cell was selected using 2 µg/mL puromycin. The resistant clones were re-cultured for further expansion and cryopreserved after being validated by western blotting. All myoblasts cells were cultured and grown in high-glucose Dulbecco's Modified Eagle Medium (DMEM) supplemented with 10% (v/v) foetal bovine serum and 1% (v/v) Penicillin-Streptomycin (10 000 units/mL-µg/mL). At about 90% confluency, skeletal muscle myoblasts were differentiated into myotubes for at least five days using high-glucose DMEM supplemented with 2% (v/v) horse serum (HS) and 1% (v/v) penicillin-streptomycin (10 000 units/mL-µg/mL). To maintain cells or myotubes viability, the medium was changed every two days until cells

were fully differentiated. For endogenous MuRF1 stability experiment, C2C12 myotubes were pre-treated with 100  $\mu$ M of dexamethasone (Dex)) for 24 h before treatment with 1  $\mu$ M bortezomib, 20  $\mu$ M MG132, and 100 nM bafilomycin A1 for the indicated time respectively. For exogenous MuRF1 stability experiment, myotubes were treated with 1  $\mu$ M bortezomib, 20  $\mu$ M MG132, and 100 nM bafilomycin A1 for the indicated time respectively.

### **5.3.3 Cell lysis**

Cells were lysed in 500  $\mu$ l sucrose lysis buffer containing 250 mM of sucrose, 50 mM of Tris-base (pH 7.5), 50 mM of sodium fluoride, 10 mM of sodium  $\beta$ -glycerolphosphate, 5 mM of sodium pyrophosphate, 1 mM of EDTA, 1 mM of EGTA, 1 mM of benzamidine, 1 mM of sodium orthovanadate, 1 x complete Mini EDTA-free protease inhibitor cocktail, and 1% of Triton X-100 and 100 mM of 2-chloroacetamide. Cells were prewashed with 5ml of cold DPBS prior to lysis on ice. Lysates were pelleted at 13,000 rpm for 15 minutes at 4°C and the supernatant was collected and stored at -80°C until analysis.

### **5.3.4 Protein Measurement**

Bradford protein quantification assay was performed on the supernatant. Briefly, 300  $\mu$ l of Coomassie Protein Assay Reagent were loaded in duplicate onto a flat bottom clear 96 well plate. 10 $\mu$ l of dH<sub>2</sub>O was used as a blank. For a standard curve 10  $\mu$ l of serial dilution of BSA protein standards (125, 250, 500, 750, 1000  $\mu$ g/ml) were used. 10  $\mu$ l of 10 x diluted sample supernatants were added to each corresponding well in duplicate and were mixed thoroughly using a plate shaker for 10 sec twice at 1250 rpm. The plate was briefly incubated at room

temperature, and the absorbance was measured at 595 nm using a BMG Labtech FluoStar Omega micro plate reader (Aylesbury, UK). MARS software was used to analyze the results.

### **5.3.5 Sample preparation**

For western blot analysis, samples were prepared in 1x NuPAGE LDS sample buffer containing 1.5% of 2-mercaptoethanol.

### **5.3.6 GFP pulldown**

20  $\mu$ l of GFP-trap agarose bead slurry (Chromotek, Germany) pre-washed with an ice-cold phosphate buffered saline (PBS) was then washed twice with ice-cold sucrose lysis buffer before incubated with 2 mg lysates overnight on a rotating wheel at 4 °C. Beads were then pelleted by centrifugation at 3500 rpm for 1 min at 4°C. After washing three times with sucrose lysis buffer containing 100 mM of 2-chloroacetamide and 150 mM of NaCl, the co-immunoprecipitated proteins were eluted with 2x NuPAGE LDS sample buffer. Samples were left overnight in 1.5% of 2-mercaptoethanol to denature at room temperature before analysis.

### **5.3.7 TUBE-ubiquitin pulldown**

Escherichia coli BL21 cells were used to expressed and purify the His-halo-ubiquitin UBA domain tetramer (UBA<sup>UBQLN1</sup>) as previously described (86). In 750  $\mu$ l of binding buffer, 1 mg of the HALOUBA<sup>UBQLN1</sup> TUBE protein was incubated for 2 hours at 4°C with 200  $\mu$ l of HaloLink resin that had been pre-washed with cold PBS (phosphate buffered saline). 1 mg of protein from cell lysates was incubated to the conjugated UBA<sup>UBQLN1</sup> TUBE protein and HaloLink resin overnight on a rotational wheel at 4°C. Following 3 washes in sucrose lysis buffer, the captured

ubiquitin and poly-ubiquitin chains were eluted in 1x LDS sample buffer (NuPAGE, Invitrogen, NP0008). Samples were left overnight in 1.5% of 2-mercaptoethanol to denature at room temperature before analysis.

### **5.3.8 Western blotting**

Sample aliquots were electrophoresed on 10% BIS-TRIS polyacrylamide gels using 1x MOPS running buffer at 140 V for approximately 1 hour 15 minutes. Proteins were electroblotted onto PVDF membrane (Millipore, Hertfordshire, UK) in a transfer buffer containing; 20 mM Tris base, 150 mM glycine and 20 % methanol for 1 h at 100V in 4°C condition. Membranes were blocked for 1 hour in 5% (w/v) dried skimmed milk diluted in Tris-buffered saline Tween 20 (TBS-T): 137 mM of sodium chloride, 20 mM of Tris-base 7.5 pH and 0.1% of Tween-20. The membranes were incubated overnight at 4°C with the appropriate primary antibody. Membranes were washed three times in TBS-T prior to incubation in horse radish peroxidase conjugated secondary antibodies at room temperature for 1 h. Membranes were washed a further three times in TBS-T prior to antibody detection using enhanced chemiluminescence horseradish peroxidase substrate detection kit (Millipore, Hertfordshire, UK). Images were acquired using a G: BOX Chemi-XR5 (Syngene, Cambridgeshire, UK).

### **5.3.9 *In vitro* Analysis**

The *in vitro* ubiquitylation assay was performed using 50 µl of reaction mixture containing 50 mM HEPES Ph7.5, 1 mM DTT, 5 µM ubiquitin, 34 nM His-UBE1, 7 µM UBE2, and 230 nM MBP-MuRF1. The mixture was mixed with freshly prepared 20 µl of 1 M MgCl<sub>2</sub>, 10 µl of 100 mM of ATP P<sup>H</sup> 7.0, and 170 µl of ddH<sub>2</sub>O prior to incubation. Reactions were incubated for 1 hr at 37 °C and were terminated by adding LDS sample buffer to a final concentration of 1 x LDS

sample buffer containing 1.25%  $\beta$ -mercaptoethanol. Samples were left overnight to denature before Western blotting.

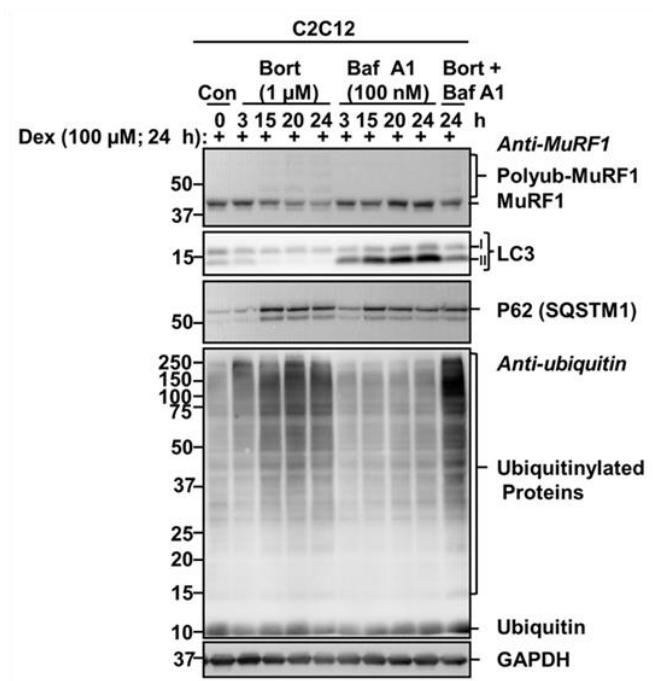
## 5.4 RESULTS

### 5.4.1 Endogenous MuRF1 is stabilised by inhibition of the proteasome and autophagy in skeletal muscle.

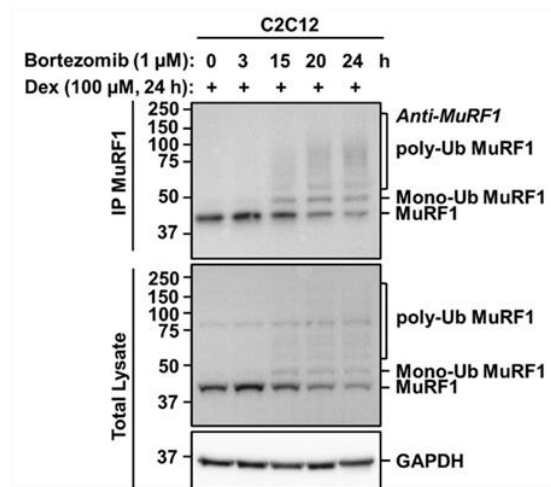
To determine the stability of endogenous MuRF1, we treated C2C12 myotubes pre-treated with dexamethasone (Dex. 100  $\mu$ M) for 24 h to induce atrophy, with the proteasome (bortezomib) and autophagy (bafilomycin A1) inhibitors, respectively. A 15-hour bortezomib treatments leads to mono-ubiquitylation and accumulation of higher molecular weight (HMW) of MuRF1 species (Fig 5.1 A, upper panel, lane 3). The HMW products continued to increase with time up to 24 h of bortezomib treatment (Fig 5.1 A, upper panel, lane 5). The mono-ubiquitylation and HMW products were enhanced in MuRF1, which was coimmunoprecipitated by a MuRF1 antibody (Fig 5.1 B, upper panel, lanes 3, 4, and 5). However, similar to the bortezomib treatment, bafilomycin A1 treatment also increase MuRF1 protein content (Fig 5.1 A upper panel, lanes 8 and 9), but in a much slower rate than bortezomib, which support the notion that proteasome degrades short-live protein, whereas the autophagy degrades long-lived protein (127). As expected, poly-ubiquitylated proteins were increased only in cells treated with bortezomib (Fig 5.1 A, fourth panel, lanes 2, 3, 4, 5, and 10), indicating blockage of proteasome functions. In addition, LC3 II proteins level were increased only in cells treated with bafilomycin A1 (Fig 5.1 A, second panel, lanes 6-10) indicating blockage of autophagic functions. However, the LC3 II protein level, an autophagy marker, were drastically reduced following proteasome inhibition (Fig 5.1 A, second panel, lanes 3, 4, and 5). Surprisingly, at these same time points, p62 level, an autophagy substrate, were increased following proteasome and autophagy inhibition respectively suggesting that the ubiquitylated MuRF1 could serves as substrate to P62 for autophagy degradation. To further investigate the crosstalk between the proteasome and autophagic

degradation of MuRF1, we adopted a strategy previously employed by (128) by comparing the effects of inhibiting each pathway alone with inhibiting both pathways simultaneously. It is interesting to note that when both pathways were inhibited, MuRF1 protein contents was increased in addition to the mono-ubiquitylation and HMW accumulated (Fig 1 A, upper panel, lane 10) compared to only bortezomib treated lane (Fig 5.1 A, upper panel, lane 5). Consistently, compared to bortezomib alone lane (Fig 5.1 A, fourth panel, lane 5), treatment with bafilomycin A1 plus bortezomib led to an extra increase in poly-ubiquitylated protein levels (Fig 5.1 A, fourth panel, lane 10). As treatment of cells with the proteasome inhibitor bortezomib and autophagy inhibition with BafA1 generated a further increase in ubiquitylated MuRF1, we infer that ubiquitylated MuRF1 is accumulated due to decreased clearance by the autophagy pathway.

**A**



**B**

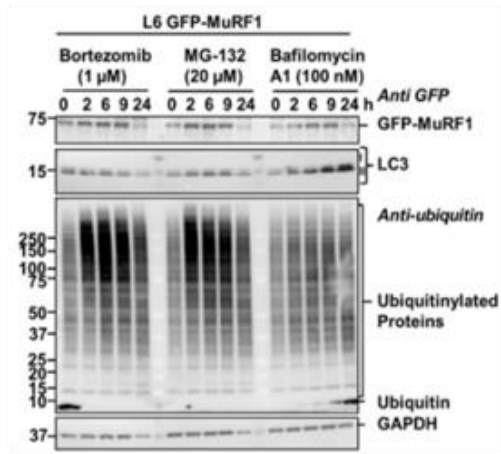
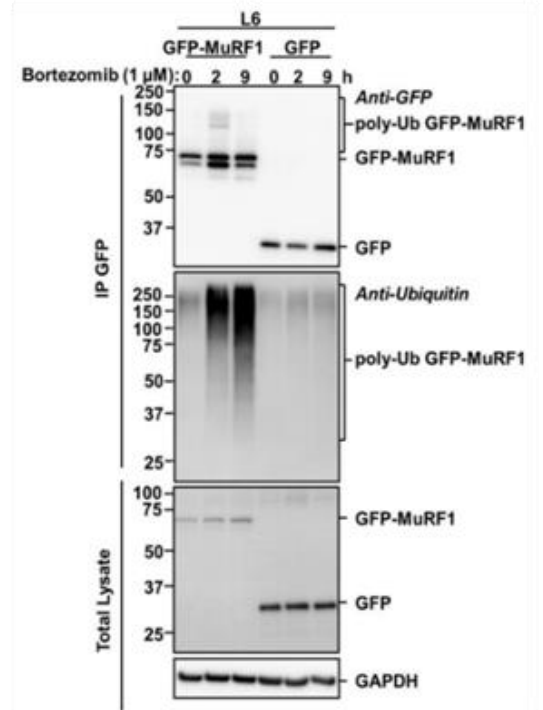
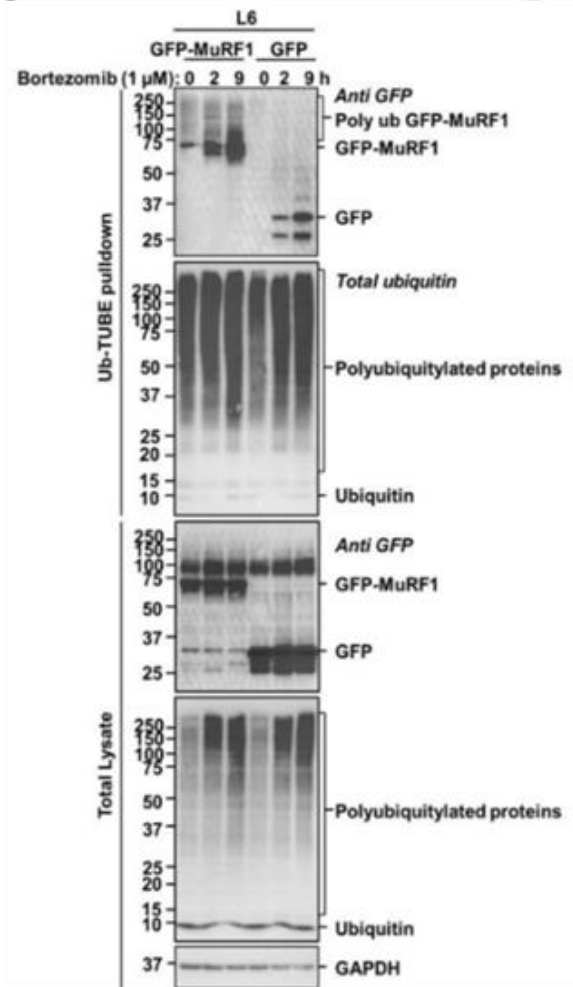
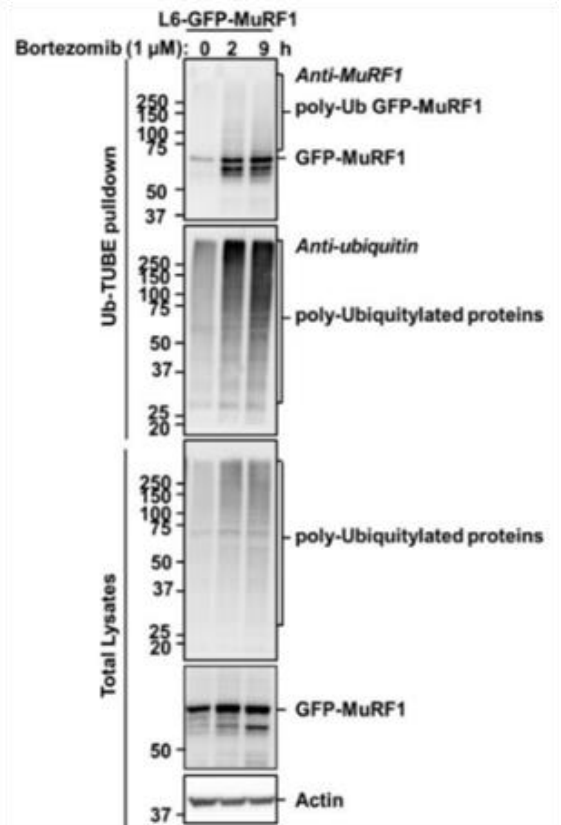


**Figure 5.1. Endogenous MuRF1 is stabilised by inhibition of the proteasome and autophagy in skeletal muscle.** (A) C2C12 mouse skeletal muscle myotubes pre-treated with dexamethasone for 24 h to induce atrophy were treated with bortezomib, MG132, and bafilomycin A1 for 0, 3, 15, 20, and 24 h, and MuRF1 expression was analysed by western blotting. (B) C2C12 mouse skeletal muscle myotubes pre-treated with dexamethasone for 24 h were treated with bortezomib for 0, 3, 15, 20, and 24 h before being immunoprecipitated using the MuRF1 antibody. Western blotting was used to analyse the immunoprecipitates and MuRF1 expression was detected using a MuRF1 antibody. The data are representative of three independent experiments.

#### **5.4.2 Exogenous MuRF1 is stabilised by inhibition of the proteasome and autophagy in skeletal muscle.**

Next, to determine the stability of the exogenous MuRF1 in skeletal muscle, a retrovirus encoding human MuRF1 protein fused with a GFP tag at the N-terminus or GFP alone was used to infect rat L6 skeletal muscle cells. We could not employ C2C12 stably expressing GFP-MuRF1 because we do not have the GFP alone control cells. Following differentiation for 6 days, we treated the myotubes with proteasome (bortezomib, MG132) and autophagy (Bafilomycin A1) inhibitors respectively. A 2-hour proteasome inhibition leads to the accumulation of MuRF1 protein content and was sustained for up to 9 h (Fig 5.2 A, upper panel, Lanes 2-4, and 8-10). Similarly, MuRF1 protein content was increased, but much slower after autophagy inhibition and was sustained up to 9 h (Fig 5.2 A, upper panel, Lanes 15-16). As expected, LC3 II proteins level were increased only in cells treated with bafilomycin A1 (Fig 5.2 A, second panel, lanes 14-17) indicating the blockage of autophagy functions. In addition, poly-ubiquitylated proteins level were increased only in cells treated with bortezomib (Fig 5.2 A, third panel, lanes 2-5); MG132 (Fig 5.2 A, third panel, lanes 8-10), indicating the blockage of proteasome functions. Notably, MuRF1 protein content was reduced considerably after 24 h of either proteasome or autophagy inhibition (Fig 5.2 A, upper panel, Lanes 5, 11, and 17), suggesting that 9 h might be the optimal treatment time to achieve proteasome and autophagy inhibition in L6 stably expressing GFP-MuRF1 cells. Consistently, GAPDH levels as a loading control were not changed by any of the treatments but were reduced considerably after 24 h of either proteasome or lysosome inhibition (Fig 5.2 A, fourth panel, Lanes 5, 11, and 17), suggesting a saturation of the 24 h treatments.

Because ubiquitylated proteins were accumulated in myotubes treated with proteasome inhibitors, we sought to establish whether MuRF1 is ubiquitylated before degradation. L6 myotubes that stably expressed GFP-MuRF1 or GFP alone (as a control) were treated with bortezomib to induce ubiquitylated protein accumulation. The myotubes were then lysed and collected in a sucrose lysis buffer containing 100 mM 2-chloroacetamide to inhibit de-ubiquitylation before being subjected to GFP pulldown using GFP-Trap agarose beads. The immunoprecipitates were extensively washed with IP sucrose lysis buffer supplemented with 150 mM NaCl to exclude non-specific protein binds to MuRF1. Probing the immunoblots containing the immunoprecipitated proteins with anti-GFP, we found mono-ubiquitylation and HMW products that resemble ubiquitylated species of the GFP-MuRF1 protein (Fig 5.2 B, upper panel, lanes 2 and 3). To ensure that MuRF1 and not its interacting proteins was ubiquitylated, same lysates were subjected to ubiquitin TUBE-pulldown analysis. Briefly, whole lysates were incubated with ubiquitin-binding resins derived from his-halo-ubiquitin 1 UBA domain tetramer (UBA<sup>UBQLN1</sup>) to captured ubiquitylated proteins. The captured ubiquitylated proteins were analysed by immunoblotting and probed with Anti-GFP antibody for MuRF1 ubiquitylation. We consistently found HMW MuRF1 species, suggesting that MuRF1 is specifically ubiquitylated as detected by a GFP antibody against the GFP tag MuRF1 (Fig 5.2 C, upper panel, lanes 2 and 3), and by a MuRF1 antibody (Fig 5.2 D, upper panel, lanes 2 and 3), respectively.

**A****B****C****D**

## **Figure 5.2. Exogenous MuRF1 is stabilised by inhibition of the proteasome and autophagy**

**in skeletal muscle.** (A) L6 rat skeletal muscle myotubes stably expressing GFP-MuRF1 were treated with bortezomib (1  $\mu$ M), MG132 (20  $\mu$ M), and bafilomycin A1 (100 nM) for 0, 2, 4, 6, 9 and 24 h. MuRF1 expression was then examined using western blotting. (B) L6 rat skeletal muscle stably expressing GFP-MuRF1 or GFP alone was treated with bortezomib for 0, 2, and 9 h prior to GFP-pulldown. The immunoprecipitates were analysed via SDS-PAGE, followed by detection with an anti-GFP antibody for MuRF1 expression and an anti-total ubiquitin antibody for MuRF1 ubiquitylation. (C) L6 rat skeletal muscles stably expressing GFP-MuRF1 or GFP alone were treated with bortezomib for 0, 2, and 9 h, before ubiquitin TUBE-pulldown. The immunoprecipitates were analysed via SDS-PAGE, followed by detection with a GFP tag antibody for MuRF1 ubiquitylation and a total ubiquitin antibody for ubiquitin expression. (D) L6 rat skeletal muscle stably expressing GFP-MuRF1 was treated with bortezomib for 0, 2, and 9 h before ubiquitin TUBE-pulldown. The immunoprecipitates were analysed via SDS-PAGE, followed by detection with the MuRF1 antibody for MuRF1 ubiquitylation and the total ubiquitin antibody for ubiquitin expression. The data are representative of three independent experiments.

### **5.4.3 MuRF1 ubiquitylation is not exclusively modified with K48 or K63 poly-ubiquitin chains in skeletal muscle.**

Next, we sought to determine whether the ubiquitylation of endogenous and exogenous MuRF1 is solely modified by k48 or k63 poly-ubiquitin chains. First, C2C12 myotubes pre-treated with dexamethasone (Dex. 100  $\mu$ M) for 24 h, were treated with the proteasome (bortezomib) and autophagy (bafilomycin A1) inhibitors before immunoblotting with anti-bodies specific to the different poly-ubiquitin chain types. As shown in Fig 5.3 A, the formations of K48- and K63-poly-ubiquitin chains were present in cells treated with proteasome and bafilomycin A1 inhibitors respectively. Interestingly, the K48 poly-ubiquitin chains (Fig 5.3 A, upper panel, lane 4) and K63 poly-ubiquitin chains (Fig 5.3 A, second panel, lane 4) exhibited additional increase when cells were treated with both inhibitors. These observations suggest that endogenous

MuRF1 is not exclusively modified with K48- or K63- poly-ubiquitin chains in skeletal muscle. Several Co-IP experiments to confirm the poly-ubiquitin chain types on modified endogenous MuRF1 were not successful. This is due to the limited availability of the poly-ubiquitin chain antibodies that recognize the endogenous MuRF1 bait protein. To close this gap, we employed the generated rat L6 skeletal muscle cell lines that stably expressed GFP-MuRF1 to confirm the characteristic chain types in the HMW GFP-MuRF1 species. Thus, we subjected extracts from L6 GFP-MuRF1 and L6 GFP myotubes under condition of proteasome inhibition to GFP pulldown. The immunoprecipitates were extensively washed with IP sucrose lysis buffer supplemented with 150 mM NaCl to exclude non-specific protein bounds to MuRF1 before detection by western blotting. Total lysate was also analysed as a positive control. The K48 poly-ubiquitin (Fig 5.3 B, upper panel, lanes 2 and 3) and K63 poly-ubiquitin chains (Fig 5.3 B, second panel, lanes 2 and 3) were present in the modified GFP-MuRF1 which was coimmunoprecipitated by a GFP pulldown. Taken together, these results suggest that ubiquitylation of endogenous and exogenous (epitope-tag) MuRF1 does not solely depend on K48- or K63- poly-ubiquitin chains.

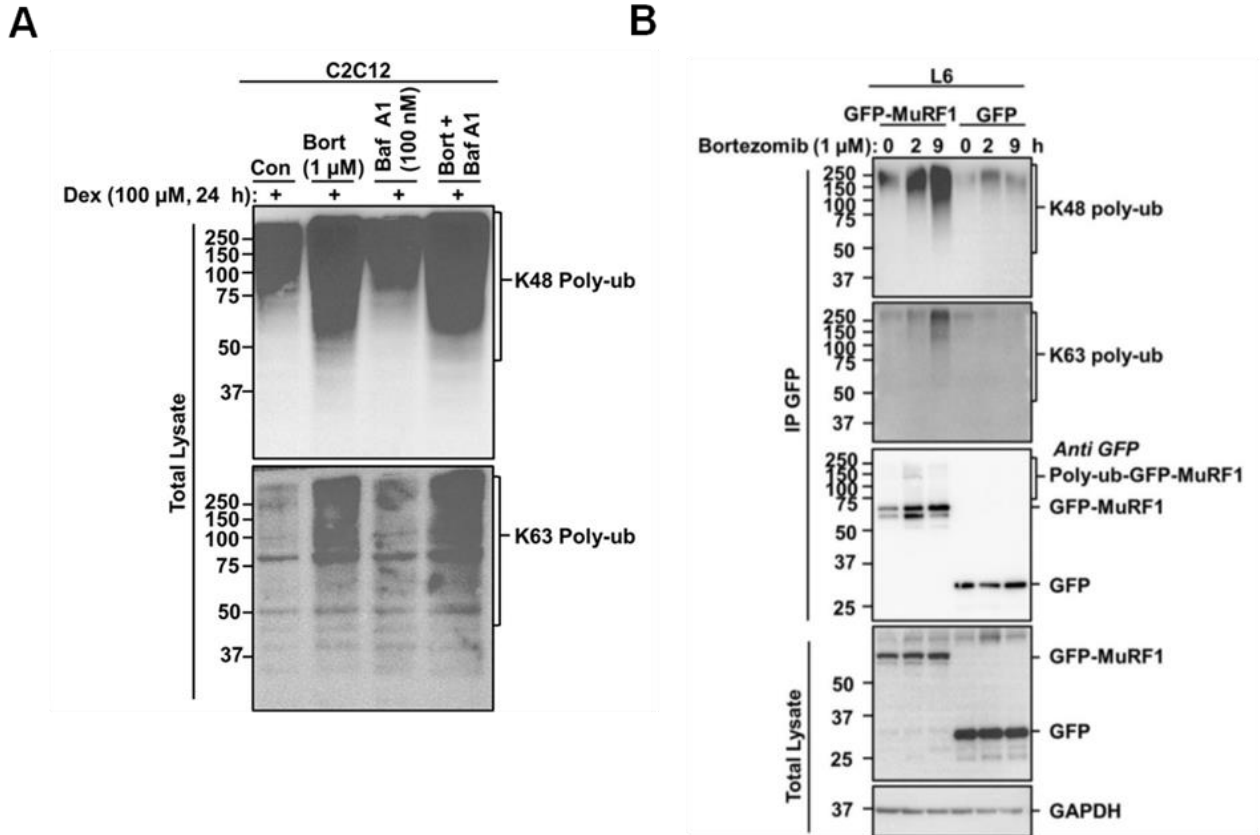
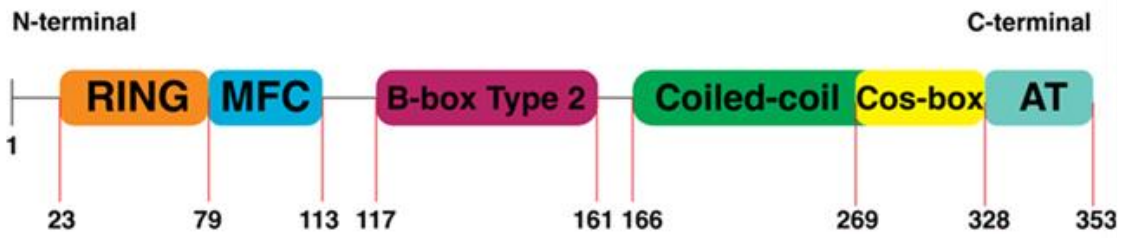


**Figure 5.3. MuRF1 ubiquitylation is not exclusively modified with K48 or K63 poly-ubiquitin chains in skeletal muscle.** (A) Endogenous MuRF1 undergoes Lys48- and Lys63-linked poly-ubiquitylation in C2C12 myotubes. Total lysates from C2C12 myotubes pre-treated with 100  $\mu$ M of dexamethasone (Dex) for 24 h, were treated with 1  $\mu$ M of bortezomib for 0, 2 and 9 h before immunoblotting with the indicated antibodies. (B) Exogenous MuRF1 undergoes Lys48- and Lys63-linked poly-ubiquitylation in L6 myotubes that stably expressed GFP-MuRF1. Total lysates (1 mg) from L6 myotubes that stably expressed GFP-MuRF1 or GFP-alone treated with 1  $\mu$ M bortezomib for 0, 2 and 9 h were subjected to GFP pulldown using GFP-Trap agarose beads. The immunoprecipitates were extensively washed with IP sucrose lysis buffer supplemented with 150 mM NaCl to exclude non-specific protein binds to MuRF1. The immunoprecipitates were analysed via immunoblotting before detecting with the indicated antibodies. The data are representative of three independent experiments.

#### **5.4.4 MuRF1 is the ubiquitin ligase that ubiquitylates itself in skeletal muscle.**

To determine whether MuRF1 stability is linked to auto-ubiquitylation, wild type and mutant RING GFP-MuRF1 at cysteine C23A that are stably expressed in C2C12 were first generated using a retroviral system (Fig 5.4 B). Following 6 days of differentiation, the proteasome inhibitor bortezomib was added for the indicated time. Control myotubes were treated with DMSO. The myotubes were then lysed and collected in a sucrose lysis buffer containing 100 mM 2-chloroacetamide to inhibit de-ubiquitylation before being subjected to GFP pulldown using GFP-Trap agarose beads. The immunoprecipitates were extensively washed with IP sucrose lysis buffer supplemented with 150 mM NaCl to exclude non-specific protein binds to MuRF1. Total lysate was also analysed as a positive control. Our result showed that wild-type GFP-MuRF1 undergo auto-ubiquitylation in the presence of an intact RING finger domain (Fig 5.4 C, upper panel, lane 2), however, in the RING finger mutant lanes, GFP-MuRF1 lacks the ability to undergo auto-ubiquitylation (Fig 5.4 C, upper panel, lane 4). Like other RING-type E3 ligases, MuRF1 auto-ubiquitylation requires intact RING finger domain. Because MuRF1 lost its auto-ubiquitylation ability when the cysteine C23 was mutated and replaced by C23A suggest that the C23 residues in the RING finger domain is essential for MuRF1 E3 ligase activity. Further reciprocal ubiquitin-TUBE pulldown assay confirmed that MuRF1 is specifically auto-ubiquitylated as detected by a GFP antibody against GFP-tag MuRF1 (Fig 5.4 D, upper panel, lane 2). GFP-MuRF1 lacks the ability to undergo auto-ubiquitylation (Fig 5.4 D, upper panel, lane 4). Taken together, these data suggest that MuRF1 undergo auto-ubiquitylation in skeletal muscle. Our result confirms the findings of earlier studies demonstrating MuRF1 auto-ubiquitylation in in vitro (82, 83) and in peripheral blood cells (81).

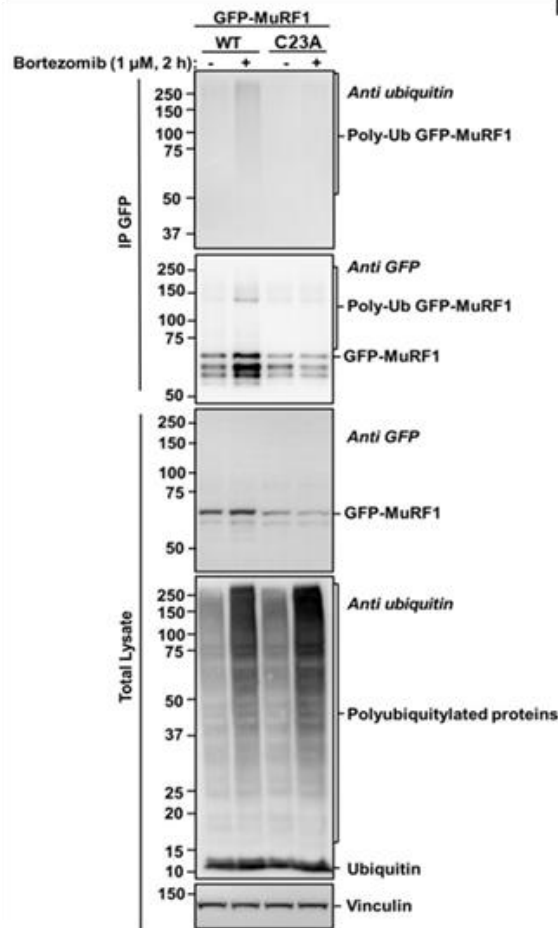
**A**



**B**



**C**



**D**

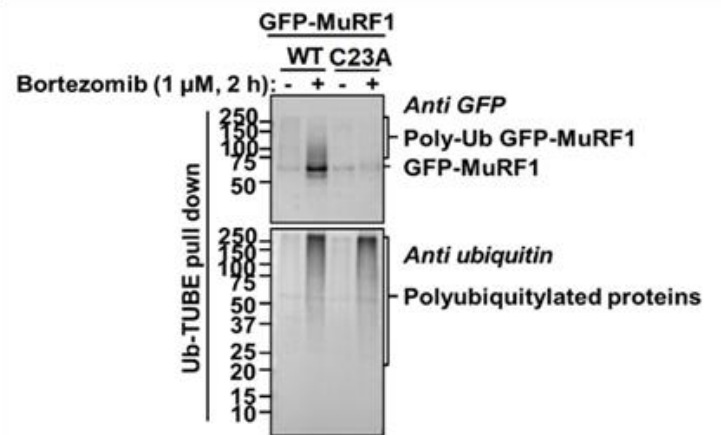


**Figure 5.4. MuRF1 undergoes auto-ubiquitylation in skeletal muscle.** (A) Human MuRF1 RING-B-box-coiled-coil domain (B) Sequence of the MuRF1 RING domain and mutant construct shown with RING finger mutation (*red*). (C) Total lysates (1 mg) from C2C12 myotubes that stably expressed GFP-MuRF1 or GFP-MuRF1 C23A (devoid of ubiquitin ligase activity) treated with 1  $\mu$ M bortezomib for 2 h were subjected to GFP pulldown using GFP-Trap agarose beads. The immunoprecipitates were extensively washed with IP sucrose lysis buffer supplemented with 150 mM NaCl to exclude non-specific protein binds to MuRF1. The immunoprecipitates were analysed by western blotting, followed by detection with a total ubiquitin antibody for MuRF1 auto-ubiquitylation and other indicated antibodies. (D) Total lysates (1 mg) from C2C12 myotubes that stably expressed GFP-MuRF1, or GFP-MuRF1, C23A (devoid of ubiquitin ligase activity) were treated with 1  $\mu$ M bortezomib, for 2 h before ubiquitin-TUBE pulldown to capture all the ubiquitylated proteins. The immunoprecipitates were analysed by western blotting, followed by detection with the GFP antibody for MuRF1 auto-ubiquitylation and the total ubiquitin antibody for ubiquitylated protein expression. 1  $\mu$ M bortezomib, a 26S proteasome inhibitor, was added for 2 h to prevent the GFP-MuRF1 from being rapidly degraded. The data are representative of three independent experiments.

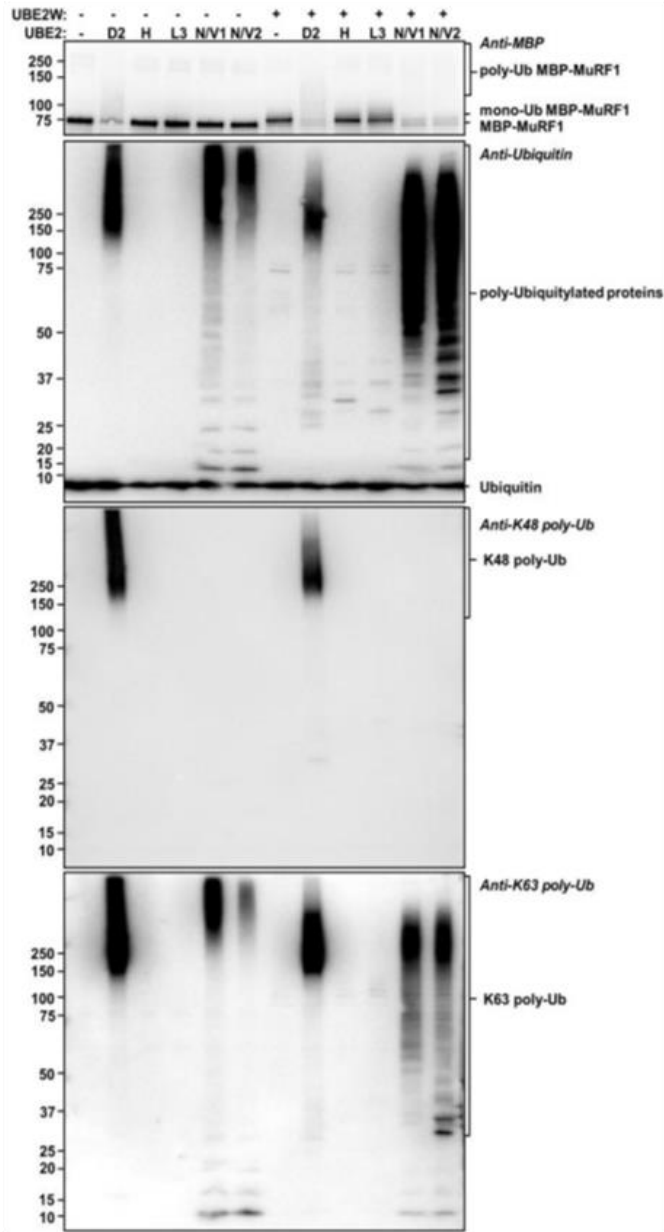
#### **5.4.5 The UBE2D, UBE2N/V1/2 and UBE2W ubiquitin-conjugating enzymes are required for MuRF1 auto-ubiquitylation *in vitro*.**

We next investigated the E2 ubiquitin-conjugating enzymes that partner with MuRF1 for its auto-ubiquitylation activity. Because MuRF1 auto-ubiquitylation generates K48- and K63- poly-ubiquitin chains, we sought to investigate the following E2 ubiquitin-conjugating enzymes that can form such chains *in vitro*. UBE2N is known to mediate K63 linkages, a signal for targeting misfolded proteins to the aggresomal-autophagy pathway (129, 130, 131). UBE2W has been shown to mediate mono-ubiquitylation as an anchor for the attachment of additional poly-ubiquitin chains (131, 132). UBE2D, which is known to mediate the formation of K48- poly-ubiquitin chains, promotes the auto-ubiquitylation of Cbl *in vitro* (82, 131). We therefore performed an *in vitro* ubiquitylation experiment to investigate this purpose. In the ubiquitylation reaction mixture, maltose-binding protein tagged MuRF1 (MBP-MuRF1) was expressed in bacteria (lacks ubiquitylation activity) and purified using amylose resin beads. MBP-MuRF1 was incubated with the reaction mixture containing ubiquitin, recombinant E1 enzyme, with/without various recombinant E2 enzymes (UBE2D2, UBE2N/V1, UBE2N/V2) and ATP in the presence or absence of UBE2W. In this reaction, MBP-MuRF1 functions as both potential E3 ligase and as a potential substrate. Negative controls were UBE2H and UBE2L3. Reactions were incubated for 1 hr at 37 °C and terminated by the addition of LDS Sample Buffer containing 1.25%  $\beta$ -mercaptoethanol before Western blotting, using the indicated antibodies. Our results show that the incubation of MBP-MuRF1 in the ubiquitylation reaction mixture containing UBE2H, UBE2L3, N/V1 or N/V2 did not lead to MBP-MuRF1 ubiquitylation (Fig 5.5 A, upper panel, lanes 3, 4, 5, and 6), whereas the incubation of MBP-MuRF1 in the ubiquitylation reaction containing UBE2D2 and UBE2W leads to both poly-ubiquitylation and mono-ubiquitylation of

MBP-MuRF1 respectively (Fig 5.5 A, upper panel, lanes 2 and 7). These results suggest that MuRF1 undergo auto-ubiquitylation that is directly catalysed by UBE2D2 and UBE2W enzymes respectively. Because UBE2W has been shown to mediate mono-ubiquitylation as an anchor for the attachment of additional poly-ubiquitin chains (131, 132), we sought to test this hypothesis with MuRF1. In a parallel ubiquitylation reaction containing recombinant UBE2D2, UBE2H, UBE2L, UBE2N/V1, or UBE2N/V2 enzymes in the presence of UBE2W show striking results. In the presence of UBE2W, UBE2D2 also catalyse MBP-MuRF1 poly-ubiquitylation (Fig 5.5 A, upper panel, lane 8). In the presence of UBE2W, the negative controls: UBE2H and UBE2L catalyse MuRF1 auto-mono-ubiquitylation implying that the mono-ubiquitin on MuRF1 was contributed by UBE2W (Fig 5 A, upper panel, lanes 9 and 10). Interestingly, the combination of UBE2N/V1 or UBE2N/V2 with UBE2W mediates the poly-ubiquitylation of MBP-MuRF1 (Fig 5.5 A, upper panel, lanes 11 and 12), implying that the mono-ubiquitin on MuRF1 acts as an anchor to attach the unanchored poly-ubiquitin chains formed by UBE2N/V1 or UBE2N/V2 (Fig 5.5, second panel, lanes 5 and 6) respectively. Our findings support the findings of previous study in which E3-ligase, TRIM5 $\alpha$ , partners with UBE2W to generate mono-ubiquitylation as an anchor to attach additional poly-ubiquitin chains (132). This modification was converted into anchored k48- and K63-poly-ubiquitin chains with further addition of UBE2D2 and UBE2N/V1 or UBE2N/V2 respectively. Because UBE2N is known to mediate K63 poly-ubiquitin chains (129, 130, 131), UBE2D can mediate the formation of K48- poly-ubiquitin chains (82, 131). We sought to identify the poly-ubiquitin specific chains that contribute to MuRF1 auto-ubiquitylation in vitro. Using antibody specific to K48 poly-ubiquitin chain and K63 poly-ubiquitin chain indicated that MBP-MuRF1 is not exclusively modified with K48- or K63- poly-ubiquitin chains in vitro like what we found in skeletal muscle. Taken together, these results

suggest that MuRF1 first undergoes auto-mono-ubiquitylation in the presence of UBE2W and this modification was converted into anchored poly-ubiquitin chains with further addition of UBE2D2 and UBE2N/V1 or UBE2N/V2 E2 enzymes respectively.

**A**



**B**

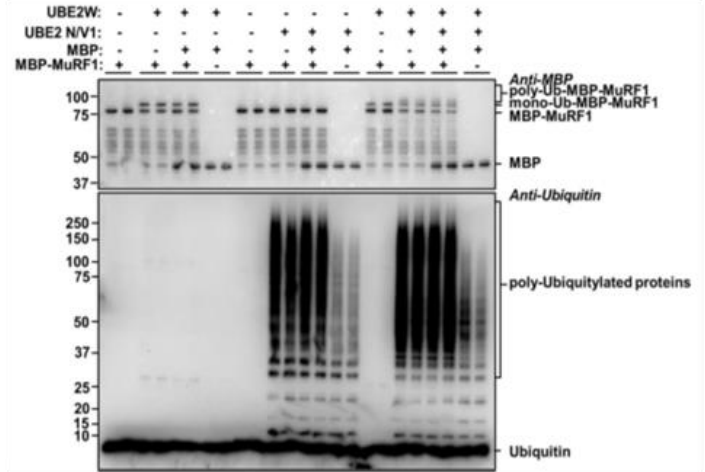


**Figure 5.5. MuRF1 auto-ubiquitylation is controlled by ubiquitin conjugating enzymes**

**UBE2s in vitro.** (A) UBE2s-dependent auto-ubiquitylation of recombinant MuRF1. Purified recombinant MBP-MuRF1 was incubated with the reaction mixture containing ubiquitin, recombinant E1 enzyme, with/without various recombinant E2 enzymes (UBE2D2, UBE2N/V1, UBE2N/V2) and ATP in the presence or absence of UBE2W. Negative controls were UBE2H and UBE2L3. Reactions were incubated for 1 hr at 37 °C and terminated by the addition of LDS Sample Buffer containing 1.25%  $\beta$ -mercaptoethanol before Western blotting, using antibody to MBP to detect both non-ubiquitylated and ubiquitylated MBP-MuRF1 (top panel), anti-ubiquitin antibody to detect ubiquitylated MBP-MuRF1 (second panel), anti-K48 poly-ubiquitin antibody to detect K48 poly-ubiquitin chain (third panel), and anti-K63 poly-ubiquitin antibody to detect K63 poly-ubiquitin chain (fourth panel). (B) Minimum requirements for the in vitro auto-ubiquitylation of MuRF1. In the in vitro ubiquitylation assay, the complete reaction mixture contained ubiquitin, E1 enzyme, E2 enzyme (UBE2N/V1), and ATP in the presence or absence of UBE2W. To determine the minimum requirements for the auto-ubiquitylation of MBP-MuRF1, MBP-MuRF1 was incubated in the incomplete reaction mixture lacking one of these components (lanes 1- 2, and 9-10). As a positive control, MBP-MuRF1 was incubated in the complete mixture (lanes 3-6, 11-14, and 17-22). As a negative control, MBP alone were incubated in the complete mixture (lanes 7-8, 15-16, and 23-24). Reactions were incubated for 1 hr at 37 °C and terminated by the addition of LDS sample buffer containing 1.25%  $\beta$ -mercaptoethanol followed by Western blotting, using antibody to MBP to detect both non-ubiquitylated and ubiquitylated MBP-MuRF1 (top panel), anti-ubiquitin antibody to detect ubiquitylated MBP-MuRF1 (second panel). The incomplete reaction mixture shown in lanes 1-2, and 9-10 lacked the E2 enzymes.

#### **5.4.6 MuRF1 function as an E3 ligase enzyme and ubiquitylates itself *in vitro***

Given that the E1, E2, and E3 proteins are the minimum requirement for a ubiquitylation to occur, we sought to know whether these enzymes are also essential for MuRF1 auto-ubiquitylation shown in Fig 5.5 B. Thus, another *in vitro* experiment was performed. As a positive control, maltose amylose resin beads tagged MuRF1 (MBP-MuRF1) were incubated in the complete reaction mixture containing ubiquitin, recombinant E1 enzyme, and UBE2N/V1 in the presence or absence of UBE2W (Fig 5.5 B, upper panel, lanes 3-6, 11-14, and 17-22). As a negative control, MBP-MuRF1 was incubated in the incomplete reaction mixture lacking one of these components (lanes 1- 2, and 9-10). Reactions were incubated for 1 hr at 37 °C and terminated by the addition of LDS sample buffer containing 1.25%  $\beta$ -mercaptoethanol followed by Western blotting, using antibody to MBP to detect both non-ubiquitylated and ubiquitylated MBP-MuRF1 (upper panel), anti-ubiquitin antibody to detect ubiquitylated MBP-MuRF1 (second panel). The incomplete reaction mixture shown in lanes 1-2, and 9-10 lacked the E2 enzymes. As shown in Fig 5.5 B, incubation of MBP-MuRF1 in the complete ubiquitylation reaction leads to ubiquitylation of MuRF1, but the incubation of MBP-MuRF1 in the incomplete ubiquitylation reaction do not leads to MBP-MuRF1 ubiquitylation (Fig 5.5 B upper panel, lanes 1- 2, and 9-10). Similarly, the incubation of MBP alone in the complete ubiquitylation reaction do not leads to MBP- ubiquitylation (Fig 5.5 B upper panel, lanes 7-8, 15-16, and 23-24). Because the ubiquitylation reaction where MBP-MuRF1 was ubiquitylated do not contains any E3 ligase other MuRF1 and MBP alone fails to ubiquitylate itself, suggest that MuRF1 functions as an E3 ligase and ubiquitylates itself *in vitro*.

## 5.5 Discussion

Using endogenous MuRF1, epitope-tagged MuRF1 from skeletal muscle cell lines, and recombinant MuRF1, we demonstrated that MuRF1 undergoes auto-ubiquitylation. However, MuRF1 auto-ubiquitylation was abolished by the point mutation of an essential cysteine residue at position 23 to alanine (C23A) in the RING domain. Furthermore, we show that MuRF1 catalyses the addition of K48- and K63-specific poly-ubiquitin chains to itself in skeletal muscle. We show that MuRF1 auto-ubiquitylation regulates its own stability in skeletal muscles. Our *in vitro* study using purified proteins shows a 2-step mechanism of MuRF1 auto-ubiquitylation, where recombinant MuRF1 first undergoes auto-mono-ubiquitylation in the presence of UBE2W and this modification was converted into anchored poly-ubiquitin chains with further addition of UBE2D2 and UBE2N/V1, or UBE2N/V2, respectively. Our data add MuRF1 to the growing list of E3 ubiquitin ligases shown to undergo UBE2W-dependent auto-mono-ubiquitylation *in vitro* (132, 133, 134, 135, 136). The cooperation between UBE2W and UBE2N/V has also been reported *in vitro* (132, 133, 135). Our novel findings provide an impetus for further exploration of the role of MuRF1 auto-ubiquitylation in the regulation of skeletal muscle mass.

Our findings suggest that auto-ubiquitylated MuRF1 could degrade MuRF1 via the canonical proteasome and the autophagy lysosomal pathway via a crosstalk mechanism. Bortezomib treatment reduced MuRF1 protein abundance with increasing higher molecular weight product as early as 15 h, which we confirmed as auto-ubiquitylation of MuRF1. This suggests that MuRF1 undergoes the proteasomal degradation. In contrast, bafilomycin A1 treatment increase MuRF1 protein content (Fig 1 A upper panel, lanes 8 and 9) at 20 h, which is a much slower rate than bortezomib. This supports the notion that proteasome degrades short-lived protein, whereas the

autophagy degrades long-lived protein (127). When bortezomib and bafilomycin A1 treatments were combined, MuRF1 protein abundance was accumulated more compared to bortezomib treatment alone. This evidence suggests that the activation of autophagy further enhanced the clearance of poly-ubiquitylated MuRF1 protein, demonstrating a crosstalk between the proteasomal and lysosomal-mediated degradation (8).

In the present study we show that proteasome inhibition-mediated poly-ubiquitylation of the MuRF1 was dependent on the formation of both K48- and K63-linked poly-ubiquitylation. A previous report provide evidence that both K48- and K63-linked poly-ubiquitin chains can be recognised by cargo receptors (P62 and NBR1) (137). In accordance with this, we found increase in the P62 protein level following proteasome inhibition-mediated poly-ubiquitylation of MuRF1, suggesting that the ubiquitylated MuRF1 could serves as substrate to P62 for autophagy degradation. It is well known that the proteasome mainly degrades unfolded proteins (30). When accumulated proteins become difficult to unfold, autophagy becomes the main degradative pathway for the removal of these abnormally folded proteins (138). Taken together, our data suggest that autophagy is critical for the stability of MuRF1 and is probably the main degradative pathway for the removal of the abnormally folded ubiquitylated MuRF1.

Our findings suggest that MuRF1 stability is regulated by its auto-ubiquitylation. The participation of MuRF1 in the ubiquitin-proteasome system owing to its RING finger domain is again mirrored in the protein stability experiments. We observed that when WT MuRF1 was overexpressed exogenously in skeletal muscle under proteasome inhibition, MuRF1 undergoes auto-ubiquitylation, which leads to the proteasomal degradation. However, MuRF1 auto-

ubiquitylation was abolished by the RING finger mutant MuRF1 at C23A in the RING domain. MuRF1 lost its auto-ubiquitylation ability when the cysteine C23 was mutated and replaced by C23A suggesting that the C23 residues in the RING finger domain of MuRF1 is essential for MuRF1 E3 ligase activity. This finding suggests that the higher molecular weight species observed on the wild-type MuRF1 was due to its ubiquitylation and could be a negative feedback mechanism that regulate its stability (139). This may help explain why MuRF1 overexpression in mice results in MuRF1 ubiquitylation on 16 lysine sites and skeletal muscle atrophy, whereas the MuRF1 RING domain mutant at C44S/C47S attenuates skeletal muscle atrophy (51). Our findings are in line with the previous evidence that auto-ubiquitylation and the subsequent auto-degradation of E6-AP (140), Mdm2 (141), and CBL (142) E3 ligases serves as a negative feedback mechanisms for their stability.

MuRF1 is a RING-type E3 ligase with no catalytic activity, but depends on its E2 partner that brings the catalytic activity (143). We show that MuRF1 requires UBE2W, UBE2D2, UBE2N/V1, and UBE2N/V2 for its auto-ubiquitylation in vitro. However, the E2 ubiquitin-conjugating enzymes that partner with MuRF1 and catalyse poly-ubiquitin chains remain to be confirmed in skeletal muscle. Our in vitro data shows that MuRF1 catalyses the formation of K48- and K63-poly-ubiquitin chains in a two-step mechanism by partnering with multiple E2 ubiquitin-conjugating enzymes. In this present finding, MuRF1 first undergoes auto-mono-ubiquitylation in the presence of UBE2W and this modification was converted into anchored k48- and K63-poly-ubiquitin chains with further addition of UBE2D2 and UBE2N/V1 or UBE2N/V2 respectively. Our findings are consistent with that of a previous study where another TRIM protein, TRIM5 alpha first undergoes auto-mono-ubiquitylation in the presence of

UBE2W and this modification was converted into anchored poly-ubiquitin chains with further addition of UBE2N/V1 (131, 132). In addition, previous studies have also shown that UBE2N can generate unanchored K63 poly-ubiquitin chain (129, 130, 131, 132) and UBE2D can generate K48-poly-ubiquitin chains (82, 131). Although our findings have provided the first evidence towards understanding the role of MuRF1 auto-ubiquitylation mechanisms in the catabolic process of skeletal muscle atrophy, future studies should determine the mechanistic roles of MuRF1 auto-ubiquitylation in skeletal muscle atrophy. Although we have demonstrated MuRF1 auto-ubiquitylation and its stability using cell-based skeletal muscle cell lines, future studies should examine auto-ubiquitylation of MuRF1 *in vivo*.

## **5.6 Conclusion**

Employing an established ubiquitin-TUBE pulldown strategy, we have demonstrated MuRF1 auto-ubiquitylation and its stability in skeletal muscle (Fig 5.6). MuRF1 auto-ubiquitylation-mediated K48- and K63-poly-ubiquitin chains signal autophagy-mediated auto-degradation of MuRF1. A mutation of C23A in the RING domain of MuRF1 abolished MuRF1 auto-ubiquitylation, making the cysteine 23 residue, one of the key players in the catabolic process of skeletal muscle atrophy. A novel two-step mechanism of MuRF1 auto-ubiquitylation was found *in vitro*, where recombinant MuRF1 first undergoes auto-mono-ubiquitylation in the presence of UBE2W, which in turn, convert into anchored poly-ubiquitin chains with further addition of UBE2D2 and UBE2N/V1, or UBE2N/V2, respectively.

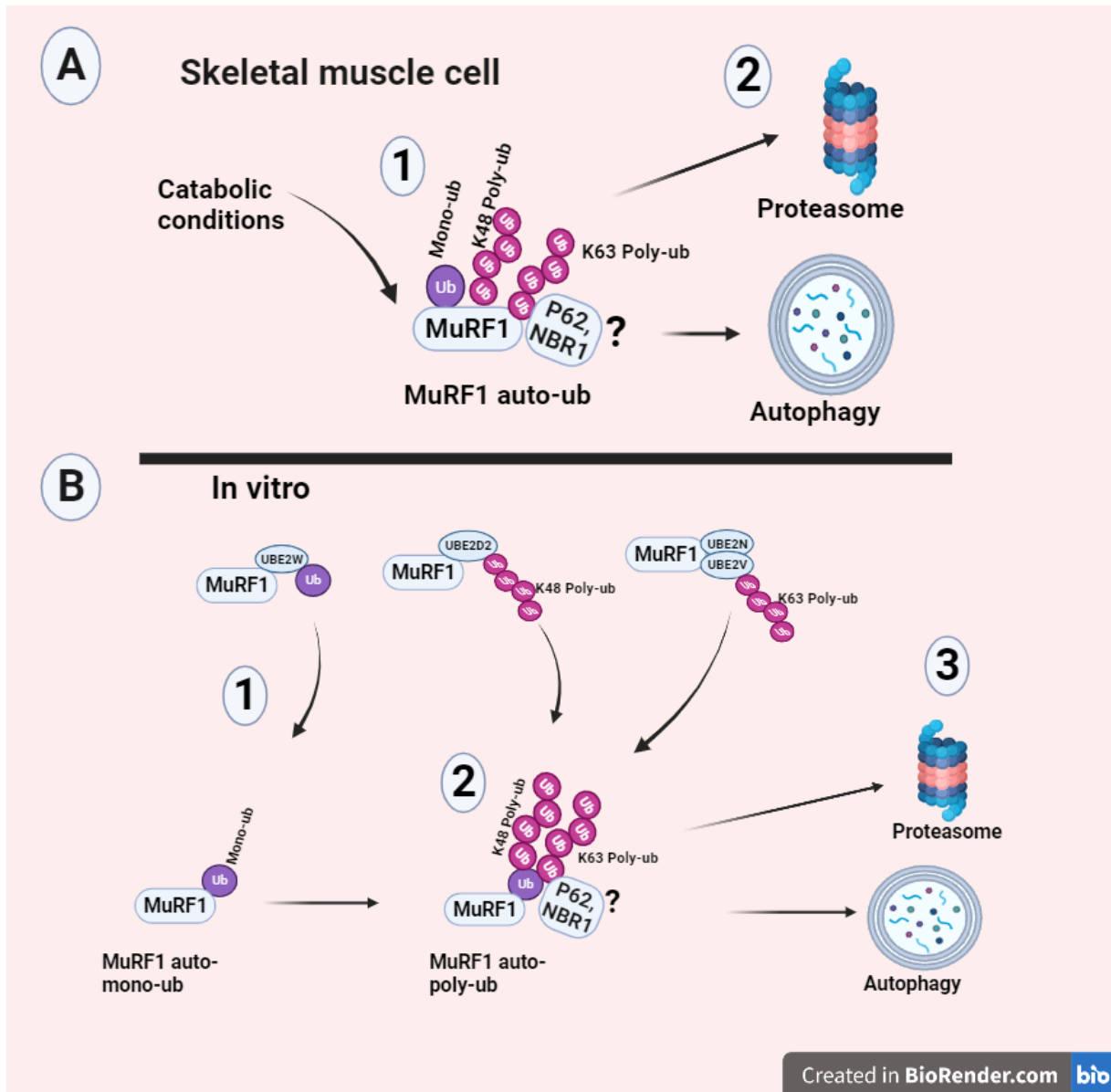


**Figure 5.6. A working model of MuRF1 auto-ubiquitylation** (A) MuRF1 auto-ubiquitylation in skeletal muscle. (1) Under catabolic conditions (Dex induced or overexpressed MuRF1), MuRF1 catalyses mono-ubiquitylation, K48, and K63 poly-ubiquitin chains to itself. (2) MuRF1 auto-ubiquitylation degrades MuRF1 via proteasome and autophagy via a crosstalk mechanism. (B) A two-step MuRF1 auto-ubiquitylation in vitro. (1) Recombinant MuRF1 first undergoes auto-mono-ubiquitylation with cognate UBE2W. (2) Mono-ubiquitylation on MuRF1 serves as an anchor to anchors K48 and K63- poly-ubiquitin chains with further addition of UBE2D2 and UBE2N/V respectively. (3) MuRF1 auto-ubiquitylation degrades MuRF1 via proteasome and autophagy via a crosstalk mechanism.

---

**CHAPTER 6**  
**GENERAL DISCUSSION**

---

## **6.1 GENERAL DISCUSSION**

The purpose of this thesis is to examine MuRF1's molecular role and its stability in the skeletal muscle. Skeletal muscle atrophy has been linked to various impairments, including muscle insulin resistance, with a significant negative impact on independence and quality of life. Thus, gaining a deeper understanding of MuRF1's molecular role and its stability in the regulation of skeletal muscle mass will help in the manipulation of the signalling molecules in future therapeutic strategies towards achieving healthy skeletal muscle mass.

Studies previously conducted have identified MuRF1 to be a valid marker for skeletal muscle atrophy (51, 52). However, how MuRF1 regulates skeletal muscle mass at the molecular level remain poorly understood. The inadequate research tools and techniques have narrowed skeletal muscle atrophy research over the previous years. Research has focused on gene expression of MuRF1 in wild type and knockout MuRF1 mice under conditions of atrophy. In these earlier studies, MuRF1 is consistently overexpressed in nearly all the skeletal muscle atrophy conditions in mice (49). In contrast, MuRF1 gene deletion partially prevented skeletal muscle from atrophy (51, 52). Given that MuRF1 is an excellent therapeutic target to prevent atrophy conditions, a better understanding of the molecular role of MuRF1 is necessary to establish an effective therapeutic strategy to ameliorate skeletal muscle atrophy.

Studies conducted in the quest to identify the interacting partners of MuRF1, have revealed multiple roles for MuRF1. While MuRF1 is crucial in the degradation of myofibrillar proteins (61, 62), other studies suggest that MuRF1 may also control a number of other non-degradative cellular functions, including protein ubiquitylation (51, 64), amino acid and carbohydrate

metabolism (66), fatty acid oxidation (75), mitochondrial function (76), apoptosis (77), endoplasmic reticulum (ER) stress response (78), and insulin resistance (54). Because MuRF1 also regulates other functions besides causing skeletal muscle atrophy, deleting MuRF1 as an option may have negative effects on other pathways and may be detrimental to muscle health. Consistently, report from a previous study indicates that Mutant MuRF1 impaired muscle protein degradation and induced hypertrophic cardiomyopathy in human (53). In addition, in one recent study, MuRF1 overexpression was sufficient to cause atrophy (51), but most of its ubiquitylated targets do not undergo degradation (51) which suggests that another co-partner is necessary.

After successfully generating skeletal muscle cell lines stably expressing GFP-MuRF1 (for the MuRF1 protein interaction study) and GFP-MuRF1 RING finger mutant at C23A (for the MuRF1 E3 ligase activity study), including MuRF1 KO (for the MuRF1 functional study), and GFP-MuRF1 knock-in (for the MuRF1 protein interaction study) using retroviral and CRISPR/Cas9 gene editing systems (Chapter 3).

Firstly, we show that the tripartite motif-containing protein 72 (TRIM72) is a novel interacting partner of MuRF1 in skeletal muscle (Chapter 4.; Figure 4.1). Importantly, the knockout and rescue experiments of MuRF1 demonstrated that TRIM72 protein abundance is positively correlated with MuRF1 protein expression (Chapter 4.; Figure 4.2). Consistently, TRIM72 protein abundance was increased by dexamethasone treatment in C2C12 myotubes, alongside MuRF1 protein expression (Chapter 4.; Figure 4.4). Interestingly, our observation in Chapter 4 (Figure 4.2) match what has been found in a recent study, where MuRF1 and TRIM72 were

downregulated in tibialis anterior (TA) muscle after MuRF1 inhibitor (MyoMed 205) was administered to obese ZSF1 rats (108). Taken together, these data clearly demonstrate that MuRF1 is required to stabilize TRIM72 in skeletal muscle. Further analysis indicate that dexamethasone treatment decreases IRS1/Akt signalling, protein synthesis, and glucose uptake in wild type myotubes, but not in MuRF1 KO myotubes (Chapter 4., Fig 4). These data suggest that MuRF1 decrease insulin induced protein synthesis and induced muscle insulin resistance by interacting and stabilising TRIM72 in dexamethasone treated C2C12 myotubes. Consistent with this propose mechanism of MuRF1, subsequent study, showed that overexpression of TRIM72, sufficiently impairs IRS1/Akt signalling in MuRF1 KO myotubes (Chapter 4.; Figure 4.5).

Previous study had suggested that TRIM72 overexpression induced muscle insulin resistance by mediating the ubiquitylation and degradation of IRS1 protein via its E3 ligase activity (71, 72). Muscle insulin resistance has been generally considered to be the major defect in type 2 diabetic patient (144). Consistent with this notion, several studies have reported that TRIM72 is significantly increased in diabetic animal and humans (71, 115, 145, 146). This is indeed a novel molecular mechanism by which MuRF1 could regulates skeletal muscle mass, in addition to its known degradative roles.

Importantly, these present findings are consistent with a previous study, where it was reported that immobilisation induced-atrophy leads to muscle insulin resistance in humans by reducing insulin-induced glucose uptake (147, 148). However, these earlier studies were unable to provide clear mechanism by which immobilisation induced atrophy leads to muscle insulin resistance.

Here, we propose a mechanism that during atrophy events, MuRF1 interacts and stabilise TRIM72 to induced muscle insulin resistance that impairs insulin induced-glucose uptake. A previous study also shows that a reduction in the activity of key signalling molecules regulating glucose uptake in immobilised induced-muscle atrophy (149).

Lastly, increased muscle protein breakdown mediated by the ubiquitin-proteasome and the autophagic system are also associated with skeletal muscle atrophy. Thus, one strategy to prevent skeletal muscle atrophy and to improve patients' condition would be to regulate the activities of the UPS or its ubiquitylating enzymes. As highlighted in chapter 5, we show that overexpressed MuRF1 undergoes auto-ubiquitylation in skeletal muscle. A mutation of C23A in the RING domain of MuRF1 abolished MuRF1 auto-ubiquitylation, indicating the importance of the RING domain in the catabolic process of skeletal muscle atrophy. MuRF1 catalyses the addition of mono-ubiquitylation, K48-, and K63- specific poly-ubiquitin chains to itself in skeletal muscle. MuRF1 auto-ubiquitylation-mediated K48- and K63-poly-ubiquitin chains signal proteasome- and autophagy-mediated auto-degradation of MuRF1. The activation of autophagy further enhanced the clearance of poly-ubiquitylated MuRF1 protein, demonstrating a crosstalk between the proteasomal and lysosomal-mediated degradation. Though the mechanism involved is not well understood. Further in vitro analysis reflects similar result as in the skeletal muscle; MuRF1 interacts with cognate UBE2D, UBE2N/Vs and UBE2W to catalyse mono-ubiquitylation, K48, and K63 specific poly-ubiquitin chains in a UBE2-dependent manner. A novel two-step mechanism of MuRF1 auto-ubiquitylation was found in vitro, where recombinant MuRF1 first undergoes auto-mono-ubiquitylation with cognate UBE2W to serves as an anchor for UBE2D2 and UBE2N/V1, or UBE2N/V2 generated poly-ubiquitin chains, respectively. Overall, we show

novel mechanisms for protein stability of MuRF1 in skeletal muscle. This suggest another strategy, whereby MuRF1 or the UPS activities can be restricted until when required.

## **6.2 Limitations**

The use of cell-based skeletal muscle cells to study MuRF1's molecular function and stability in skeletal muscle is a big limitation. Although cell-based skeletal muscle models can provide valuable molecular insights into muscle-specific signalling, they do not fully mimic mature skeletal muscle tissue. This is because mature skeletal muscle tissue consists of neurons, blood vessels, smooth muscle cells, fibroblasts, and immunological cells. This clearly indicates that the structural composition and metabolic demands of mature skeletal muscle tissue differ from those of cell-based skeletal muscle cells. In addition, these various cell types could contribute to the muscle's diverse functions. Based on these significant differences, it is important to consider that findings made in cell-based skeletal muscle may not reflect those made in mature skeletal muscle tissue.

Another notable limitation of this thesis is the absence of *in vivo* data. Despite the recent developed MuRF1 knockout mouse model by Sue Bodine's laboratory at the Oklahoma Medical Research Foundation, USA (49), through collaboration and a kindly donation of frozen lysates, it was not possible conducting experiments using these lysates. The reason is that validation of MuRF1 protein expression via western blot has been difficult because MuRF1 protein bands were indeed visible in the lanes containing samples from MuRF1 knockout mice. Thus, MuRF1 protein levels could not accurately be quantified. This observation has been reported by a

previous study and the authors concluded that most of the commercially available MuRF1 antibodies lack specificity in mice (150).

### **6.3 Conclusion**

In conclusion, the present thesis contributes a novel finding towards our understanding of the molecular function of MuRF1 and its stability in skeletal muscle. Specifically, the findings in this present thesis demonstrate that MuRF1 down regulate muscle protein synthesis and mediates muscle insulin resistance by interacting and stabilising TRIM72 protein in skeletal muscle. Furthermore, this thesis also demonstrates that overexpressed MuRF1 undergoes auto-ubiquitylation via K48-and K63-poly-ubiquitin chains to regulate its own stability in skeletal muscle. A mutation of C23A in the RING domain of MuRF1 abolished MuRF1 auto-ubiquitylation, indicating the importance of the RING domain in the catabolic process of skeletal muscle atrophy. The activation of autophagy further enhanced the clearance of poly-ubiquitylated MuRF1 protein, demonstrating a crosstalk between the proteasomal and lysosomal-mediated degradation. A novel two-step mechanism of MuRF1 auto-ubiquitylation was found in vitro, where recombinant MuRF1 first undergoes auto-mono-ubiquitylation in the presence of UBE2W and was converted into anchored poly-ubiquitin chains with further addition of UBE2D2 and UBE2N/V1, or UBE2N/V2, respectively.

---

**CHAPTER 7**  
**REFERENCE**

---

1. Frontera WR, Ochala J. Skeletal muscle: a brief review of structure and function. *Calcif Tissue Int.* 2015;96(3):183-95.
2. Baskin KK, Winders BR, Olson EN. Muscle as a "mediator" of systemic metabolism. *Cell Metab.* 2015;21(2):237-48.
3. Defronza RA, Jacot, E., Jequier, E., Maeder, E., Wahren, J., and Felber, J. P. The Effect of Insulin on the Disposal of Intravenous Glucose Results from Indirect Calorimetry and Hepatic and Femoral Venous Catheterization  
DIABETES. 1981;30:8.
4. Rai M, Demontis F. Systemic Nutrient and Stress Signaling via Myokines and Myometabolites. *Annu Rev Physiol.* 2016;78:85-107.
5. Argiles JM, Campos N, Lopez-Pedrosa JM, Rueda R, Rodriguez-Manas L. Skeletal Muscle Regulates Metabolism via Interorgan Crosstalk: Roles in Health and Disease. *J Am Med Dir Assoc.* 2016;17(9):789-96.
6. Meyer CD, M. J. Welle L. S. & Gerich E. J. . Role of human liver, kidney, and skeletal muscle in postprandial glucose homeostasis. *Am J Physiol Endocrinol Metab.* 2002;282:9.
7. Sartori R, Romanello V, Sandri M. Mechanisms of muscle atrophy and hypertrophy: implications in health and disease. *Nat Commun.* 2021;12(1):330.
8. Nishimura Y, Musa I, Holm L, Lai YC. Recent advances in measuring and understanding the regulation of exercise-mediated protein degradation in skeletal muscle. *Am J Physiol Cell Physiol.* 2021;321(2):C276-C87.
9. Bodine SC, Stitt TN, Gonzalez M, Kline WO, Stover GL, Bauerlein R, et al. Akt/mTOR pathway is a crucial regulator of skeletal muscle hypertrophy and can prevent muscle atrophy in vivo. *Nat Cell Biol.* 2001;3(11):1014-9.
10. Sandri M. Signaling in muscle atrophy and hypertrophy. *Physiology (Bethesda).* 2008;23:160-70.
11. Jacinto E, Facchinetti V, Liu D, Soto N, Wei S, Jung SY, et al. SIN1/MIP1 maintains rictor-mTOR complex integrity and regulates Akt phosphorylation and substrate specificity. *Cell.* 2006;127(1):125-37.
12. Sarbassov DD, Ali SM, Sabatini DM. Growing roles for the mTOR pathway. *Curr Opin Cell Biol.* 2005;17(6):596-603.
13. Sandri M, Sandri C, Gilbert A, Skurk C, Calabria E, Picard A, et al. Foxo Transcription Factors Induce the Atrophy-Related Ubiquitin Ligase Atrogin-1 and Cause Skeletal Muscle Atrophy. *Cell.* 2004;117(3):399-412.
14. Stitt TN, Drujan D, Clarke BA, Panaro F, Timofeyeva Y, Kline WO, et al. The IGF-1/PI3K/Akt pathway prevents expression of muscle atrophy-induced ubiquitin ligases by inhibiting FOXO transcription factors. *Mol Cell.* 2004;14(3):395-403.
15. Ito N, Ruegg UT, Takeda S. ATP-Induced Increase in Intracellular Calcium Levels and Subsequent Activation of mTOR as Regulators of Skeletal Muscle Hypertrophy. *Int J Mol Sci.* 2018;19(9).
16. Rommel C, Bodine SC, Clarke BA, Rossman R, Nunez L, Stitt TN, et al. Mediation of IGF-1-induced skeletal myotube hypertrophy by PI(3)K/Akt/mTOR and PI(3)K/Akt/GSK3 pathways. *Nat Cell Biol.* 2001;3(11):1009-13.

17. Peng XD, Xu PZ, Chen ML, Hahn-Windgassen A, Skeen J, Jacobs J, et al. Dwarfism, impaired skin development, skeletal muscle atrophy, delayed bone development, and impeded adipogenesis in mice lacking Akt1 and Akt2. *Genes Dev.* 2003;17(11):1352-65.
18. Pallafacchina G, Calabria E, Serrano AL, Kalhovde JM, Schiaffino S. A protein kinase B-dependent and rapamycin-sensitive pathway controls skeletal muscle growth but not fiber type specification. *Proc Natl Acad Sci U S A.* 2002;99(14):9213-8.
19. Rossetti ML, Fukuda DH, Gordon BS. Androgens induce growth of the limb skeletal muscles in a rapamycin-insensitive manner. *Am J Physiol Regul Integr Comp Physiol.* 2018;315(4):R721-r9.
20. Collins GA, Goldberg AL. The Logic of the 26S Proteasome. *Cell.* 2017;169(5):792-806.
21. Masiero E, Agatea L, Mammucari C, Blaauw B, Loro E, Komatsu M, et al. Autophagy is required to maintain muscle mass. *Cell Metab.* 2009;10(6):507-15.
22. Costelli P, Reffo P, Penna F, Autelli R, Bonelli G, Baccino FM. Ca(2+)-dependent proteolysis in muscle wasting. *Int J Biochem Cell Biol.* 2005;37(10):2134-46.
23. Du J, Wang X, Miereles C, Bailey JL, Debigare R, Zheng B, et al. Activation of caspase-3 is an initial step triggering accelerated muscle proteolysis in catabolic conditions. *J Clin Invest.* 2004;113(1):115-23.
24. Park J, Cho J, Song EJ. Ubiquitin-proteasome system (UPS) as a target for anticancer treatment. *Arch Pharm Res.* 2020;43(11):1144-61.
25. Zhao J, Zhai B, Gygi SP, Goldberg AL. mTOR inhibition activates overall protein degradation by the ubiquitin proteasome system as well as by autophagy. *Proc Natl Acad Sci U S A.* 2015;112(52):15790-7.
26. Vainshtein A, Sandri M. Signaling pathways that control muscle mass. *International journal of molecular sciences.* 2020;21(13):4759.
27. Yin L, Li N, Jia W, Wang N, Liang M, Yang X, et al. Skeletal muscle atrophy: From mechanisms to treatments. *Pharmacol Res.* 2021;172:105807.
28. Komander D, Rape M. The ubiquitin code. *Annual review of biochemistry.* 2012;81:203-29.
29. Kulathu Y, Komander D. Atypical ubiquitylation - the unexplored world of polyubiquitin beyond Lys48 and Lys63 linkages. *Nat Rev Mol Cell Biol.* 2012;13(8):508-23.
30. Baumeister W, Walz J, Zühl F, Seemüller E. The proteasome: paradigm of a self-compartmentalizing protease. *Cell.* 1998;92(3):367-80.
31. Ohtake F, Saeki Y, Ishido S, Kanno J, Tanaka K. The K48-K63 Branched Ubiquitin Chain Regulates NF- $\kappa$ B Signaling. *Molecular cell.* 2016;64(2):251-66.
32. Ohtake F, Tsuchiya H, Saeki Y, Tanaka K. K63 ubiquitylation triggers proteasomal degradation by seeding branched ubiquitin chains. *Proceedings of the National Academy of Sciences of the United States of America.* 2018;115(7):E1401-E8.
33. Yau RG, Doerner K, Castellanos ER, Haakonsen DL, Werner A, Wang N, et al. Assembly and Function of Heterotypic Ubiquitin Chains in Cell-Cycle and Protein Quality Control. *Cell.* 2017;171(4):918-33 e20.
34. Bachiller S, Alonso-Bellido IM, Real LM, Pérez-Villegas EM, Venero JL, Deierborg T, et al. The Ubiquitin Proteasome System in Neuromuscular Disorders: Moving Beyond Movement. *Int J Mol Sci.* 2020;21(17).

35. Peris-Moreno D, Taillandier D, Polge C. MuRF1/TRIM63, Master Regulator of Muscle Mass. *Int J Mol Sci.* 2020;21(18).
36. Amemiya Y, Azmi P, Seth A. Autoubiquitination of BCA2 RING E3 ligase regulates its own stability and affects cell migration. *Mol Cancer Res.* 2008;6(9):1385-96.
37. Jackman RW, Kandarian SC. The molecular basis of skeletal muscle atrophy. *Am J Physiol Cell Physiol.* 2004;287(4):C834-43.
38. Lecker SH, Jagoe RT, Gilbert A, Gomes M, Baracos V, Bailey J, et al. Multiple types of skeletal muscle atrophy involve a common program of changes in gene expression. *FASEB J.* 2004;18(1):39-51.
39. Fitts RH, Romatowski JG, Peters JR, Paddon-Jones D, Wolfe RR, Ferrando AA. The deleterious effects of bed rest on human skeletal muscle fibers are exacerbated by hypercortisolemia and ameliorated by dietary supplementation. *Am J Physiol Cell Physiol.* 2007;293(1):C313-20.
40. Huang L, Li M, Deng C, Qiu J, Wang K, Chang M, et al. Potential Therapeutic Strategies for Skeletal Muscle Atrophy. *Antioxidants (Basel).* 2022;12(1).
41. Belavy DL, Miokovic T, Armbrecht G, Richardson CA, Rittweger J, Felsenberg D. Differential atrophy of the lower-limb musculature during prolonged bed-rest. *Eur J Appl Physiol.* 2009;107(4):489-99.
42. Tan BH, Fearon KC. Cachexia: prevalence and impact in medicine. *Curr Opin Clin Nutr Metab Care.* 2008;11(4):400-7.
43. Reid MB, Judge AR, Bodine SC. CrossTalk opposing view: The dominant mechanism causing disuse muscle atrophy is proteolysis. *J Physiol.* 2014;592(24):5345-7.
44. Attaix D, Ventadour S, Codran A, Béchet D, Taillandier D, Combaret L. The ubiquitin–proteasome system and skeletal muscle wasting. *Essays in Biochemistry.* 2005;41:173-86.
45. Murton AJ, Constantin D, Greenhaff PL. The involvement of the ubiquitin proteasome system in human skeletal muscle remodelling and atrophy. *Biochim Biophys Acta.* 2008;1782(12):730-43.
46. Khodabukus A, Baar K. Factors That Affect Tissue-Engineered Skeletal Muscle Function and Physiology. *Cells Tissues Organs.* 2016;202(3-4):159-68.
47. Khodabukus A. Tissue-Engineered Skeletal Muscle Models to Study Muscle Function, Plasticity, and Disease. *Front Physiol.* 2021;12:619710.
48. Nagashima T, Hadiwidjaja S, Ohsumi S, Murata A, Hisada T, Kato R, et al. In Vitro Model of Human Skeletal Muscle Tissues with Contractility Fabricated by Immortalized Human Myogenic Cells. *Adv Biosyst.* 2020;4(11):e2000121.
49. Bodine SC, Latres E, Baumhueter S, Lai VK, Nunez L, Clarke BA, et al. Identification of ubiquitin ligases required for skeletal muscle atrophy. *Science.* 2001;294(5547):1704-8.
50. Taillandier D, Polge C. Skeletal muscle atrogenes: From rodent models to human pathologies. *Biochimie.* 2019;166:251-69.
51. Baehr LM, Hughes DC, Lynch SA, Van Haver D, Maia TM, Marshall AG, et al. Identification of the MuRF1 Skeletal Muscle Ubiquitylome Through Quantitative Proteomics. *Function (Oxf).* 2021;2(4):zqab029.
52. Bodine SC, Latres E., Baumhueter, S., Lai, V.K., Nunez, L., Clarke, B.A., Poueymirou, W.T., Panaro, F.J., Dharmarajan, E. Na, K., Pan, Z.Q., Valenzuela, D.M., DeChiara, T.M., Stitt,

- T.N., Yancopoulos, G.D., Glass, D.J., . Identification of ubiquitin ligases required for skeletal muscle atrophy. *Science (New York, NY)*. 2001;294 (5547).
53. Chen SN, Czernuszewicz G, Tan Y, Lombardi R, Jin J, Willerson JT, et al. Human molecular genetic and functional studies identify TRIM63, encoding Muscle RING Finger Protein 1, as a novel gene for human hypertrophic cardiomyopathy. *Circ Res*. 2012;111(7):907-19.
54. Scalabrin M, Adams V, Labeit S, Bowen TS. Emerging Strategies Targeting Catabolic Muscle Stress Relief. *International Journal of Molecular Sciences*. 2020;21(13):4681.
55. Bodine SC, Baehr LM. Skeletal muscle atrophy and the E3 ubiquitin ligases MuRF1 and MAFbx/atrogen-1. *Am J Physiol Endocrinol Metab*. 2014;307(6):E469-84.
56. Vogel C, Marcotte EM. Insights into the regulation of protein abundance from proteomic and transcriptomic analyses. *Nature reviews genetics*. 2012;13(4):227-32.
57. Buccitelli C, Selbach M. mRNAs, proteins and the emerging principles of gene expression control. *Nat Rev Genet*. 2020;21(10):630-44.
58. Sandri M. Protein breakdown in muscle wasting: role of autophagy-lysosome and ubiquitin-proteasome. *Int J Biochem Cell Biol*. 2013;45(10):2121-9.
59. Nishimura Y, Musa I, Holm L, Lai YC. Recent advances in measuring and understanding the regulation of exercise-mediated protein degradation in skeletal muscle. *American journal of physiology Cell physiology*. 2021.
60. Bodine SC. Edward F. Adolph Distinguished Lecture. Skeletal muscle atrophy: Multiple pathways leading to a common outcome. *Journal of Applied Physiology*. 2020;129(2):272-82.
61. Clarke BA, Drujan D, Willis MS, Murphy LO, Corpina RA, Burova E, et al. The E3 Ligase MuRF1 Degrades Myosin Heavy Chain Protein in Dexamethasone-Treated Skeletal Muscle. *Cell Metabolism*. 2007;6(5):376-85.
62. Cohen S, Brault JJ, Gygi SP, Glass DJ, Valenzuela DM, Gartner C, et al. During muscle atrophy, thick, but not thin, filament components are degraded by MuRF1-dependent ubiquitylation. *J Cell Biol*. 2009;185(6):1083-95.
63. Budhidarmo R, Nakatani Y, Day CL. RINGs hold the key to ubiquitin transfer. *Trends Biochem Sci*. 2012;37(2):58-65.
64. Baehr LM, Furlow JD, Bodine SC. Muscle sparing in muscle RING finger 1 null mice: response to synthetic glucocorticoids. *The Journal of Physiology*. 2011;589(19):4759-76.
65. Shoji S, Pennington RJ. The effect of cortisone on protein breakdown and synthesis in rat skeletal muscle. *Mol Cell Endocrinol*. 1977;6(3):159-69.
66. Koyama S, Hata S, Witt CC, Ono Y, Lerche S, Ojima K, et al. Muscle RING-Finger Protein-1 (MuRF1) as a Connector of Muscle Energy Metabolism and Protein Synthesis. *Journal of Molecular Biology*. 2008;376(5):1224-36.
67. Nakao R, Hirasaka K, Goto J, Ishidoh K, Yamada C, Ohno A, et al. Ubiquitin ligase Cbl-b is a negative regulator for insulin-like growth factor 1 signaling during muscle atrophy caused by unloading. *Mol Cell Biol*. 2009;29(17):4798-811.
68. Ochi A, Abe T, Nakao R, Yamamoto Y, Kitahata K, Takagi M, et al. N-myristoylated ubiquitin ligase Cbl-b inhibitor prevents on glucocorticoid-induced atrophy in mouse skeletal muscle. *Arch Biochem Biophys*. 2015;570:23-31.
69. Shi J, Luo L, Eash J, Ibebunjo C, Glass DJ. The SCF-Fbxo40 complex induces IRS1 ubiquitination in skeletal muscle, limiting IGF1 signaling. *Dev Cell*. 2011;21(5):835-47.

70. Ye J, Zhang Y, Xu J, Zhang Q, Zhu D. FBXO40, a gene encoding a novel muscle-specific F-box protein, is upregulated in denervation-related muscle atrophy. *Gene*. 2007;404(1-2):53-60.
71. Song R, Peng W, Zhang Y, Lv F, Wu H-K, Guo J, et al. Central role of E3 ubiquitin ligase MG53 in insulin resistance and metabolic disorders. *Nature*. 2013;494(7437):375-9.
72. Yi J-S, Park JS, Ham Y-M, Nguyen N, Lee N-R, Hong J, et al. MG53-induced IRS-1 ubiquitination negatively regulates skeletal myogenesis and insulin signalling. *Nature Communications*. 2013;4(1).
73. Lee CS, Yi JS, Jung SY, Kim BW, Lee NR, Choo HJ, et al. TRIM72 negatively regulates myogenesis via targeting insulin receptor substrate-1. *Cell Death Differ*. 2010;17(8):1254-65.
74. Cohen S, Lee D, Zhai B, Gygi SP, Goldberg AL. Trim32 reduces PI3K-Akt-FoxO signaling in muscle atrophy by promoting plakoglobin-PI3K dissociation. *J Cell Biol*. 2014;204(5):747-58.
75. Rodriguez JE, Liao JY, He J, Schisler JC, Newgard CB, Drujan D, et al. The ubiquitin ligase MuRF1 regulates PPARalpha activity in the heart by enhancing nuclear export via monoubiquitination. *Mol Cell Endocrinol*. 2015;413:36-48.
76. Adams V, Bowen TS, Werner S, Barthel P, Amberger C, Konzer A, et al. Small-molecule-mediated chemical knock-down of MuRF1/MuRF2 and attenuation of diaphragm dysfunction in chronic heart failure. *J Cachexia Sarcopenia Muscle*. 2019;10(5):1102-15.
77. Bowen TS, Adams V, Werner S, Fischer T, Vinke P, Brogger MN, et al. Small-molecule inhibition of MuRF1 attenuates skeletal muscle atrophy and dysfunction in cardiac cachexia. *Journal of Cachexia, Sarcopenia and Muscle*. 2017;8(6):939-53.
78. Hwee DT, Baehr LM, Philp A, Baar K, Bodine SC. Maintenance of muscle mass and load-induced growth in Muscle RING Finger 1 null mice with age. *Aging Cell*. 2014;13(1):92-101.
79. Hershko A, Ciechanover A. The ubiquitin system. *Annu Rev Biochem*. 1998;67:425-79.
80. Weissman AM, Shabek N, Ciechanover A. The predator becomes the prey: regulating the ubiquitin system by ubiquitylation and degradation. *Nat Rev Mol Cell Biol*. 2011;12(9):605-20.
81. Mota R, Rodríguez JE, Bonetto A, O'Connell TM, Asher SA, Parry TL, et al. Post-translationally modified muscle-specific ubiquitin ligases as circulating biomarkers in experimental cancer cachexia. *Am J Cancer Res*. 2017;7(9):1948-58.
82. Kim HT, Kim KP, Lledias F, Kisselev AF, Scaglione KM, Skowryra D, et al. Certain pairs of ubiquitin-conjugating enzymes (E2s) and ubiquitin-protein ligases (E3s) synthesize nondegradable forked ubiquitin chains containing all possible isopeptide linkages. *J Biol Chem*. 2007;282(24):17375-86.
83. Bowen TS, Adams V, Werner S, Fischer T, Vinke P, Brogger MN, et al. Small-molecule inhibition of MuRF1 attenuates skeletal muscle atrophy and dysfunction in cardiac cachexia. *J Cachexia Sarcopenia Muscle*. 2017;8(6):939-53.
84. Uchiki T, Kim HT, Zhai B, Gygi SP, Johnston JA, O'Bryan JP, et al. The ubiquitin-interacting motif protein, S5a, is ubiquitinated by all types of ubiquitin ligases by a mechanism different from typical substrate recognition. *J Biol Chem*. 2009;284(19):12622-32.
85. Dawson PWJ. Assessment of commercial versus custom-made MuRF1 antibodies: University of Birmingham; 2020.
86. Kristariyanto YA, Abdul Rehman SA, Campbell DG, Morrice NA, Johnson C, Toth R, et al. K29-selective ubiquitin binding domain reveals structural basis of specificity and heterotypic nature of k29 polyubiquitin. *Mol Cell*. 2015;58(1):83-94.

87. Goodman CA, Mabrey DM, Frey JW, Miu MH, Schmidt EK, Pierre P, et al. Novel insights into the regulation of skeletal muscle protein synthesis as revealed by a new nonradioactive in vivo technique. *Faseb j.* 2011;25(3):1028-39.
88. Walhout AJ, Vidal M. High-throughput yeast two-hybrid assays for large-scale protein interaction mapping. *Methods.* 2001;24(3):297-306.
89. Guest PC, Gottschalk MG, Bahn S. Proteomics: improving biomarker translation to modern medicine? *Genome Med.* 2013;5(2):17.
90. Sandri M. Protein breakdown in muscle wasting: role of autophagy-lysosome and ubiquitin-proteasome. *The international journal of biochemistry & cell biology.* 2013;45(10):2121-9.
91. Rojas-Fernandez A, Herhaus L, Macartney T, Lachaud C, Hay RT, Sapkota GP. Rapid generation of endogenously driven transcriptional reporters in cells through CRISPR/Cas9. *Sci Rep.* 2015;5:9811.
92. Cong L, Ran FA, Cox D, Lin S, Barretto R, Habib N, et al. Multiplex genome engineering using CRISPR/Cas systems. *Science.* 2013;339(6121):819-23.
93. Zhou Y, Zhu S, Cai C, Yuan P, Li C, Huang Y, et al. High-throughput screening of a CRISPR/Cas9 library for functional genomics in human cells. *Nature.* 2014;509(7501):487-91.
94. Liao J, Karnik R, Gu H, Ziller MJ, Clement K, Tsankov AM, et al. Targeted disruption of DNMT1, DNMT3A and DNMT3B in human embryonic stem cells. *Nature Genetics.* 2015;47(5):469-78.
95. Seabright AP, Lai YC. Regulatory Roles of PINK1-Parkin and AMPK in Ubiquitin-Dependent Skeletal Muscle Mitophagy. *Front Physiol.* 2020;11:608474.
96. Sackey JM, Hyatt JP, Raffaello A, Jagoe RT, Roy RR, Edgerton VR, et al. Rapid disuse and denervation atrophy involve transcriptional changes similar to those of muscle wasting during systemic diseases. *Faseb j.* 2007;21(1):140-55.
97. Hirner S, Krohne C, Schuster A, Hoffmann S, Witt S, Erber R, et al. MuRF1-dependent regulation of systemic carbohydrate metabolism as revealed from transgenic mouse studies. *J Mol Biol.* 2008;379(4):666-77.
98. McElhinny AS, Kakinuma K, Sorimachi H, Labeit S, Gregorio CC. Muscle-specific RING finger-1 interacts with titin to regulate sarcomeric M-line and thick filament structure and may have nuclear functions via its interaction with glucocorticoid modulatory element binding protein-1. *J Cell Biol.* 2002;157(1):125-36.
99. Centner T, Yano J, Kimura E, McElhinny AS, Pelin K, Witt CC, et al. Identification of muscle specific ring finger proteins as potential regulators of the titin kinase domain. *J Mol Biol.* 2001;306(4):717-26.
100. Nowak M, Suenkel B, Porras P, Migotti R, Schmidt F, Kny M, et al. DCAF8, a novel MuRF1 interaction partner, promotes muscle atrophy. *J Cell Sci.* 2019;132(17).
101. Manring H, Smith EM, Beck EX, Mcelhanon KE, Gushchina L, He WA, et al. Multiple Tripartite Motif E3 Ubiquitin Ligases Facilitate Skeletal Muscle Atrophy. *The FASEB Journal.* 2016;30(S1):1244.9-9.
102. Ran FA, Hsu PD, Wright J, Agarwala V, Scott DA, Zhang F. Genome engineering using the CRISPR-Cas9 system. *Nat Protoc.* 2013;8(11):2281-308.
103. Borden KLB. RING fingers and B-boxes: zinc-binding protein– protein interaction domains. *Biochem Cell Biol* 1998;76:8.

104. Eo H, Reed CH, Valentine RJ. Imoxin prevents dexamethasone-induced promotion of muscle-specific E3 ubiquitin ligases and stimulates anabolic signaling in C2C12 myotubes. *Biomed Pharmacother.* 2020;128:110238.
105. Kayali AG, Young VR, Goodman MN. Sensitivity of myofibrillar proteins to glucocorticoid-induced muscle proteolysis. *Am J Physiol.* 1987;252(5 Pt 1):E621-6.
106. Schmidt EK, Clavarino G, Ceppi M, Pierre P. SUNSET, a nonradioactive method to monitor protein synthesis. *Nature Methods.* 2009;6(4):275-7.
107. Witt CC, Witt SH, Lerche S, Labeit D, Back W, Labeit S. Cooperative control of striated muscle mass and metabolism by MuRF1 and MuRF2. *EMBO J.* 2008;27(2):350-60.
108. Adams V, Wunderlich S, Mangner N, Hommel J, Esefeld K, Gielen S, et al. Ubiquitin-proteasome-system and enzymes of energy metabolism in skeletal muscle of patients with HFpEF and HFrEF. *ESC Heart Fail.* 2021;8(4):2556-68.
109. Bonaldo P, Sandri M. Cellular and molecular mechanisms of muscle atrophy. *Disease Models & Mechanisms.* 2013;6(1):25-39.
110. Tamemoto H, Kadowaki T, Tobe K, Yagi T, Sakura H, Hayakawa T, et al. Insulin resistance and growth retardation in mice lacking insulin receptor substrate-1. *Nature.* 1994;372(6502):182-6.
111. Araki E, I., Lipes, Myra, A., Patti, Mary-Elizabeth, BriinIng, Jens, Claus, Haag, Ill Burritt, Johnson, Randall S., & Kahn, C., Ronald. Alternative pathway of insulin signalling in mice with targeted disruption of the IRS-1 gene. *NATURE.* 1994;372.
112. Crossland H, Skirrow S, Puthuchery ZA, Constantin-Teodosiu D, Greenhaff PL. The impact of immobilisation and inflammation on the regulation of muscle mass and insulin resistance: different routes to similar end-points. *J Physiol.* 2019;597(5):1259-70.
113. Du H, Zhao Y, Yin Z, Wang DW, Chen C. The role of miR-320 in glucose and lipid metabolism disorder-associated diseases. *Int J Biol Sci.* 2021;17(2):402-16.
114. Labeit S, Hirner S, Bogomolovas J, Cruz A, Myrزابekova M, Moriscot A, et al. Regulation of Glucose Metabolism by MuRF1 and Treatment of Myopathy in Diabetic Mice with Small Molecules Targeting MuRF1. *Int J Mol Sci.* 2021;22(4).
115. Wu H-K, Zhang Y, Cao C-M, Hu X, Fang M, Yao Y, et al. Glucose-Sensitive Myokine/Cardiokine MG53 Regulates Systemic Insulin Response and Metabolic Homeostasis. *Circulation.* 2019;139(7):901-14.
116. Feng H, Shen H, Robeson MJ, Wu YH, Wu HK, Chen GJ, et al. MG53 E3 Ligase-Dead Mutant Protects Diabetic Hearts From Acute Ischemic/Reperfusion Injury and Ameliorates Diet-Induced Cardiometabolic Damage. *Diabetes.* 2022;71(2):298-314.
117. Wang Q, Bian Z, Jiang Q, Wang X, Zhou X, Park KH, et al. MG53 Does Not Manifest the Development of Diabetes in db/db Mice. *Diabetes.* 2020;69(5):1052-64.
118. Philouze C, Turban S, Cremers B, Caliez A, Lamarche G, Bernard C, et al. MG53 is not a critical regulator of insulin signaling pathway in skeletal muscle. *PLoS One.* 2021;16(2):e0245179.
119. Cockram PE, Kist M, Prakash S, Chen SH, Wertz IE, Vucic D. Ubiquitination in the regulation of inflammatory cell death and cancer. *Cell Death Differ.* 2021;28(2):591-605.
120. Chen RH, Chen YH, Huang TY. Ubiquitin-mediated regulation of autophagy. *J Biomed Sci.* 2019;26(1):80.
121. Yang Y, Yu X. Regulation of apoptosis: the ubiquitous way. *Faseb j.* 2003;17(8):790-9.

122. Oh E, Akopian D, Rape M. Principles of Ubiquitin-Dependent Signaling. *Annu Rev Cell Dev Biol.* 2018;34:137-62.
123. Glickman MH, Ciechanover A. The ubiquitin-proteasome proteolytic pathway: destruction for the sake of construction. *Physiol Rev.* 2002;82(2):373-428.
124. Cohen P, Kellsall IR, Nanda SK, Zhang J. HOIL-1, an atypical E3 ligase that controls MyD88 signalling by forming ester bonds between ubiquitin and components of the Myddosome. *Adv Biol Regul.* 2019:100666.
125. Meroni G, Diez-Roux G. TRIM/RBCC, a novel class of 'single protein RING finger' E3 ubiquitin ligases. *Bioessays.* 2005;27(11):1147-57.
126. Seabright AP, Fine NHF, Barlow JP, Lord SO, Musa I, Gray A, et al. AMPK activation induces mitophagy and promotes mitochondrial fission while activating TBK1 in a PINK1-Parkin independent manner. *Faseb j.* 2020;34(5):6284-301.
127. Komatsu M, Waguri S, Ueno T, Iwata J, Murata S, Tanida I, et al. Impairment of starvation-induced and constitutive autophagy in Atg7-deficient mice. *J Cell Biol.* 2005;169(3):425-34.
128. Korolchuk VI, Mansilla A, Menzies FM, Rubinsztein DC. Autophagy inhibition compromises degradation of ubiquitin-proteasome pathway substrates. *Mol Cell.* 2009;33(4):517-27.
129. Olzmann JA, Chin LS. Parkin-mediated K63-linked polyubiquitination: a signal for targeting misfolded proteins to the aggresome-autophagy pathway. *Autophagy.* 2008;4(1):85-7.
130. Olzmann JA, Li L, Chudaev MV, Chen J, Perez FA, Palmiter RD, et al. Parkin-mediated K63-linked polyubiquitination targets misfolded DJ-1 to aggresomes via binding to HDAC6. *J Cell Biol.* 2007;178(6):1025-38.
131. Liyasova MS, Ma K, Voeller D, Ryan PE, Chen J, Klevit RE, et al. Cbl interacts with multiple E2s in vitro and in cells. *PLoS One.* 2019;14(5):e0216967.
132. Fletcher AJ, Christensen DE, Nelson C, Tan CP, Schaller T, Lehner PJ, et al. TRIM5 $\alpha$  requires Ube2W to anchor Lys63-linked ubiquitin chains and restrict reverse transcription. *Embo j.* 2015;34(15):2078-95.
133. Christensen DE, Brzovic PS, Klevit RE. E2-BRCA1 RING interactions dictate synthesis of mono- or specific polyubiquitin chain linkages. *Nat Struct Mol Biol.* 2007;14(10):941-8.
134. Vittal V, Stewart MD, Brzovic PS, Klevit RE. Regulating the Regulators: Recent Revelations in the Control of E3 Ubiquitin Ligases. *J Biol Chem.* 2015;290(35):21244-51.
135. Tatham MH, Plechanovová A, Jaffray EG, Salmen H, Hay RT. Ube2W conjugates ubiquitin to  $\alpha$ -amino groups of protein N-termini. *Biochem J.* 2013;453(1):137-45.
136. Zhang Y, Zhou X, Zhao L, Li C, Zhu H, Xu L, et al. UBE2W interacts with FANCL and regulates the monoubiquitination of Fanconi anemia protein FANCD2. *Mol Cells.* 2011;31(2):113-22.
137. Zhang L, Xu M, Scotti E, Chen ZJ, Tontonoz P. Both K63 and K48 ubiquitin linkages signal lysosomal degradation of the LDL receptor. *J Lipid Res.* 2013;54(5):1410-20.
138. Gandhi J, Antonelli AC, Afridi A, Vatsia S, Joshi G, Romanov V, et al. Protein misfolding and aggregation in neurodegenerative diseases: a review of pathogenesis, novel detection strategies, and potential therapeutics. *Rev Neurosci.* 2019;30(4):339-58.
139. Fang S, Weissman AM. A field guide to ubiquitylation. *Cell Mol Life Sci.* 2004;61(13):1546-61.

140. Kao WH, Beaudenon SL, Talis AL, Huibregtse JM, Howley PM. Human papillomavirus type 16 E6 induces self-ubiquitination of the E6AP ubiquitin-protein ligase. *J Virol.* 2000;74(14):6408-17.
141. Fang S, Jensen JP, Ludwig RL, Vousden KH, Weissman AM. Mdm2 is a RING finger-dependent ubiquitin protein ligase for itself and p53. *J Biol Chem.* 2000;275(12):8945-51.
142. Ryan PE, Davies GC, Nau MM, Lipkowitz S. Regulating the regulator: negative regulation of Cbl ubiquitin ligases. *Trends Biochem Sci.* 2006;31(2):79-88.
143. Alpi AF, Chaugule V, Walden H. Mechanism and disease association of E2-conjugating enzymes: lessons from UBE2T and UBE2L3. *Biochem J.* 2016;473(20):3401-19.
144. DeFronzo RA, Tripathy D. Skeletal muscle insulin resistance is the primary defect in type 2 diabetes. *Diabetes Care.* 2009;32 Suppl 2(Suppl 2):S157-63.
145. Qi J, Yang B, Ren C, Fu J, Zhang J. Swimming Exercise Alleviated Insulin Resistance by Regulating Tripartite Motif Family Protein 72 Expression and AKT Signal Pathway in Sprague-Dawley Rats Fed with High-Fat Diet. *J Diabetes Res.* 2016;2016:1564386.
146. Reddy SS, Shruthi K, Prabhakar YK, Sailaja G, Reddy GB. Implication of altered ubiquitin-proteasome system and ER stress in the muscle atrophy of diabetic rats. *Arch Biochem Biophys.* 2018;639:16-25.
147. Dirks ML, Wall BT, van de Valk B, Holloway TM, Holloway GP, Chabowski A, et al. One Week of Bed Rest Leads to Substantial Muscle Atrophy and Induces Whole-Body Insulin Resistance in the Absence of Skeletal Muscle Lipid Accumulation. *Diabetes.* 2016;65(10):2862-75.
148. Mikines KJ, Richter EA, Dela F, Galbo H. Seven days of bed rest decrease insulin action on glucose uptake in leg and whole body. *J Appl Physiol (1985).* 1991;70(3):1245-54.
149. Biensø RS, Ringholm S, Kiilerich K, Aachmann-Andersen NJ, Krogh-Madsen R, Guerra B, et al. GLUT4 and glycogen synthase are key players in bed rest-induced insulin resistance. *Diabetes.* 2012;61(5):1090-9.
150. Baehr LM, West DWD, Marshall AG, Marcotte GR, Baar K, Bodine SC. Muscle-specific and age-related changes in protein synthesis and protein degradation in response to hindlimb unloading in rats. *J Appl Physiol (1985).* 2017;122(5):1336-50.